MECHANICAL SURFACE WAVES IN SOLID LAYERED MEDIA

by T L KOH

Thesis submitted to the University of London in candidature for the degree of Doctor of Philosophy

Imperial College (University of London)
Department of Physics

and

Chelsea College (University of London)
Department of Physics

August 1976

ABSTRACT

A numerical analysis is given for a layered media with no loss of generality when imposing the necessary boundary constraints. In the present work, the particle motion of mechanical surface wave is considered to have three dimensional displacements rather than being conveniently confined on a plane in a crystalline solid. The approach towards the inclusion of piezoelectricity in plane wave propagation is carried out by establishing a relation in amplitude between the mechanical displacements and the associated electric potential.

The surface wave velocity and the coupling efficiency are also found and discussed in various combinations of crystalline material for the layered media. Several cases including the combinations of $ZnO/LiNbO_3$, ZnO/Si and $LiNbO_3$, are investigated with the aid of a computer programme which has been developed for this purpose. In conjunction with the analysis, an attempt is made with the concept of wave slowness to give a physical picture of mechanical surface wave behaviour in layered media. Within that context, a surface wave can be regarded as composed of the three basic bulk waves in a crystalline solid which has boundary constraints.

In order to utilize the results of the theoretical work an experiment was designed to assess the feasibility of a dispersive delay line compounded from layered media. An overlay ZnO layer was reactively sputtered onto a thermally oxidized silicon substrate. The silicon substrate was intended to have low resistivity such as those commercially used in micro-electronics. At the present stage, the total insertion loss in operating the device at a fundamental

frequency of 130 MHz would be extremely high (i.e. 70 dB). The inherent difficulties of realization are fully discussed and suggestions made for better transducer layout and construction of the acoustic device.

ACKNOWLEDGEMENT

The author wishes to express his deep appreciation to Dr R W B Stephens for his guidance throughout this research work. He also learned many important lessons from Dr M J P Musgrave, Department of Mathematics, and Professor J C Anderson, Department of Electrical Engineering at the Imperial College. Special thanks are due to Dr T C Lim, American Rockwell U.S.A., for his advice at the early stage of this project and to the Ministry of Defence, England, for its financial support. Finally, he is very grateful to his parents for their unfailing encouragement and support.

TABLE OF CONTENTS

CHAPTER 1		INTRODUCTION	PAGE
	1.1	General Remarks	1
	1.2	Objective	1 - 4
	1.3	Contents of Thesis	4 - 5
CHAPTER 2		PLANE WAVE PROPAGATION IN A CRYSTAL	
	2.1	Basic Concepts	6 - 8
	2.2	Mechanical Bulk Waves in a Purely Elastic Crystal	8 - 12
	2.3	Mechanical Bulk Waves in a Piezoelectric Crystal	12 - 22
CHAPTER 3		WAVE PHENOMENA AT A BOUNDED SOLID MEDIA	
	3.1	Waves occur at an Interface of Two Media	23 - 24
	3.2	Complex Direction Cosines	24 - 28
	3.3	Boundary conditions for a Layered Media	28 - 35
	3.4	A Method for calculating the Surface Wave Velocity	35 - 39
	3.5	Energy Flow and Group Velocity of the Surface Wave	39 - 41
CHAPTER 4		THEORETICAL STUDIES OF A LAYERED MEDIA	
	4.1	Effect of Piezoelectricity on Wave Velocity and Group Delay Time	42 - 46
	4.2	Dispersion Characteristics of ZnO/Si and $LiNbO_3$/Si	46 - 51
	4.3	Coupling Efficiencies of CdS/Si and $LiNbO_3$/Si	51 - 61
	4.4	Associated Electric Potential in CdS/Si	61
	4.5	Comparison of Coupling Efficiencies of ZnO/$LiNbO_3$, $LiNbO_3$/Si and PbTe/$LiNbO_3$	61 - 65
	4.6	Particle Displacements of the Mechanical Surface Waves in PbTe/SiO_2, PbTe/$LiNbO_3$, $LiNbO_3$/Si and ZnO/$LiNbO_3$	65 - 82
	4.7	Comments	82 - 85

CHAPTER 5		EXPERIMENTAL PROCEDURE	
	5.1	Thin Film Deposition by Radio Frequency Sputtering	86 - 93
	5.2	Fabrication of Interdigital Transducer	94 - 102
	5.3	Insertion Loss of the SAW Transducer	102 - 107
	5.4	Comments	107 - 109
CONCLUSION			110 - 111
APPENDIX A1		PIEZOELECTRICALLY STIFFENED ELASTIC CONSTANTS	112
APPENDIX A2		PHYSICAL SIGNIFICANCE OF ELECTROMECHANICAL AMPLITUDE RATIO	113 - 115
APPENDIX A3		CONCEPT OF COMPLEX PLANE WAVE	116 - 118
APPENDIX A4		VARIOUS BOUNDARY CONDITIONS FOR DIFFERENT COMBINED CRYSTALS IN LAYERED STRUCTURE	119 - 126
APPENDIX A5		ELECTRIC POTENTIAL ABOVE FREE SURFACE OF PIEZOELECTRIC CRYSTAL	127 - 128
APPENDIX A6		COMPUTER PROGRAMME 'SNOOPY'	129 - 136
APPENDIX A7		ASSOCIATED ELECTRIC ENERGY ACCOMPANYING THE MECHANICAL SURFACE WAVE IN A PIEZOELECTRIC CRYSTAL	137 - 138
GLOSSARY			139 - 140
REFERENCES			141 - 143

CHAPTER 1

INTRODUCTION

1.1 General Remarks

There are many areas of science which have social relevance, but it is difficult at times to predict which particular investigation is going to produce practical results in the immediate future. Since World War II, serious attention has been given to device-oriented research in the region of the electromagnetic spectrum between the near infrared and beyond. The travelling wave tube was operating in 1946 and later in 1950, saw the advent of transistor in solid-state devices. In parallel with this work, exciting research and development programmes were being undertaken in the field of mechanical acoustic waves in the frequency range extending from a few cycles to microwave region. Recently many techniques in signal analysis and data processing have changed the older tendency in considering only the output power from devices.

1.2 Objective

It was hoped that the present work would serve a two-fold purpose: to achieve a fundamental understanding on the behaviour of mechanical surface waves and to present a practical low-cost method in miniature device fabrication. The device considered is a velocity-frequency dispersive delay line by propagating mechanical surface waves in layered media. For many years, workers in seismology and in applied mathematics have compiled a good list on literature for wave propagation relating to the present topic (e.g. W M Ewing et al 1957, L M Brekhovskikh 1960, L Cagniard 1962 and V I Keilis-Borok et al 1967). A few references which led to the present work, are of interest in saying out the prime intention of the author.

It has been suggested by J L Synge 1956 & 1957 that generalized Rayleigh waves can propagate without attenuation in certain directions of an anisotropic elastic medium. This fact was later illustrated by V T Buchwald 1961 that if these waves exist with no attenuation, the waves can only propagate on certain plane of crystal symmetry. In a review paper by M J.P Musgrave 1961, these waves in anisotropic media cannot in general be separated into purely longitudinal or purely transverse particle displacements. R Stoneley 1955, concluded that there were no Rayleigh waves in materials such as aluminium, copper and nickel because the wave vectors of these waves become complex. It should be added that such complex wave vectors do not debar the existence of a mechanical surface wave. This is in agreement with T C Lim and G W Farnell 1968, who failed to find 'forbidden directions' in any crystal surface for propagating Rayleigh waves and instead they proposed to call a surface wave with small attenuation on that surface as the 'pseudo-surface waves'. In a paper by R Burridge 1970, it can be found that the above statement made by Lim and Farnell is fairly satisfactorily demonstrated by a 'reductio ad absurdum' argument.

Since 1965 when R M White and F W Voltmer introduced interdigital deposited electrodes for a direct excitation and detection of surface waves on piezoelectric crystals, there were two interesting areas of studying the behaviour of mechanical surface waves. The first interest lies in a general investigation of surface waves in piezoelectric crystals. For instance, G A Coquin and H F Tiersten 1966, gave a good analysis of the aforementioned interdigital surface wave transducer. In 1968, J J Campbell and W R Jones underlined a criterion for estimating piezoelectric coupling efficiency

of surface waves and further suggested that the criterion is based on a wave velocity change in the presence of a conducting film. This aspect of the matter is also pointed out by K A Ingebrigtsen 1969. Concurrently, J L Bleutein 1968 and Yu V Gulyaew 1969 reported that transverse waves, with particle displacements parallel to free surface, could propagate as surface waves only on piezoelectric crystals. The second interest is shown by P Schnitzler 1967 and R V Schmidt et al 1969 that a velocity-frequency dispersion can be realized by propagating surface waves in piezoelectric layered substrate, e.g. CdS film overlay onto Ge substrate. The studies of wave propagation in layered media can also be found in other papers by C Lardat et al 1970, G W Farnell 1970 and L P Solie 1973. In calculations, the piezoelectric crystal is treated as for a piezoelectrically stiffened medium and surface wave is considered as one which can propagate in a purely Rayleigh mode and a purely Love mode. However, it has been shown by F E Borguis 1955, K Brugger 1956 and G Koerber 1971, that it is not always possible to propagate 'pure modes' of bulk waves and surface waves in anisotropic crystals. From a theoretical viewpoint, it is generally not advisable to presume that particle motion of a surface wave is two dimensional, but there are three mutually coupled displacements. Moreover, the author is aware of a more elaborate but complicated way in which wave propagation behaviour is separately induced by the mechanical stress field and by the electromagnetic stress field. This approach is not followed since the prime interest here is with the slow velocity mechanical surface wave.

Finally, the second purpose of this work should also be briefly mentioned. Apart from presenting a practical method in device fab-

rication, it was in the mind of the author to corroborate the theoretical work by experimental results. Hence, dispersive delay line was to be made and tested. In parallel to this thought, the acoustic delay materials and the technique of this film deposition were to be chosen such that both would be attractive for the commercialized electronic industries. Hence, piezoelectric materials, e.g. CdS and ZnO, were selected to be deposited on semiconductor substrates, e.g. Ge and Si, by means of radio frequency sputtering.

1.3 Contents of the Thesis

The author proposes the mechanical surface wave is generated from the three basic bulk waves at a boundary surface of interface of an anisotropic crystal. In general, the mechanical surface wave cannot be regarded as one with the particle displacements of a pure Rayleigh or Love wave. In chapter 2, the fundamentals of the bulk wave behaviour in piezoelectric media are discussed and how the introduction of a piezomechanical amplitude ratio, used as a conversion factor, enables a solution of the wave equations to be realized. An attempt, in chapter 3, is made to introduce an explanation of complex wave vectors to account for wave problem at boundary interface. In the same chapter, a numerical analysis is described and following that in chapter 4, the theoretical results for various two-material combinations are given and discussed. It is essential to point out that the theoretical studies are very much device-oriented, but it is believed that a simple physical picture of a layered system has been established by chapter 3 and 4. Although it was not possible, due to time and cost limitations, to corroborate the theoretical predictions by experimental results, the

work as described in chapter 5 has enabled the author to acquire a good and valuable experience in microwave technology.

CHAPTER 2

PLANE WAVE PROPAGATION IN A CRYSTAL

2.1 Basic Concepts

With a view to better understanding of wave behaviour in a medium, it is necessary to resolve the problem into three regions of discussion:

excitation

propagation and

detection

The objective of this work is to describe the physical phenomena of wave propagation in a crystal in terms of wave characteristics arising from anisotropy and piezoelectricity. The geometry and the intrinsic physical properties of a medium define the possible modes of wave propagation. Mathematical analysis employed to predict the feature of wave propagation differs accordingly, but a fact remains that in most cases it is desirable for practical interests to provide the simplest and most useful approach. From a theoretical point of view, it is possible to divide wave propagation into two main categories:

1) A wave that possesses a complex resonant frequency, giving time dependence viz exp ($i\omega t$) with Imag (ω) > 0.
2) A wave that possesses a complex wave vector, giving variation with distance viz exp ($i\bar{k}t$) with ($\bar{k}$) > 0.

When dealing with wave propagation in a homogeneous and unlimited medium, it is sufficient to use a plane wave solution with a real propagation vector which is defined by the direction cosines (l_1, l_2, l_3), if a set of orthogonal axes (OX_1, OX_2, OX_3) in the medium is used as reference. The wave surface is often referred to as the surface of equiphase that would move to a distance in unit time associated with a disturbance

occurring at zero time at the origin of the reference. Due to this disturbance, the energy flux along the wave normal would cross the wave surface at a rate that could be identified with the phase velocity, V, of the plane wave. Now let the energy direction be defined by the direction cosines (L_1, L_2, L_3), in the same axis reference, the angle of deviation Δ between the energy direction and the propagation direction can be obtained from the relation:

$\cos \Delta = l_i L_i$; $i = 1, 2, 3$

Since any single crystal can be regarded as isotropic or anisotropic, the above quantity can have the following implications:

$\cos \Delta = 1$ for an isotropic, $\cos \Delta \leq 1$ for an anisotropic crystal.

Hence for an isotropic crystal, Δ is zero and thus the velocity surface coincides with the wave surface.

In order to give a geometrical relationship between the directions of energy flow, mechanical displacement and phase velocity, it is desirable to introduce the concepts of the velocity, slowness and wave surfaces. The three surfaces can be briefly represented as:

1) A velocity surface which is formed by the locus of a length proportional to the phase velocity in the propagation direction.
2) A slowness surface which is formed in the same way as the velocity surface except the length is inversely proportional to the phase velocity. However, Musgrave (1954) in his work chose a proportionality constant as K/ρ where K is associated with wave energy and its value is arbitrarily chosen but according to the symmetry of a crystal.
3) A wave surface is the envelope of plane waves which have moved to their corresponding distances in unit time associated with a disturbance which has occurred at zero time at the origin of reference.

Alternatively, the envelope of planes which is described by

$l_i x_i - Vt = 0.$

Now let O be the origin of the reference, a line $ON = V\,(l_1, l_2, l_3)$ and $OI = K/\rho V$, as shown graphically in Fig. 2.1. N is thus a point on the velocity surface and I, the slowness surface. IP is drawn in the direction (L_1', L_2', L_3') and of a length equal to $(V - K/\rho V)/l_i L_i'$. Therefore, P is a point on the wave surface. With respect to ON, the angles subtended by OP and IP are respectively equal to Δ and Δ'. Δ' defines the angle between the particle displacement direction and that of the wave propagation.

2.2 Mechanical Bulk Waves in a Purely Elastic Crystal

To achieve further insight into the wave characteristics in a crystal, it is essential to reveal the behaviour of mechanical displacements of the three possible waves: a longitudinal and two transverse modes. The stresses in the crystal are related to the mechanical displacements by the stress/strain relation:

$$T_{ij} = C_{ijkl}\, S_{kl} \quad ; \quad i,j,k,l = 1,2,3 \tag{2.1}$$

with

$$S_{kl} = \tfrac{1}{2}\,(U_{k,l} + U_{l,k}) \tag{2.2}$$

where T_{ij} are the components of the stress tensor, C_{ijkl} of the elastic stiffness, S_{kl} of the strain tensor and U_k of the mechanical displacement. If the body force is absent in the crystal, the equation of motion becomes:

$$T_{ij,i} = \rho\, \ddot{U}_j \tag{2.3}$$

where ρ is the material density of the crystal. From the above equations the combined effect describes the propagation of the

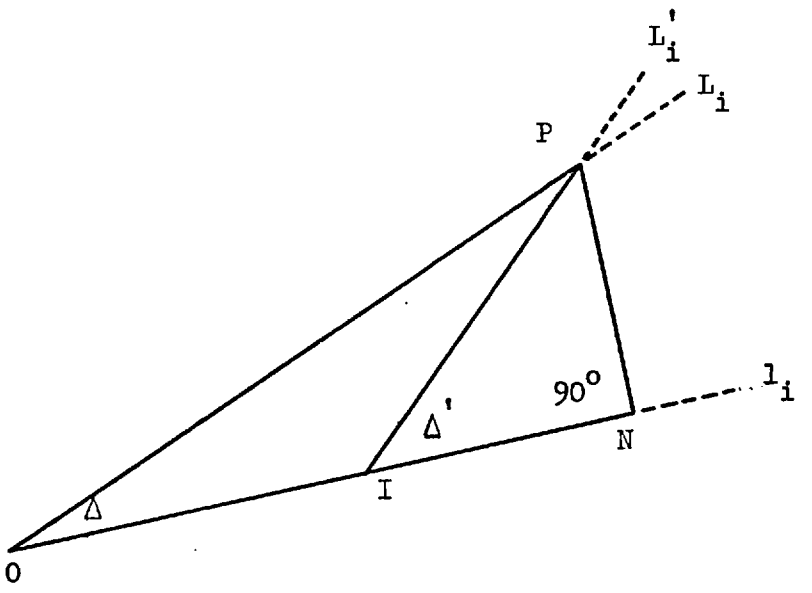

(a) $V > 1/V$

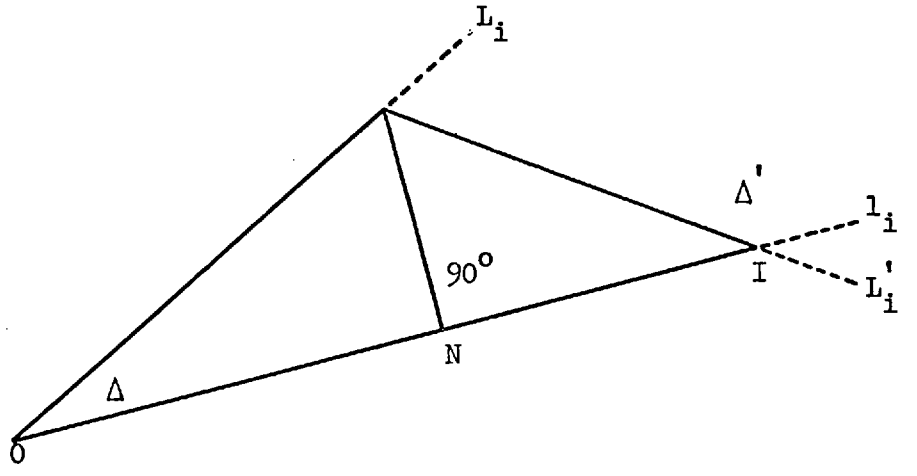

(b) $V < 1/V$

Fig. 2.1 GEOMETRICAL RELATIONSHIP BETWEEN DIRECTIONS OF ENERGY FLOW, MECHANICAL DISPLACEMENT AND PHASE VELOCITY

mechanical wave displacements:

$$C_{ijkl} \quad U_{k,li} \quad - \quad \rho \ddot{U}_j \quad = \quad 0 \qquad (2.4)$$

For the same reference of co-ordinates wherein OX_1 and OX_3 are the perpendicular axes in the plane of the paper with OX_2 axis normal to the plane, then the infinite plane wave solution for the mechanical displacements take the form:

$$U_j \quad = \quad \alpha_j \quad \exp \quad ik \cdot (l_i x_i - Vt) \qquad (2.5)$$

where x_i and t are space and time variables respectively, k is the modulus of the wave vector and V, the wave velocity. Finally, α_i are the amplitudes of mechanical displacement. By substituting Eq. 2.5 into Eq. 2.3, the propagation of the disturbance can therefore be represented by the three velocity surfaces given as:

$$\left| \Gamma_{jk} - \rho V^2 \quad \delta_{jk} \right| \quad \left| \alpha_j \right| \quad = 0 \; ; \quad \delta_{jk} = \begin{matrix} 1 & \text{for } j = k \\ 0 & j \neq k \end{matrix} \qquad (2.6)$$

with

$$\Gamma_{jk} \quad = \quad C_{ijkl} \quad l_1 \quad l_i$$

where Γ_{jk} are the Christoffel stiffnesses and δ_{jk} is the Kronecker delta. It follows that for the above equations in matrix form to have physical meaning, the condition below is to be fulfilled:

$$\det \quad \left| \Gamma_{jk} - \mu \delta_{jk} \right| \quad = \quad 0 \; ; \quad \mu = \rho V^2 \qquad (2.7)$$

where μ is the characteristic (eigen) value such that there exist a set of non-zero values of the amplitudes, α_j, which are thus the corresponding characteristic (eigen) vectors. Since the Christoffel stiffnesses are subjected to the condition ($\Gamma_{jk} = \Gamma_{kj}$), the above matrix is diagonal symmetric and thus the value for μ must be real. This result implies a physically possible wave velocity, V, associated with the mechanical displacement. It is also legitimate to regard μ

as the root of a characteristic polynomial of the above matrix. In this case, it is obvious that the polynomial is cubic and thus three distinct values of μ can be obtained and associated with the three possible waves in a crystal. In fact experimentally this is found to be the case in any anisotropic crystal. It should be noted that only two distinct values exist in an isotropic crystal since the two transverse modes are coupled together with the same phase velocity.

From the above considerations, the results may be expressed in the following manner:

(a) There are in general three different velocities associated with the distinct values of μ, regardless of the direction of wave propagation in a crystal.

(b) Since α_i are the eigenvectors for each velocity, their values can be normalized to give the direction cosines (L_1', L_2', L_3') of the mechanical displacement for each bulk wave. Subsequently, the angle between the displacement direction and the propagation direction is related by:

$$\cos \Delta' = l_i L_i'$$

This aspect indicates that the three displacement directions are usually neither orthogonal to, nor coincident with, the propagation direction. A similar relation can also exist with the energy direction. Furthermore, it is revealed that in calculations on many crystals the mechanical displacements are not necessarily always orthogonal but are predominantly so. The bulk waves are therefore in general regarded as quasi-longitudinal and quasi-transverse in nature.

(c) It is worthy of note that this approach in computing the wave propagating characteristics does not provide information on the relative wave intensity.

Consequently, if waves travel with the same velocity as for example in the case of the two transverse modes in an isotropic crystal, it is impossible to deduce any information about the interchange of energy from the mechanical displacements of the waves.

2.3 Mechanical Bulk Waves in a Piezoelectric Crystal

A necessary condition for the occurrence of piezoelectricity is the absence of a centre of symmetry. Piezoelectric media are therefore intrinsically anisotropic. Since piezoelectricity provides a coupling between elastic and dielectric phenomena, stress in a medium is a function not only of geometric strain but also of electric field. It is known that due to the piezoelectric effect, there is a change in the mechanical wave velocity in a piezoelectric medium. The change in velocity could be very substantial in magnitude depending on the piezoelectric coupling factor and the orientation of the crystal axis. This part of the present work emphasizes an extension of the concept of piezoelectrically stiffened components of the elastic tensor (see Appendix A 1) of a piezoelectric medium. The piezoelectric coupling factor K_p of the medium can be estimated from the following expression (D A Berlincourt et al, 1964):

$$K_p^2 = 1 - (V / V_\infty)^2 \qquad (2.8)$$

V is the wave velocity deducible from elastic stiffnesses, C_{ijkl}, when the medium is considered hypothetically as elastic and V_∞ is the wave velocity modified from the physical constants comprising elastic stiffnesses, C_{ijkl}, dielectric constants, ε_{ik}, and piezoelectric constants, e_{kij}, when the medium is regarded as piezoelectric. Before discussing the calculation of the wave velocity in a piezo-

electric crystal, it is essential to know that through piezoelectric coupling, every electromagnetic wave is associated with an elastic wave. For a non-piezoelectric crystal, two electromagnetic waves and three mechanical waves can be propagated independently. However, the two types of waves are coupled together in a piezoelectric crystal and thus there are five wave velocities for both electromagnetic and mechanical waves.

It should be noted that the two mechanical waves will be associated with the propagated electromagnetic waves while the slower electromagnetic waves will arise from electric field accompanying the naturally slower mechanical waves. The present discussion is concerned with the latter and hence it is the slower electromagnetic waves which are dealt with in the following theory of linear piezoelectricity. Now it is assumed that for all practical purposes the piezoelectric crystal is purely non-conductive such that the varying electric field would be able to sustain itself and follow the mechanical wave. This restriction implies the physical system is quasi-static in the sense that so far, the fast mechanical waves associated with the velocity of the electromagnetic waves have been neglected and also the medium is essentially charge free. Hence the components of the electric field may be derived from a scalar potential as in the following analysis. In addition to the preceding equations 2.2, 2.3, and 2.5, used in wave propagation, the following equations are required for a piezoelectric crystal:

Associated electric scalar potential:-

$$\phi = \alpha_4 \exp ik (l_i x_i - Vt) \tag{2.9}$$

Components of electric field:-

$$E_k = - \phi_{,k} \tag{2.10}$$

Charge equation of electrostatics:-

$$D_{i,i} = 0 \tag{2.11}$$

Equations of constitutive relations:-

$$T_{ij} = C_{ijkl}\, S_{kl} - e_{kij}\, E_k \;;\; i,j,k,l = 1,2,3 \tag{2.12}$$

$$D_i = e_{ikl}\, S_{kl} + \varepsilon_{ik}\, E_k \tag{2.13}$$

where α_4 is the amplitude of the electric potential, E_k is the component of the electric potential, D_i of the electrical displacement, e_{kij} of the piezoelectric tensor and ε_{ik} of dielectric tensor. The resulting equations obtained to represent the velocity surfaces for a piezoelectric crystal are as follows:

$$\begin{vmatrix} \Gamma_{jk} - \mu\delta_{jk} & , & \Gamma_{j4} \\ \Gamma_{4j} & , & \Gamma_{44} \end{vmatrix} \begin{vmatrix} \alpha_k \\ \alpha_4 \end{vmatrix} = 0 \tag{2.14}$$

where Γ's are the Christoffel stiffnesses given as:

$$\Gamma_{jk} = C_{ijkl}\, l_l l_i \;,\; \Gamma_{j4} = e_{kij}\, l_k l_i \;,$$
$$\Gamma_{4j} = \Gamma_{j4} \;,\; \Gamma_{44} = -\varepsilon_{ik}\, l_k l_i \;. \tag{2.15}$$

The above may be regarded numerically as an eigen value and vector problem. In computation, a difficulty arises from the fact that the different physical constants (i.e. c_{ijkl}, e_{kij} and ε_{ik}) are of highly contrasting magnitude. It is obvious that in the characteristic matrix, the elements of the last row and column are relatively small in magnitude and thus the matrix can be reduced to that for the elastic medium. In order to estimate the piezoelectric effect on the velocity surfaces, it is necessary to obtain a relative ratio of magnitude between the mechanical and electrical amplitude. Since the equations for piezoelectricity are linear, it is legitimate and possible to estimate a relative ratio of α_4 for

an arbitrary set of α_k. This aspect implies that the relative ratio, α_o can be associated with the modulus of electric polarization due to elastic waves in piezoelectric media. Henceforth, α_o may be used as a 'coupling' factor between the elastic and dielectric phenomena akin to the concept of piezoelectric constant in piezoelectricity. The value of the relative ratio can be obtained readily if the calculation for velocity surfaces is done by using the actual physical constants to find a set of values for α_k and α_4 corresponding to a case of trivial solution. The values obtained for α_k and α_4 are related to α_o in the following way, (also see Appendix A 2):

$$\frac{|\alpha_k|}{|\alpha_4|} = \alpha_o \qquad (2.16)$$

In subsequent calculation of the velocity surfaces, the value α_o is used as a scaling factor for the physical constants of the piezoelectric medium and thus the modified Christoffel stiffnesses are given as:

$$\Gamma'_{jk} = \Gamma_{jk}\,\alpha_o \;,\; \Gamma'_{j4} = \Gamma_{j4} \;,\; \Gamma'_{4j} = \Gamma_{4j} \;, \text{ and } \Gamma'_{44} = \Gamma_{44}/\alpha_o \qquad (2.17)$$

As a result of the modification, the characteristic value of the modified matrix is now equal to $\rho V^2\,\alpha_o$. Thus the wave velocity in a piezoelectric medium could become higher than that when the same medium is considered as purely elastic. The increase in wave velocity could be used to estimate the piezoelectric coupling factor, as indicated in equation 2.8. To illustrate the results obtained by this approach, both the mechanical bulk wave velocities and the corresponding piezoelectric coupling constants are calculated for the crystals, $Ba_2NaNb_5O_{15}$ and $5PbO.3GeO_2$. The elastic and piezoelectric properties can be found respectively from the recent papers of

A W Warner et al (1969) and T Yamada et al (1972). From the same papers, their calculated and measured results for the bulk wave velocities and the piezoelectric coupling constants are shown in Table 2.1 and 2.2 for comparison. The variation of the coupling constants as a function of angle of rotation of the crystal are compared and given in Figs. 2.2 and 2.3. It is relevant to point out what degree of relation exists between the piezoelectric coupling and other characteristic parameters associated with bulk waves in piezoelectric media. Fig. 2.4 shows that the associated electric potential for the three bulk waves in the $5PbO_3GeO_2$ crystal inherently manifests the anisotropy of the crystal. Although the coupling constant is not directly expressed by the associated electric potential of the piezoelectric crystal, but especially in the angular range between 30° and 50° for the vertical shear wave, the profile of the two curves closely resemble each other. It is important to make clear the associated electric potential changes in sign thus going through a zero value as shown in Fig. 2.5. Moreover, the wave energy direction in the plane of the wave propagation and being defined by an angle φ_e from the latter direction, will be also affected by a change of sign. This occurs within the angular range between 41° and 42° of the wave propagation direction. The apparent relation between the associated electric potential and the wave energy direction inversely implies that the latter direction could be electrically steered to comply with the requirements of practical applications. Finally, the results obtained by this approach are evidently not in serious conflict with those obtained by previous workers (loc cit).

TABLE 2.1

COMPARISON OF THE RESULTS OBTAINED BY A W WARNER ET AL AND THE AUTHOR FOR WAVE VELOCITIES AND COUPLING CONSTANTS OF $Ba_2NaNb_5O_{15}$ AT ROOM TEMPERATURE; VELOCITY IS IN METRES/SECOND AND IN THE DIRECTION NORMAL TO THE PLATE

ORIENTATION AND COUPLING CONSTANT	LONGITUDINAL			HORIZONTAL SHEAR			VERTICAL SHEAR		
	meas. (WARNER ET AL)	calc. (WARNER ET AL)	calc. (AUTHOR)	meas. (WARNER ET AL)	calc. (WARNER ET AL)	calc. (AUTHOR)	meas. (WARNER ET AL)	calc. (WARNER ET AL)	calc. (AUTHOR)
X	6730	6716	6715		3786	3787	3646	3634	3623
K_p							0.21	0.24	0.23
Y	6830	6826	6827		3786	3787	3650	3654	3641
K_p							0.25	0.28	0.27
Z	6150	6146	5748	3520	3528	3529	3500	3502	3502
K_p	0.57	0.57	0.48						
(ZX1) 45°	6216	6190	6152	3658	3660	3660	3592	3580	3569
(XY1) 45°	6084	6112	6085	3642	3648	3647	3560	3568	3558
(YZ1) 45°	6860	6862	6861	3650	3642	3634		3620	3621
K_p				0.16	0.26	0.24			

NOTE: THE NOTATION OF CRYSTAL ORIENTATION IS CONFORMED WITH THE I.R.E. STANDARDS FOR CRYSTALS, 1949

TABLE 2.2

COMPARISON OF THE RESULTS OBTAINED BY YAMADA ET AL AND THE AUTHOR FOR WAVE VELOCITIES OF $5PbO.3GeO_2$ AT ROOM TEMPERATURE; VELOCITY IS IN METRES/SECOND AND IN THE DIRECTION NORMAL TO THE PLATE

ORIENTATION	LONGITUDINAL			HORIZONTAL SHEAR			VERTICAL SHEAR		
	meas. (YAMADA ET AL)	calc. (YAMADA ET AL)	calc. (AUTHOR)	meas. (YAMADA ET AL)	calc. (YAMADA ET AL)	calc. (AUTHOR)	meas. (YAMADA ET AL)	calc. (YAMADA ET AL)	calc. (AUTHOR)
X	3058	3056	3056	1744	1756	1756	1694	1688	1686
Y	3056	3056	3056	1780	1780	1780	1660	1660	1660
Z	3620	3620	3619	1756	1756	1756	1756	1756	1756
(XZl) + 45°	3168	3164	3163		2040	2040	1780	1770	1768
(XZl) - 45°	3210	3206	3206		2054	2054	1672	1672	1673
(YZl) + 45°	3194	3188	3187	2050	2050	2045		1718	1718
(YZl) - 45°	3178	3182	3183		2050	2048	1734	1718	1718

NOTE: THE NOTATION OF CRYSTAL ORIENTATION IS CONFORMED WITH THE I.R.E. STANDARDS FOR CRYSTALS, 1949

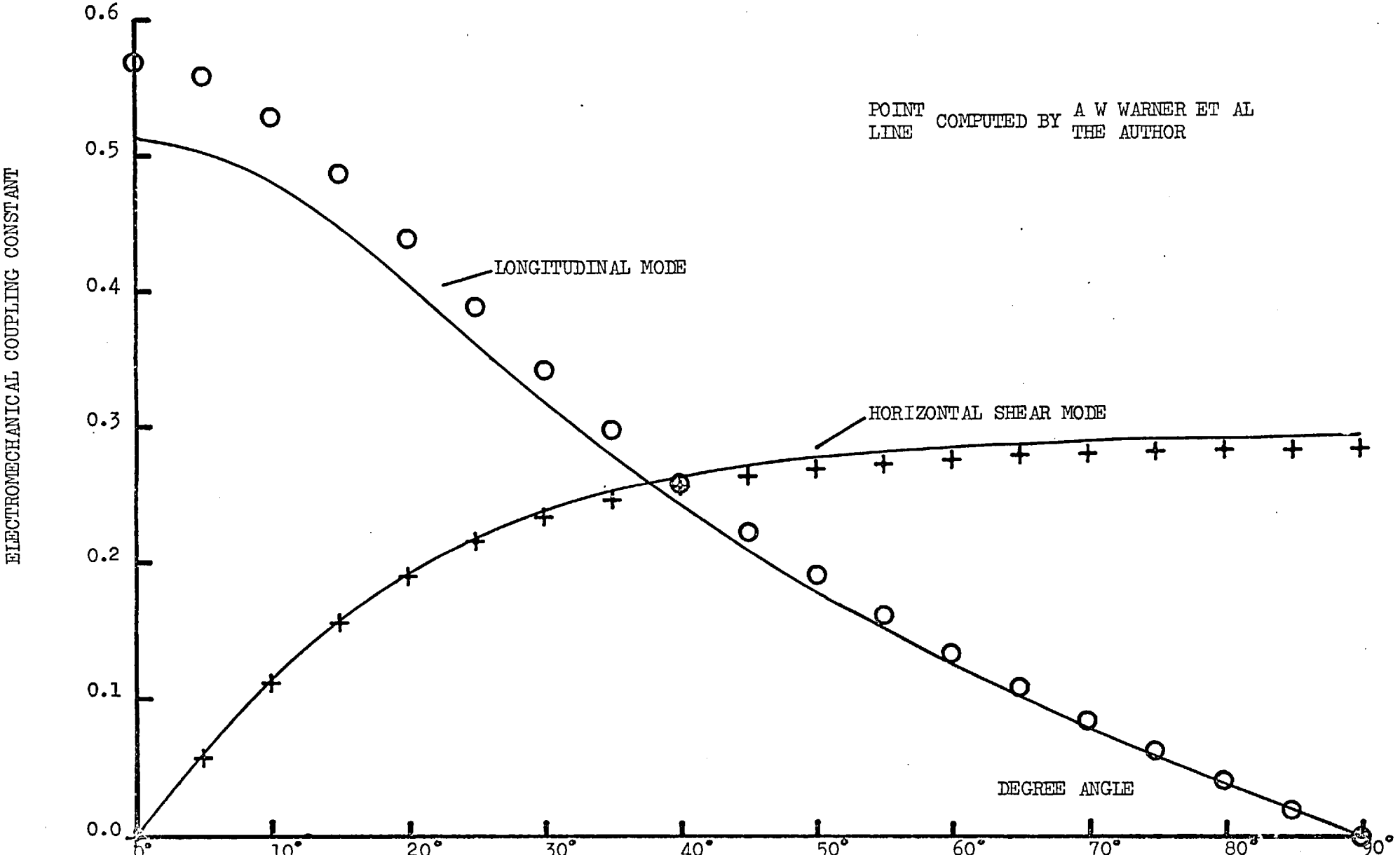

Fig. 2.2 ELECTROMECHANICAL COUPLING CONSTANT FOR TWO BULK WAVES VARYING WITH ANGULAR ORIENTATION FROM [001] to [010] IN $Ba_2NaNb_5O_{15}$ CRYSTAL

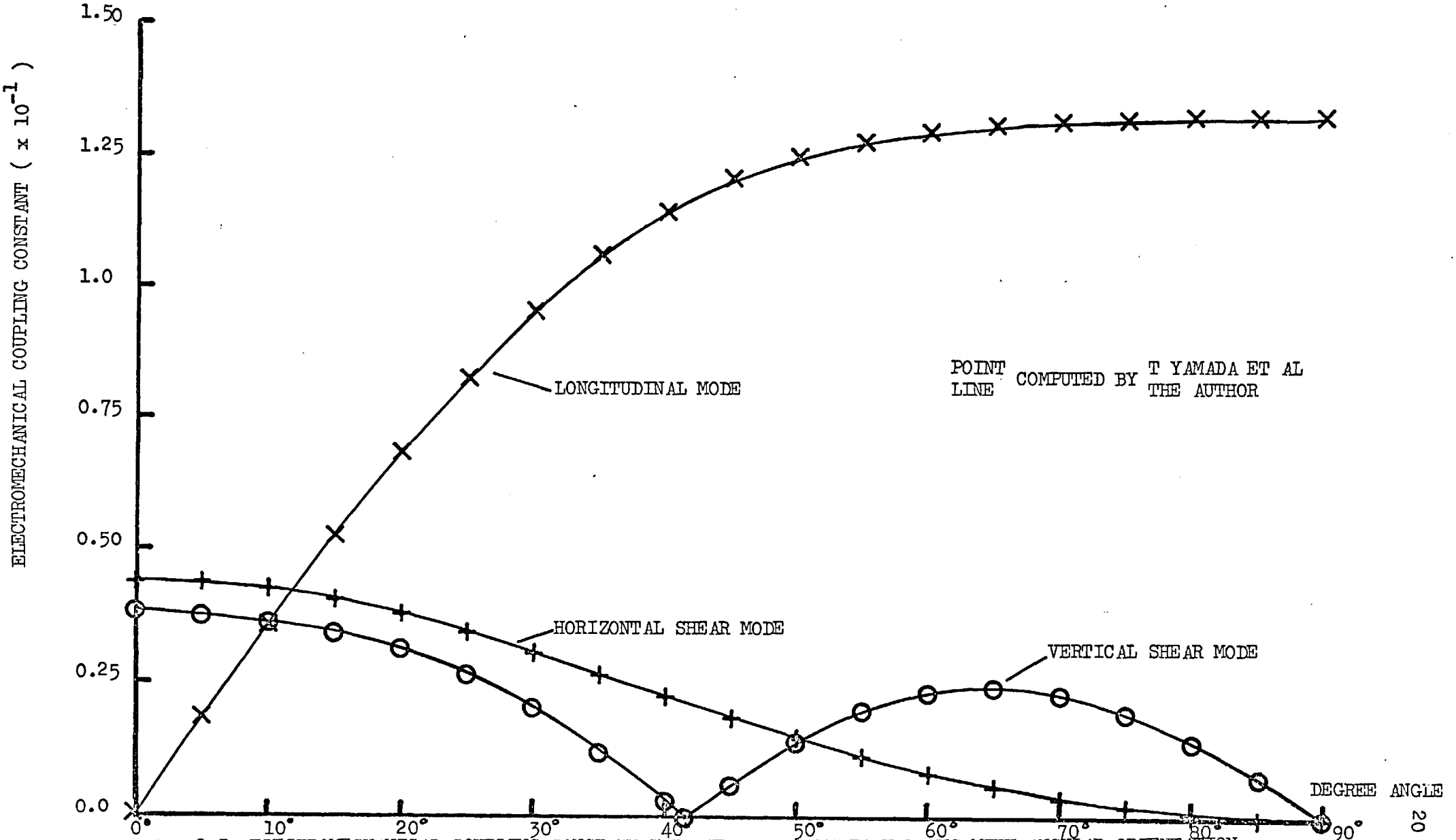

Fig. 2.3 ELECTROMECHANICAL COUPLING CONSTANT FOR THREE BULK WAVES VARYING WITH ANGULAR ORIENTATION FROM {100} TO {001} IN $5PbO_3GeO_2$ CRYSTAL

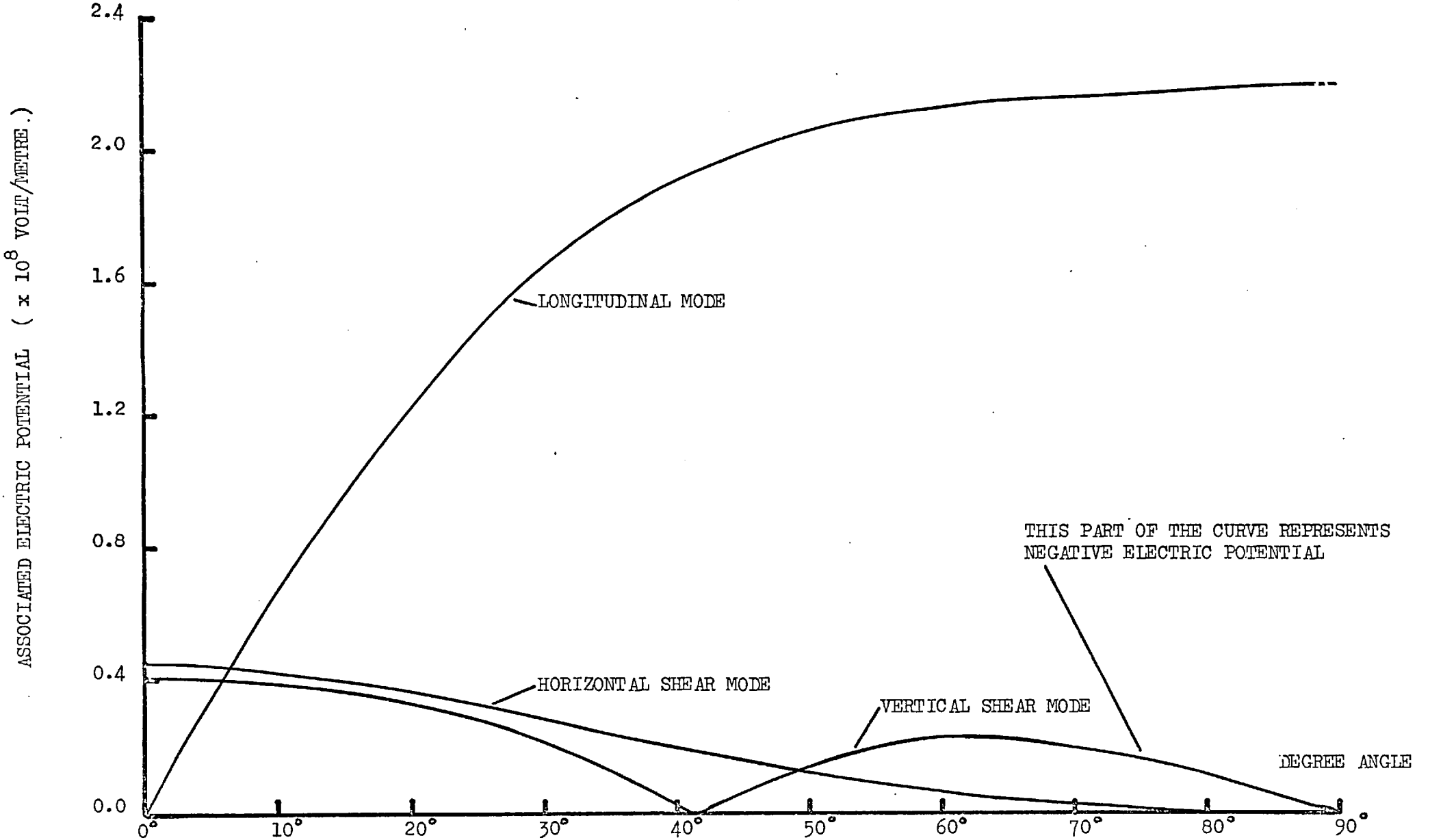

Fig. 2.4 ELECTRIC POTENTIALS ASSOCIATED WITH BULK WAVES IN Y-CUT $5PbO_3GeO_2$ VARYING WITH ANGULAR ORIENTATION FROM [100] TO [001]

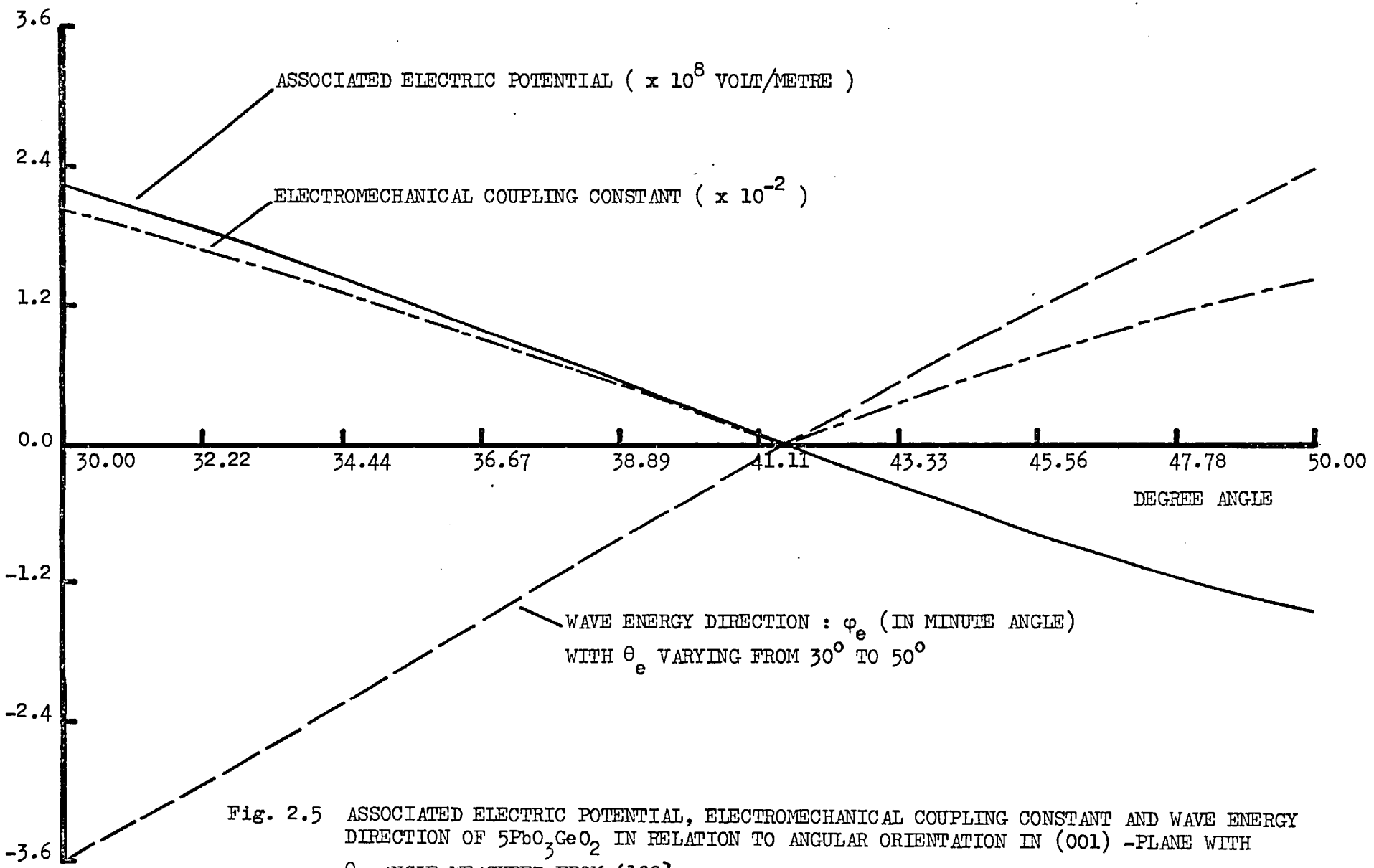

ASSOCIATED ELECTRIC POTENTIAL, ELECTROMECHANICAL COUPLING CONSTANT AND WAVE ENERGY DIRECTION

Fig. 2.5 ASSOCIATED ELECTRIC POTENTIAL, ELECTROMECHANICAL COUPLING CONSTANT AND WAVE ENERGY DIRECTION OF $5PbO_3GeO_2$ IN RELATION TO ANGULAR ORIENTATION IN (001) -PLANE WITH θ_e-ANGLE MEASURED FROM [100]

CHAPTER 3

WAVE PHENOMENA AT A BOUNDED SOLID MEDIA

3.1 Waves occur at an Interface of Two Media

When a plane wave impinges on a plane interface of two homogeneous and lossless media of different acoustic impedance, depending on the angle of incidence, it gives rise to reflected and refracted waves. Normally it is argued that for incidence at the critical angle, total reflection of the incident wave will be obtained and this is also the initial condition for the non-existence of the refracted wave in the second medium. Beyond the angle of critical incidence, it is observed that wave propagation takes place parallel to the plane interface. Wave phenomena of this type are usually classed as 'lateral waves'. Since a lateral wave cannot be adequately explained by conventional geometrical optics, it may be regarded as a combined effect of radiation and diffraction and may be referred to as a 'complex wave' (see Appendix A 3). However the characteristics of the complex wave may be interpreted in terms of wave coupling and this aspect supports the fact that if a medium can support different wave velocities, complex wave may arise at the boundary surface without the presence of another medium, i.e. in a vacuum. It is also known that the complex wave can exist in a situation where the propagation velocities in two media differ as for the case of a fluid interface. The general term complex wave may under different conditions refer to a lateral wave, a leaky wave or a surface wave but there can be interaction between them leading to intertransference of energy e.g. a leaky wave may be regarded as a regenerate lateral or surface wave over a certain velocity range. Directly following critical incidence lateral waves are generated along the surface with accompanying radiation into the body of the

medium so that two velocities are propagated at the same instant as shown in Fig. 3.1. In discussion of the surface wave, it is essential to make clear that the surface wave energy is strictly confined near to the interface. Its depth of penetration is approximately proportional to its λ. Fig. 3.2 shows vividly that wave propagation in a layer consists of multi-reflections and lateral displacements of the possible partial (or bulk) waves in the layer. The two photographs are taken from 'Acousto-Optic Investigation of Layer Wave Properties' by C J Kramer et al, in Ultrasonics Symposium Proceedings 1973.

3.2 Complex Direction Cosines

In view of the fact that the propagation vector of a surface wave is complex but is real for a bulk wave, it is not usual to link together the two types of waves. If the propagation vector of the bulk wave can be regarded as having a complex value with a zero imaginary part, then a linear compounding of the responses of each of the various bulk waves, under defined boundary conditions, can be legitimately considered to constitute the surface wave.

With the same coordinates of reference, it is usual to define the direction of the propagation vector by θ and φ, as shown in Fig.3.3. The direction cosines of this vector can therefore be given as:

$$l_1 = \cos\theta \sin\varphi, \quad l_2 = \sin\theta \sin\varphi, \text{ and } l_3 = \cos\varphi. \qquad (3.1)$$

In what follows, it is necessary to assign φ as a complex angle in order to describe the physical motion of a surface wave along a boundary of two media. Thus, l_3 is replaced by $\bar{l}_3$ and it takes the form:

$$\bar{l}_3 = l_3^* + i\, l_3^+ \qquad (3.2)$$

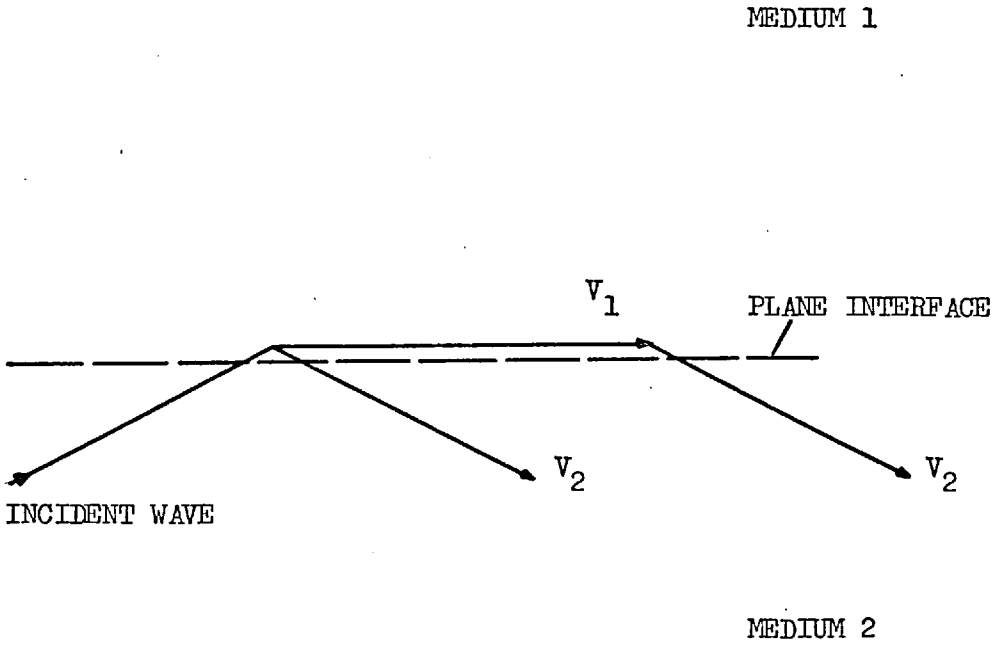

Fig. 3.1 A SIMPLE GRAPHICAL PRESENTATION OF LATERAL WAVE TRAVELLING WITH TWO VELOCITIES, V_1 AND V_2, AT A PLANE INTERFACE

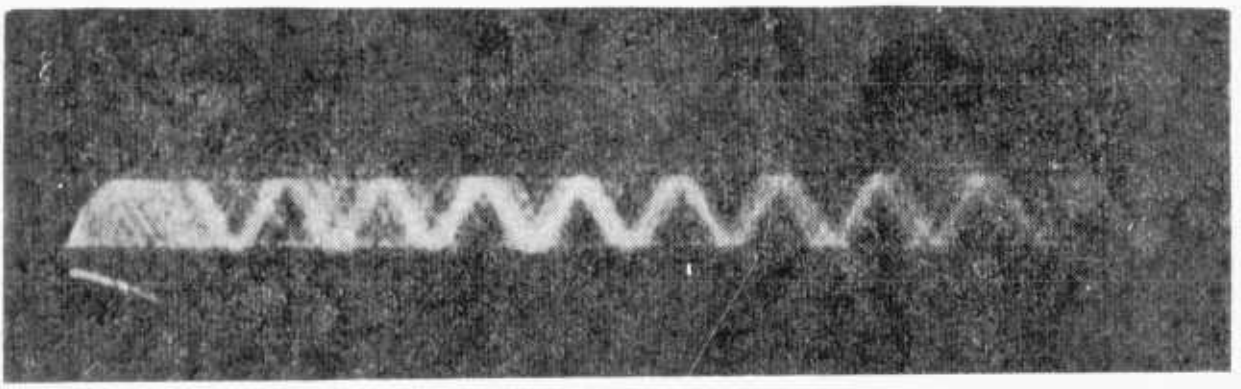

(a) SIDE VIEW OF WAVE PROPAGATION IN FLUID LAYER

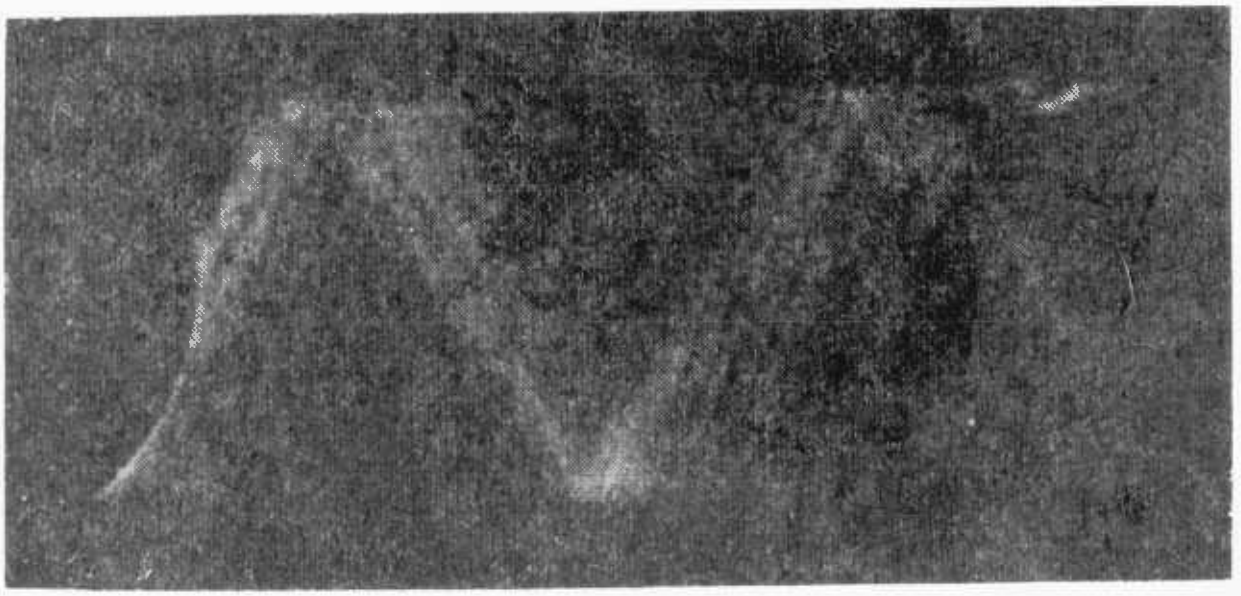

(b) MAGNIFICATION OF AN AREA IN (a)

Fig. 3.2 DIRECT VISUALIZTION OF MULTI-REFLECTIONS LATERAL DISPLACEMENTS OF WAVE PROPAGATION FLUID LAYER

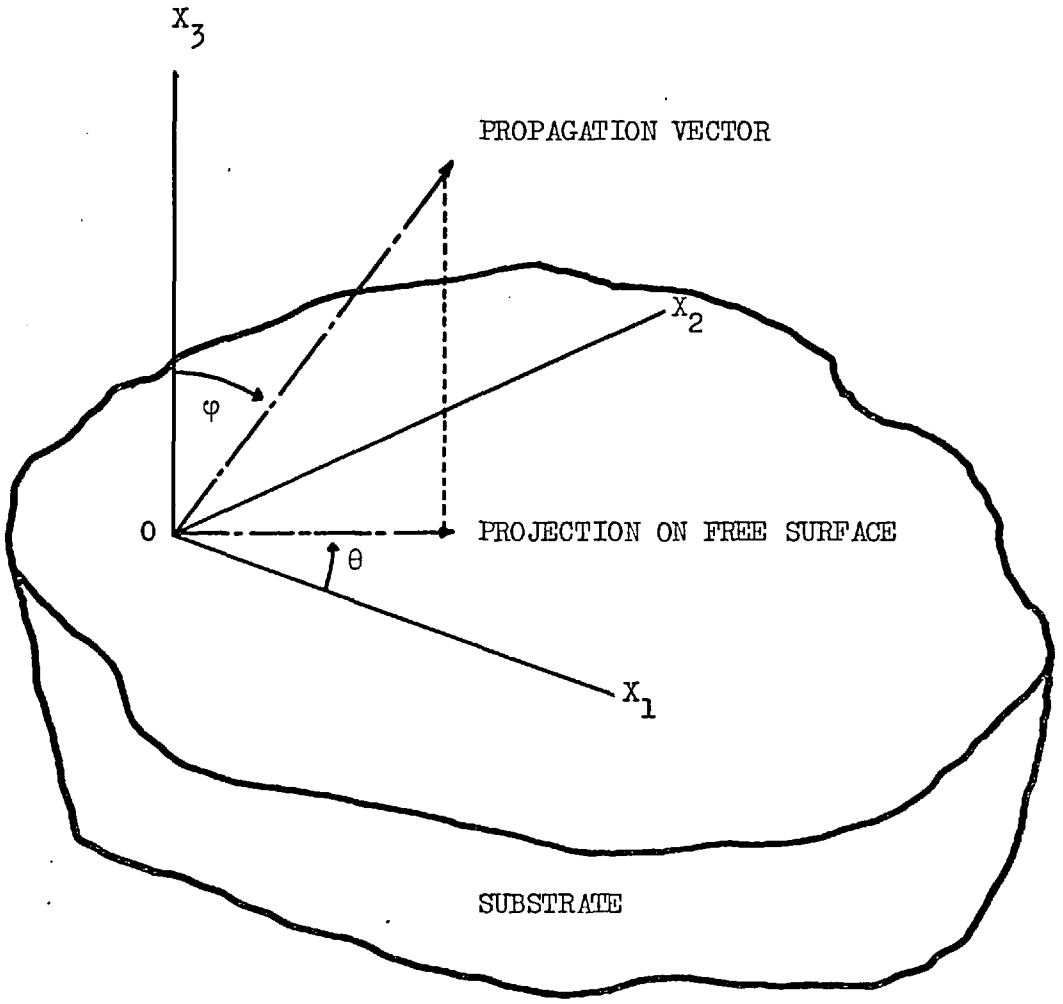

Fig. 3.3 THE PROPAGATION VECTOR AND THE ORIENTATION DEFINED BY THE EULAR ANGLES, θ AND φ

where the wave propagates in the direction given by $(\cos\theta, \sin\theta, l_3^*)$ and its amplitude is modulated exponentially by l_3^+ in the perpendicular direction; in this case, l_3^* can be expressed as $\cot\varphi$, and l_3^+ a propagation constant for the wave.

Let us consider, as an example of surface wave, a case where $\theta = 0^\circ$, and $\varphi = x + i\,y$ in which x and y are real. By substituting Eqs. 3.1 and 3.2 into Eg. 2.5, the form of the mechanical displacement becomes:

$$U_j = \alpha_j \exp(-k \sinh y \cdot x_3) \exp ik(\cosh y \cdot x_1 - Vt) \qquad (3.3)$$

This mechanical disturbance is thought of as a wave propagating in the x_1 direction with a varying amplitude along the x_3 direction and thus the wave is an inhomogeneous plane wave.

As follows from Eq. 3.3, the phase velocity of the surface wave is therefore equal to

$V/(\cosh y)$

where V is the bulk wave velocity and the corresponding wavelength of the surface wave is $\lambda/(\cosh y)$ where λ is wavelength of bulk wave. Hence the surface wave velocity and its wavelength are always less than the corresponding values for the bulk wave. Moreover, the concept of an inhomogeneous plane wave which can be transformed from an ordinary homogeneous plane wave, and vice versa, is readily illustrated by the aid of complex direction cosines (see Appendix A 3).

3.3 Boundary Conditions for a Layered Media

For each medium, there are three possible bulk waves with appropriate slownesses and energy fluxes. If an incident bulk wave meets the interface of two different media, a redistribution of energy associated

with six possible waves will, in the general case, occur in accordance with the boundary conditions. A number of possible reflected and refracted waves are governed by the fact that phases of all the waves at the interface must be equal at any instant. It may be suitable to use a geometrical presentation as in Fig. 3.4(a) to visualize the physical problem to which the above generalisation is applicable. It shows the reflected and refracted waves are bulk waves resulting from the intersections $(w_1, w_2, \ldots, w_6)$ of the various slowness surfaces with the normal line (NN') based on the common slowness along the interface and the associated $\bar{l}_3$'s (i.e. the polynomial roots) are real. However, in Fig. 3.5, if a bulk wave meets the interface at an incident angle exceeding its critical angle, a wave having the same elliptical particle motion like a Rayleigh wave can exist at the interface. In this case, the surface wave velocity is a function of the incident angle of the bulk wave and is never smaller than the Rayleigh wave velocity. The $\bar{l}_3$ root corresponding to the surface wave is therefore complex (its real part may be zero) which implies the wave suffers an exponential attenuation or amplification ruled by $\exp (i\omega l_3^+ x_3)$ and at the same time, a sinusoidal variation $\exp (i\omega l_3^* x_3)$ along the direction (l_1, l_2, l_3^*). The inverse of kl_3^+ is also regarded as the 'penetration depth' by analogy with the skin depth of the electromagnetic wave in a conductor. Thus it indicates the spreading of the energy associated with the surface wave. To summarise the effect of the above argument, Fig. 3.4(a & b) shows the various positions for which the normal line can intersect with the slowness surfaces and also the number of possible $\bar{l}_3$ roots which are expected for a purely elastic or a piezoelectricity stiffened medium. In a piezoelectric medium, there is an additional complex conjugate pair to the number

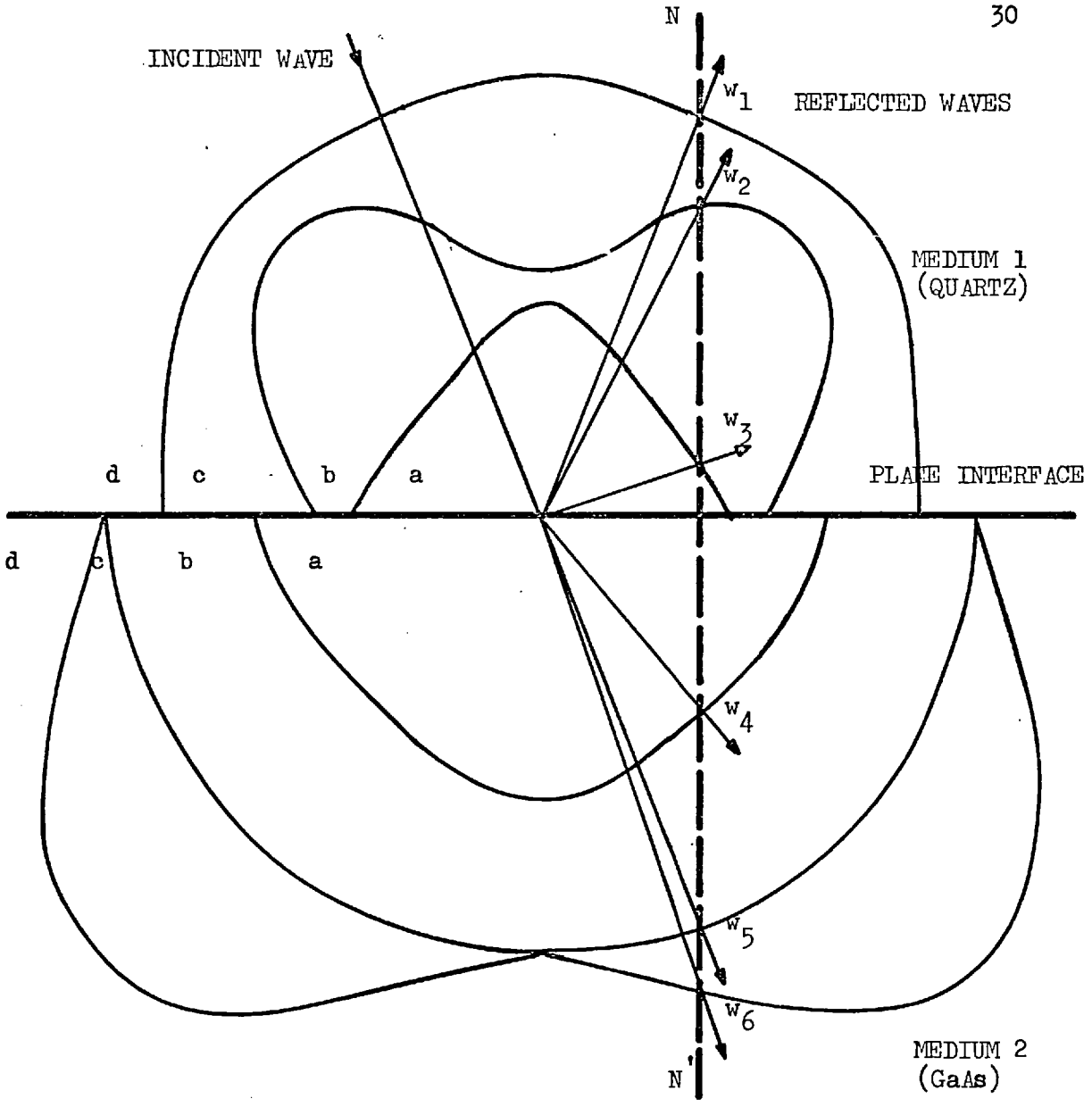

(a) SCATTERED WAVES AT PLANE INTERFACE

(b) TABLE FOR $\bar{l}_3$ ROOTS

POSITION OF NN' LINE AT	NUMBER OF $\bar{l}_3$ ROOTS FOR ONE MEDIUM	
	real	complex conjugate pair
a	6	0
b	4	1
c	2	2
d	0	3

NOTES: IF THE MEDIUM IS PIEZOELECTRIC THERE IS AN ADDITIONAL COMPLEX CONJUGATE PAIR, DUE TO THE ELECTROMAGNETIC WAVE, TO THE ABOVE NUMBER OF $\bar{l}_3$ ROOTS

Fig. 3.4 GRAPHICAL PRESENTATION OF SLOWNESS SURFACES FOR TWO ANISOTROPIC MEDIA SHARING A PLANE INTERFACE, INDICATING NUMBER OF SCATTERED WAVES AND POSSIBLE NUMBER OF $\bar{l}_3$ ROOTS

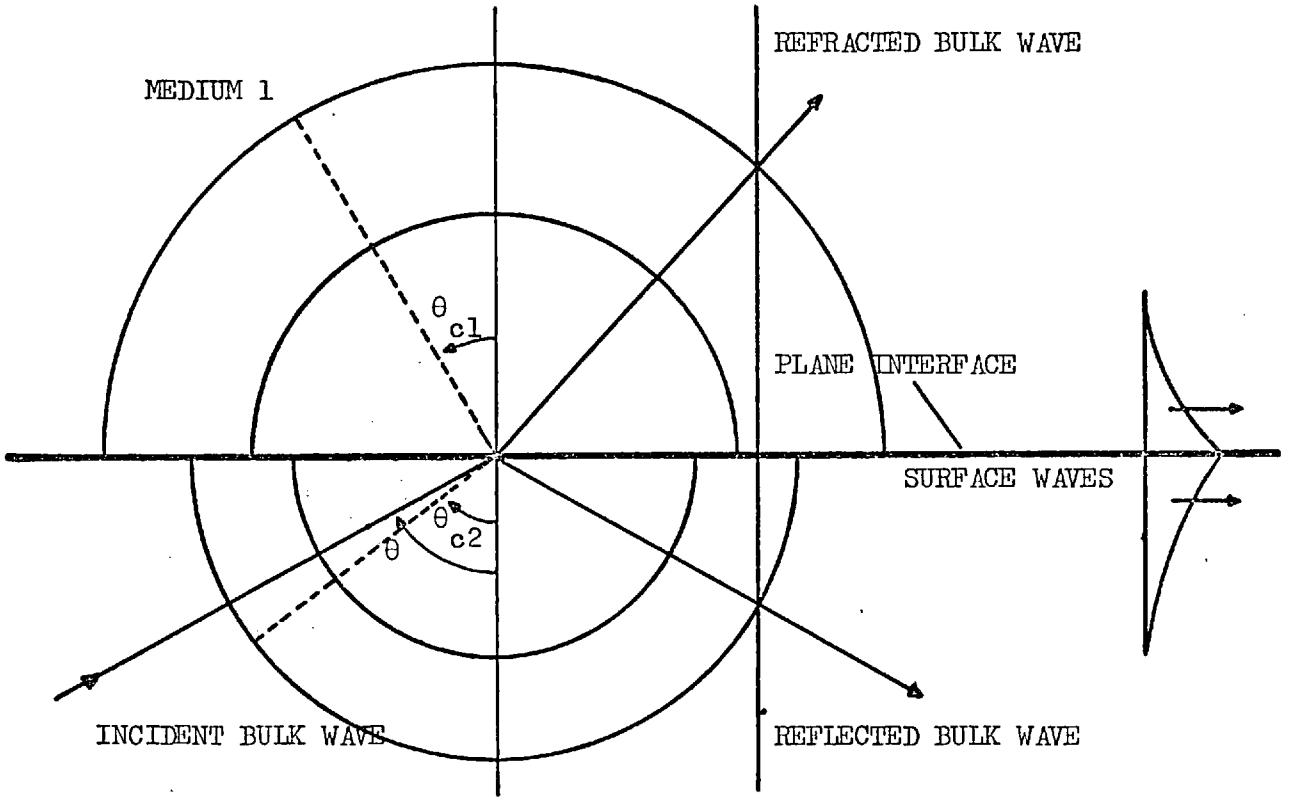

CONCENTRIC SPHERES REPRESENT SLOWNESS SURFACES OF
TWO ISOTROPIC MEDIA
θ = INCIDENT ANGLE
θ_{c1} = CRITICAL ANGLE OF MEDIUM 1
θ_{c2} = CRITICAL ANGLE OF MEDIUM 2

Fig. 3.5 GRAPHICAL PRESENTATION OF SURFACE WAVES EMERGING AT THE PLANE INTERFACE OF TWO ISOTROPIC MEDIA

required for the above cases since the electromagnetic wave velocity is always greater than that of any mechanical wave.

The characterisation of a surface wave may be obtained from a geometrical synthesis of its constituent 'partial' waves, depending upon the interaction amongst the 'partials' under the imposed boundary constraints. Applying this concept the infinite plane wave solutions for a surface wave are:-

$$U_j = C^n \alpha_j^n \quad \exp ik \left(l_i^n x_i - Vt \right) ; \quad i,j = 1,2,3 \tag{3.4}$$

$$\phi = C^n \alpha_4^n \quad \exp ik \left(l_i^n x_i - Vt \right) \tag{3.5}$$

where U_j and ϕ are the mechanical displacements and the electric potential respectively. C^n are the weighting factors for the partial waves and thus the index, n, is determined by the number of partial waves required in a specified system. In the case of a half space, n is equal to 3 for a purely elastic or a piezoelectrically stiffened medium, but it is 4 for a piezoelectric medium. For a layer, there are again two possible values except that in this situation, the number involved is twice that in a half space since there are both the growth and the decay partial waves travelling away from each interface of the layer. In a half space, only the waves with decaying amplitude are considered in the plane wave solutions. The individual contribution from each partial wave is subjected to the imposed boundary constraints and therefore weighted in the linear superposition of the mechanical field.

Since a solid medium can be theoretically considered as purely elastic, piezoelectrically stiffened or piezoelectric, it seems unnecessary to describe all possible combinations of the different

cases in the computation (see Appendix A 4) for the mechanical surface wave velocity in a layered media (see Fig. 3.6). . The author proposes therefore to consider one example, that of two solid piezoelectric media and in this case the required boundary conditions are:-

At the free space/layer interface, we have

a. Zero Mechanical Stresses

b. Continuity of Scalar Electric Potential

c. Continuity of Normal Electric Displacement

and at the layer/half space interface,

d. Continuity of Mechanical Displacements

e. Continuity of Mechanical Stresses

f. Continuity of Scalar Electric Potential

g. Continuity of Normal Electric Displacement.

With the above boundary conditions, the boundary determinant obtained is of the order of (13x13). The order of the determinant changes in accordance with the physical properties of the layered media. However, the boundary conditions for a piezoelectrically stiffened layered media are the same as that for a purely elastic case. Thus the boundary determinant is (9x9) since the scalar electric potential is either directly or indirectly excluded in both cases.

To complete the discussion on the boundary conditions for a piezoelectric layered media, it is also necessary to mention the effect of a conducting film at the vicinity of the free surface. The associated field of the mechanical surface wave will not only remain within the piezoelectric layer, but also extend into the free space

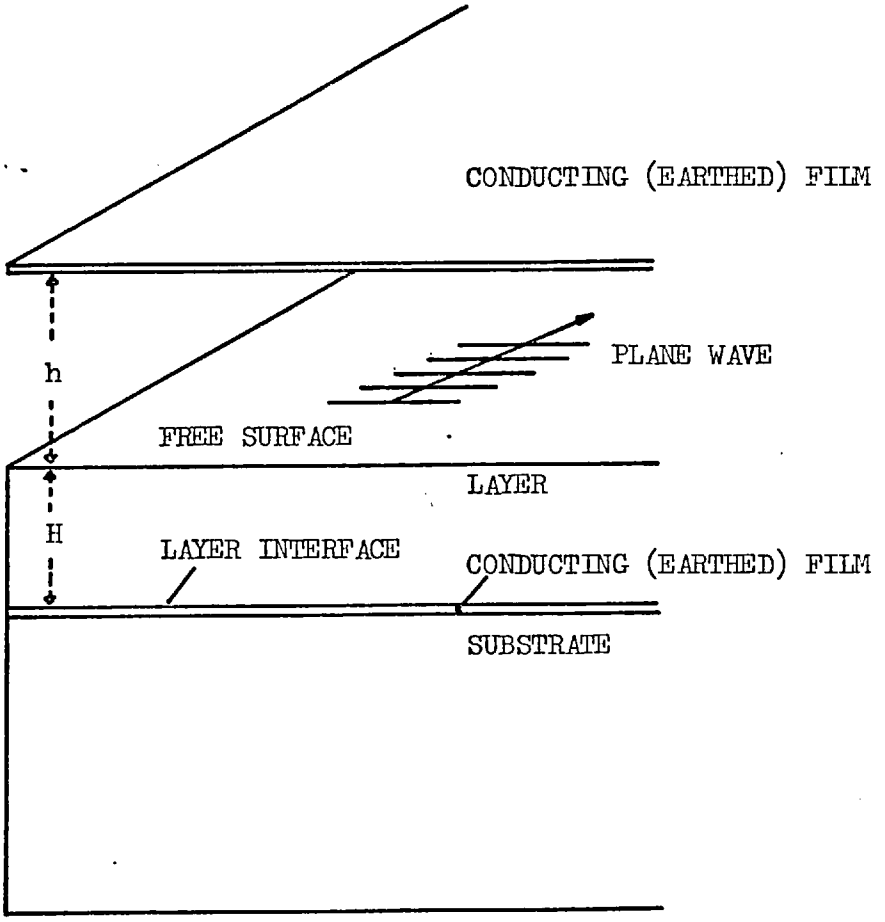

Fig. 3.6 A LAYERED SUBSTRATE WITH CONDUCTING (EARTHED) FILM ABOVE FREE SURFACE OR AT INTERFACE OF THE LAYER

region. If the conducting film is placed upon the free surface of the layer, the associated electric field will be terminated. The layer is thus regarded as piezoelectric under electrical boundary constraint as the electric field exists below the surface. Since the electric field is coupled to the mechanical field, it is expected that the surface wave velocity can be perturbed by the position, h, of the conducting film above the piezoelectric surface. Hence the electric potential of the surface wave in the free space region takes the form as (see Appendix A 5):

$$\phi = C_o \left(\sinh k(h - x_3) \;/\; \sinh kh \right) \exp ik(l_1 x_1 + l_2 x_2 - Vt) \qquad (3.6)$$

and the corresponding normal electrical displacement is given as:

$$D_3 = -i\varepsilon_o C_o \left(\cosh k(h - x_3) \;/\; \sinh kh \right) \exp ik(l_1 x_1 + l_2 x_2 - Vt) \qquad (3.7)$$

In the above expressions, C_o is the weighting factor of the associated electric field in the free space and for a case where x_3 is zero, it is equal to $C^n \alpha_4^n$. The equality implies that the value of C_o is quantitatively the sum of the electric fields associated by the partial waves at the free surface.

3.4 A Method for Calculating the Surface Wave Velocity

The approach described is not strictly analytical since no explicit form of solution is possible in deriving a feasible mechanical surface wave velocity. It is not proposed to give details of the actual calculations of surface wave velocity, but a compact computer programme has been developed (see Appendix A 6) and a concise outline of the computation is given as follows:

The equations required for the mechanical surface waves are essentially the same as those used, Eqs. 2.2, 2.3, 2.10/13, for the basic bulk waves. Apart from the infinite plane wave solutions, Eqs. 3.4 and 3.5, and the

specified boundary conditions (a,b, ...and g), there is a fresh scaling of the amplitude of both mechanical displacements and electrical potential. Subsequently, the modified Christoffel stiffnesses are used in the characteristic matrix of the velocity surfaces as previously indicated for a piezoelectric medium. If H is the layer thickness and λ is the wavelength in the layered media then for a given ratio of H/λ, there are two unknown quantities, $\bar{l}_3$ and V, in the characteristic matrix, because $\bar{l}_3$ is the additional quantity to the wave velocity,V, as in the case of the bulk waves. In the present case, the wave propagation vector is assumed to lie on the plane of either the free layer surface or the layer/half space interface. Both the direction cosines, l_1 and l_2, are initially defined at the plane interface and thus have real values. l_3 which is along the direction of the depth into the layered media, becomes the complex quantity, $\bar{l}_3$, as previously explained.

By assigning an arbitrary value to the surface wave velocity V the characteristic matrix can be expanded into a polynomial of $\bar{l}_3$. Normally, the assumed velocity, as shown in Fig. 3.7, is in the range confined by V_{s1} and 0.8 V_{s2}, where V_{s1} and V_{s2} are respectively the velocity of the fast and the slow shear waves. If both values are equal, the velocity range will be between V_{s2} and 0.8 V_{s2}. The order m of the polynomial is 2n where n is the number of partial waves involved in a particular medium. It is therefore expected that the order of the polynomial is 6 and 8 respectively for non-piezoelectric and piezoelectric media. Moreover, the odd power terms of the polynomial are found in the calculation of many crystals with propagation vector along the symmetry axis to be zero (or in other directions are

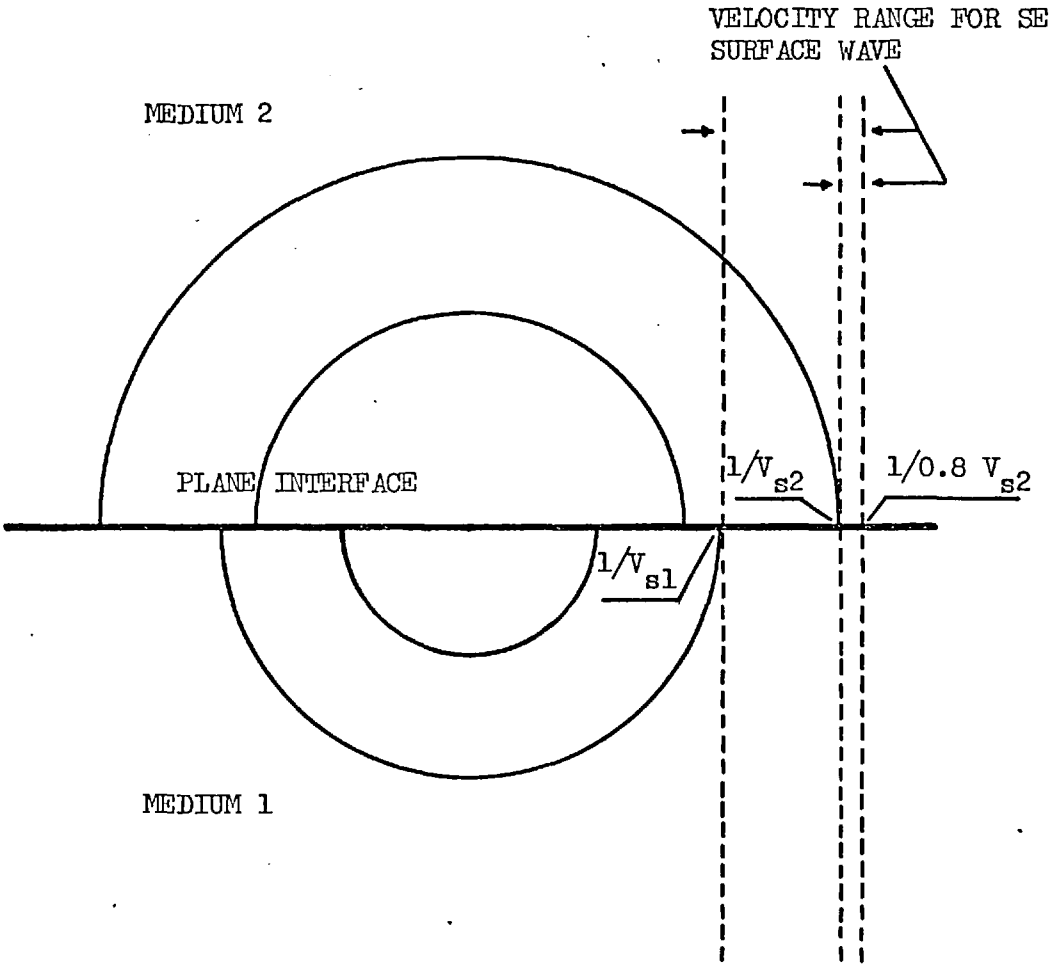

CONCENTRIC SPHERES REPRESENT SLOWNESS SURFACES OF TWO ISOTROPIC MEDIA

Fig. 3.7 POSSIBLE EXISTENCE RANGE OF SURFACE WAVE

small) so the following form is assumed:

$$Z_o \bar{I}_3^m + Z_2 \bar{I}_3^{m-2} + Z_4 \bar{I}_3^{m-4} + \ldots + Z_m = 0 \; ; \quad m = 2n \tag{3.8}$$

where Z's are the real coefficients of the polynomial. This implies that the above polynomial can be expressed into a bi-cubic or bi-quartic equation depending respectively on whether the medium is non-piezoelectric or piezoelectric. Thus the $\bar{I}_3$ roots will always occur in conjugate pairs. Subsequently, $\bar{I}_3$ roots are selected to accord with the axis of reference in the layered media such that the energy flux of the surface wave will be parallel to the boundaries. Since a set of $\bar{I}_3$ roots are obtained for one value of V, both quantities are substituted into the characteristic matrix to find a set of scaled amplitudes, $'\alpha_j^n$ and $'\alpha_4^n$ which are related to the unscaled amplitudes α_j^n and α_4^n in the form $'\alpha_j^n = \alpha_j^n/\alpha_o$ and $'\alpha_4^n = \alpha_4^n/1$. Hence the only unknown quantites are the weighted factors C^n of a given medium. The above procedure is repeated for both media. With the linear piezoelectric constitutive relations and the infinite plane wave solutions, a matrix of the boundary conditions can be established. The modulus of the boundary determinant can thus be calculated for a given surface wave velocity. The 'correct' surface wave velocity will set the determinant of the boundary conditions to a minimum value. In consequence, the weighting factors for both media, and additionally C_o for the free space region, can be readily evaluated. Therefore, the computation of the mechanical surface wave velocity is complete for a given value of H/λ. If the characteristic features of the surface wave velocity are needed for the entire thickness of the layer, the prescribed calculation has to be repeated for different ratio values of the H/λ (abbreviated as Λ).

3.5 Energy Flow and Group Velocity of the Surface Wave

A mechanical wave propagated through a piezoelectric medium has energy stored both in mechanical displacement and in the associated electric field but the former is by far the most important (see Appendix A 7). The governing parameters in determining both the energy flux and the energy density are the physical constants C_{ijkl}, e_{kij} and ε_{ik}. However, both the mechanical displacements and the associated electric potential are regarded as complex. It should be pointed out that it is not the energy flow at any instant in the harmonic field which is of interest, but the average flow of energy that takes place. A convenient average flow is obtained by evaluating the total energy change during a complete cycle and dividing by the period of the cycle. Such a manipulation enables the energy flux, P_i, to take such a form as:

$$P_i = 0.5 \text{ Real } (- T_{ij} \dot{U}_j^{*}) \tag{3.9}$$

where the asterisk indicates the complex conjugate of U_j, and similarly, the energy density, E_i, is given as:

$$E_i = 0.5 \text{ Real } (T_{ij} S_{ij}^{*}) \tag{3.10}$$

where S_{ij}^{*} is the complex conjugate of S_{ij}.

Since the present theory is limited to the ideal surface wave, it is logical to assume the net energy flow is zero across any plane interface. With the same axis of reference in the layered media, it implies that the energy flux component, P_3, can be assumed zero and thus the other energy flux components, P_1 and P_2, are both integrated with respect to x_3. Using Eq. 3.9 and integrating over the range from R_1 to R_2 $(R_1 > R_2)$, the energy flux at the plane interface is given by:

$$Pl_i = (V k^2 C^n C^{n*} \alpha_j^{n*} f g) / ik (\bar{l}_3^n - \bar{l}_3^{n*}); \quad i = 1,2,3 \qquad (3.11)$$

where $f = 0.5 \; C_{ijkl} ({}'\alpha_k^n l_j^n + {}'\alpha_l^n l_k^n) + e_{kij} \; {}'\alpha_4^n \; l_k^n$

and $g = \exp ik (\bar{l}_3^n - \bar{l}_3^{n*}) R_2 - \exp ik (\bar{l}_3^n - \bar{l}_3^{n*}) R_1$

Similarly, the energy density is obtained from Eq. 3.10 by integration with respect to x_3 and is given by:

$$El_i = (k^2 C^n C^{n*} \; 0.5 \; ({}'\alpha_i^{n*} l_j^{n*} + {}'\alpha_j^{n*} \; l_i^{n*}) fg) / ik (\bar{l}_3^n - l_3^n)$$

The direction of the energy flow away from the wave propagation vector which is defined by $(l_1, l_2, 0)$ is given by $\cos^{-1} (L_1 l_1 + L_2 l_2)$ where L_i is the normalized form of Pl_i. So far, the description of equations is applicable to any medium. For the layered media, the energy flux is regarded as the sum of the components from both the layer and the half space; the same procedure is applied to the energy density of the layered media.

The group velocity for a surface wave is described as the ratio of the real part of the complex energy flux, integrated over the full thickness of the layer and partial depth of the half space, to the corresponding integral of the energy density. For an infinite plane wave in a homogeneous, dispersive, anisotropic medium which is but lossless and linear, the group velocity is equal to the velocity of energy transported by the plane wave. Hence the group velocity for the surface wave is given by:

$$V_g = \frac{Pl_i' + Pl_i''}{El_i' + El_i''} \qquad ; \quad i = 1,2,3$$

where Pl_i' and Pl_i'' are the components of the energy flux respectively

for the half space and the layer. Similarly, El_i' and El_i'' are the corresponding components of the energy density. This method is more suitable for the present numerical computation than the gradient method since the latter requires three successive calculations of the phase velocity for three neighbouring values of Λ in order to deduce the group velocity.

CHAPTER 4

THEORETICAL STUDIES OF A LAYERED MEDIA

4.1 Effect of Piezoelectricity on Wave Velocity and Group Delay Time

From the earlier discussion (Sec. 2.3) it was pointed out how the material became modified as a result of the existence of piezoelectricity and the calculated change was consistent with observations of the wave velocity of propagation in such media (C.C. Tseng, 1967 ; F.W. Voltmer, 1968). In strong piezoelectric media the influence of piezoelectricity can lead to the velocity being increased by 10% or more from that for the purely elastic material. Fig. 4.1 provides a comparison of the different phase velocities when the materials, ZnO and $LiNbO_3$, are both regarded as purely elastic, as simply piezoelectric and as piezoelectrically stiffened layered media. It is apparent from the phase velocity curves that it is inaccurate to perform any calculation of the wave velocity in a piezoelectric material when it is simply considered as purely elastic. As regards applying piezoelectrically stiffened constants in calculation, there is generally a difference in phase velocity and moreover, no other information on piezoelectric interaction with an external electric field would be available for studies.

The other immediate effect is the influence of a conducting film on the associated electric field at the plane boundary of the piezoelectric material. The change in magnitude is significant for material with strong piezoelectric coupling. It follows that the wave velocity can be externally modified by perturbing the associated electric field. Fig. 4.2 illustrates the variation of the group delay time (i.e. inverse of group velocity) with the Λ ratio in the two cases (I) and

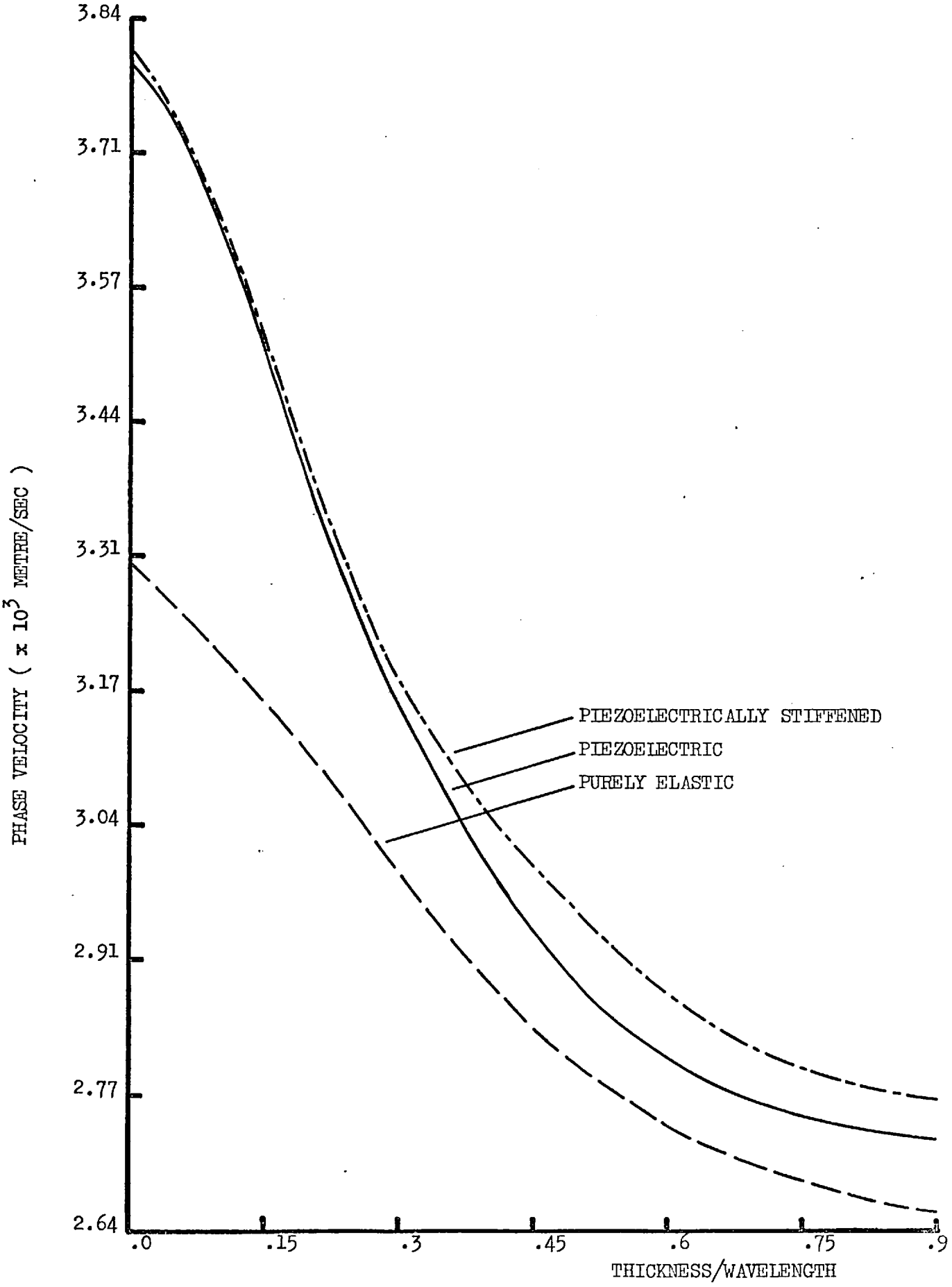

Fig. 4.1 PHASE VELOCITIES IN $ZnO/LiNbO_3$ OBTAINED BY REGARDING THE MEDIA AS PIEZOELECTRICALLY STIFFENED, PIEZOELECTRIC AND PURELY ELASTIC

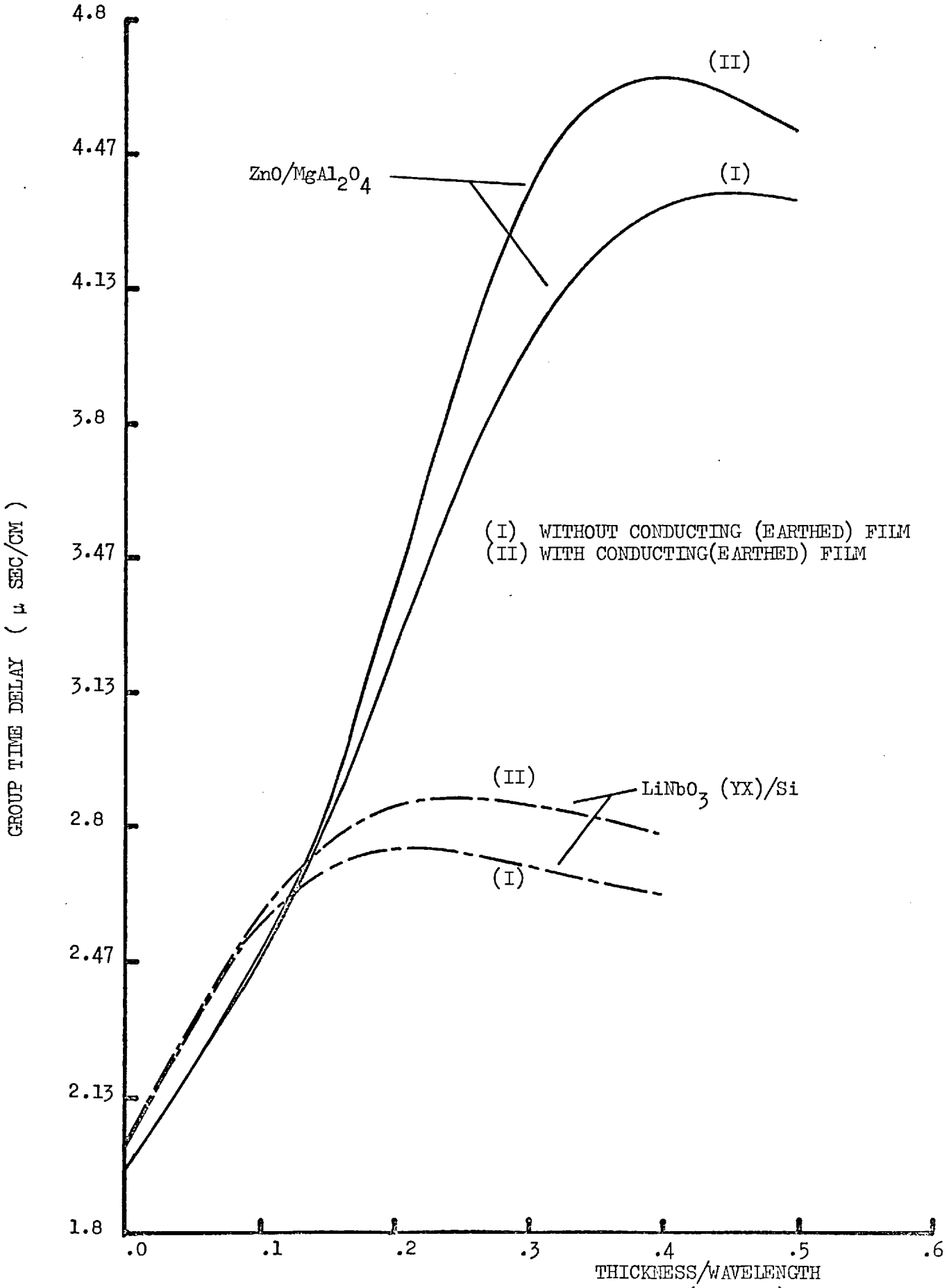

Fig. 4.2 GROUP DELAY TIME AFFECTED BY CONDUCTING (EARTHED) FILM AT FREE SURFACE AND 'TERMINAL' DELAY TIMES IN $ZnO/MgAl_2O_4$ AND $LiNbO_3$ (YX)/Si

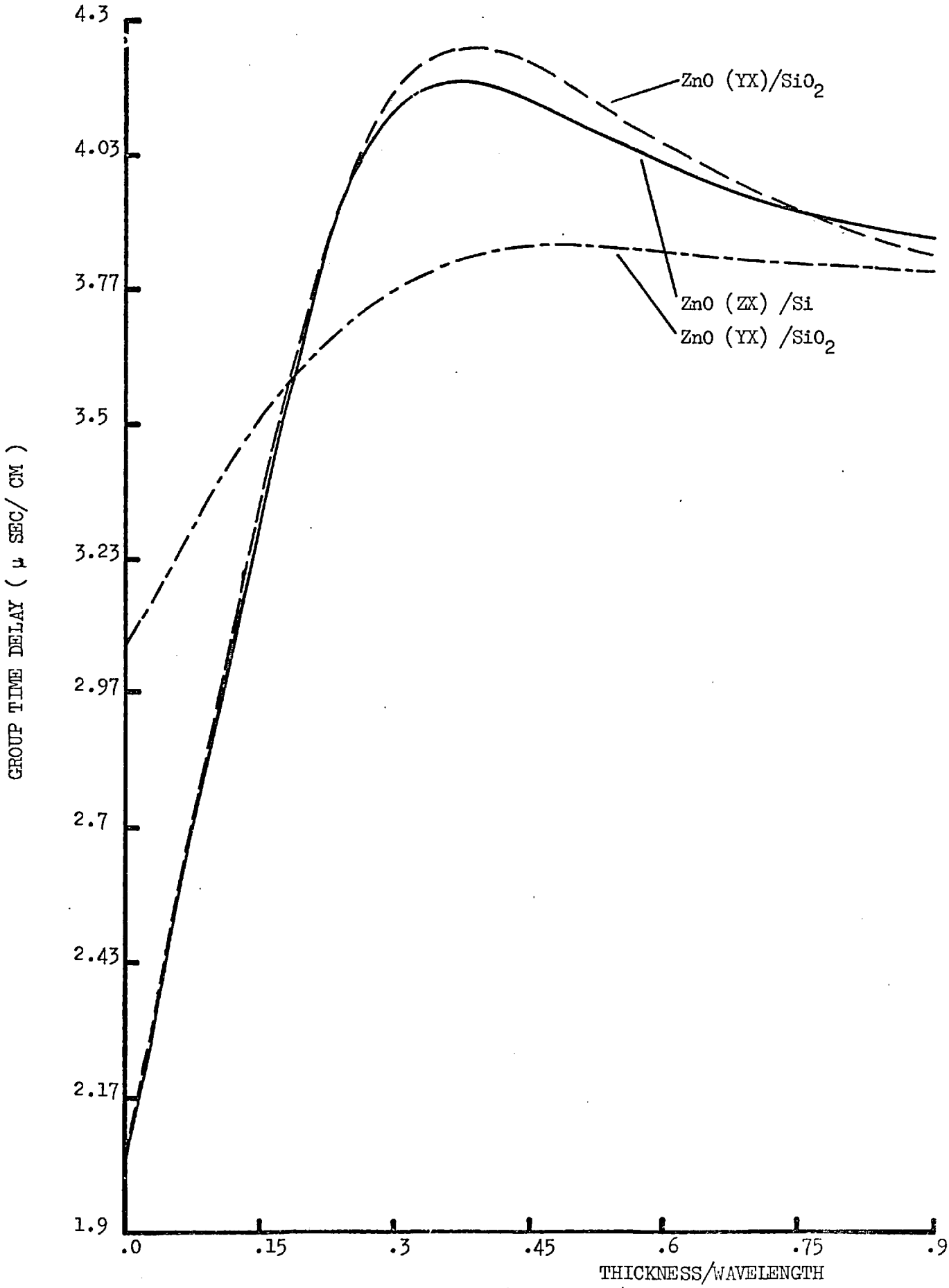

Fig. 4.3 GROUP TIME DELAY VERSUS (THICKNESS/WAVELENGTH) FOR VARIOUS COMBINATIONS OF ZnO LAYER WITH Si AND SiO_2 SUBSTRATES

(II) for both combinations, i.e. $ZnO/MgAl_2O_4$ and $LiNbO_3/Si$. With the conducting film deposited on the free surface of the ZnO layer, the time-bandwidth product with a good linearity is 52% larger than that is the case without the conducting film. For a $LiNbO_3$ layer, there is no effective change in the time-bandwidth product, because the difference in the delay times of the two materials, $LiNbO_3$ and Si, is relatively small in magnitude. The linear portion between the 'terminal' delay times is shorter in $LiNbO_3/Si$ than in $ZnO/MgAl_2O_4$. It is therefore advantageous to select a combination of materials with large delay times and high piezoelectric coupling along a specified direction for wave propagation. It should be added that the linearity of the group delay time curve is in general not good owing to the variation of piezoelectricity with the Λ ratio. It inversely implies that it is possible to correct and design a particular form of variation of group delay time by placing metallic electrodes on the propagating wave path to influence the associated electric field. By so doing, the wave velocity could be modified at various sections of the layered media with piezoelectric layer.

4.2 Dispersion Characteristics of ZnO/Si and $LiNbO_3/Si$

If a direct comparison is made between Figs. 4.2 and 4.3, it is quite apparent that the linearity of the group delay time curve is better for ZnO/Si than it is for $ZnO/MgAl_2O_4$. By approximate estimation, the time-bandwidth product is 160% larger for ZnO/Si with respect to the latter combination. In fact, the former combination was used in the experiment of the present project. The silicon surface was thermally oxidized to form an extremely thin insulating layer for the interdigital electrodes to be placed upon it. A similar arrange-

ment was also applied independently by F S Hickernell et al, 1972. It is interesting to point out that if the silicon oxide layer is made too thick, the dispersion characteristic curve is essentially the same as that for ZnO/SiO_2. As the result, the range of group delay time is largely reduced. It is equally undesirable to have the silicon oxide layer compatible to the operating wavelength of the wave in the layered media. If the thickness of SiO_2 is approximately that of the ZnO, wave energy would be channelled independently into the two layered media. For this case, a signal would arrive separately and their separation in time would subsequently merge together as it were when wave energy tends to propagate with a similar velocity at certain Λ values of the layers. Another example of the matter is unfortunately found in the experimental result by Hickernell, 1970 and 1972. The aforesaid effect is illustrated by Figs. 4.4 and 4.5. It may be important to point out that the experimental phase velocity was computed by Hickernell from the relation, frequency times wavelength, where the frequency was the observed quantity based on the transmission characteristics and the wavelength was set by the geometry of the interdigital transducer.

Fig. 4.6 gives a comparison of theoretical results obtained by R M White, 1972, and the author, for the dispersive curves and the points of the phase and the group velocities of ZnO/Si layered media. In spite of the different methods used, there is a close numerical agreement. However, there is a discrepancy in the results obtained in the case of $LiNbO_3/Si$ studied by White and the author. Firstly, the two extreme electrical conditions upon the $LiNbO_3$ layer were

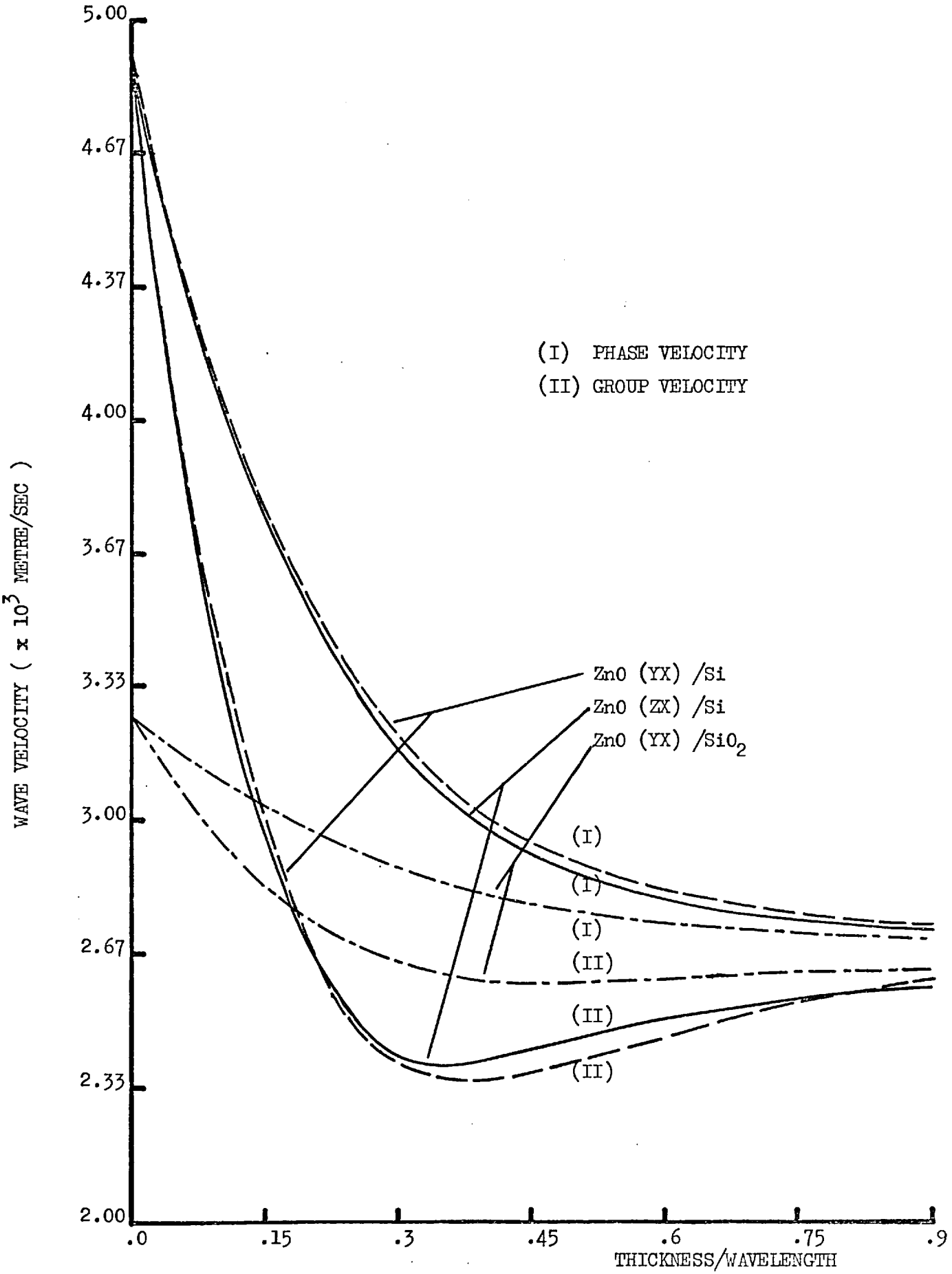

Fig. 4.4 WAVE VELOCITIES VERSUS (THICKNESS/WAVELENGTH) FOR VARIOUS COMBINATIONS OF ZnO LAYER WITH Si and SiO_2 SUBSTRATES

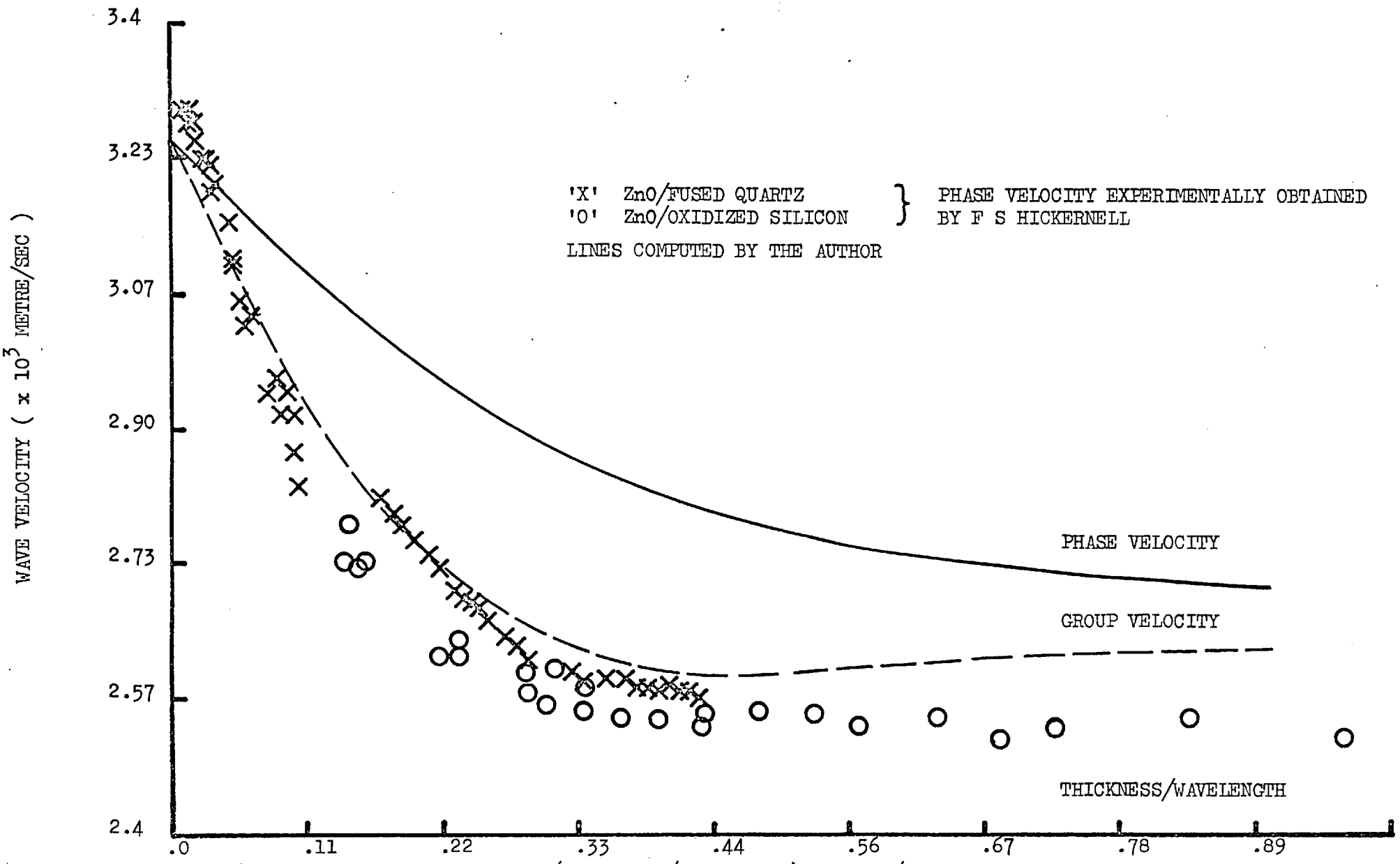

Fig. 4.5 WAVE VELOCITIES VERSUS (THICKNESS/WAVELENGTH) FOR ZnO/SiO_2 SEPARATELY OBTAINED BY F S HICKERNELL AND THE AUTHOR

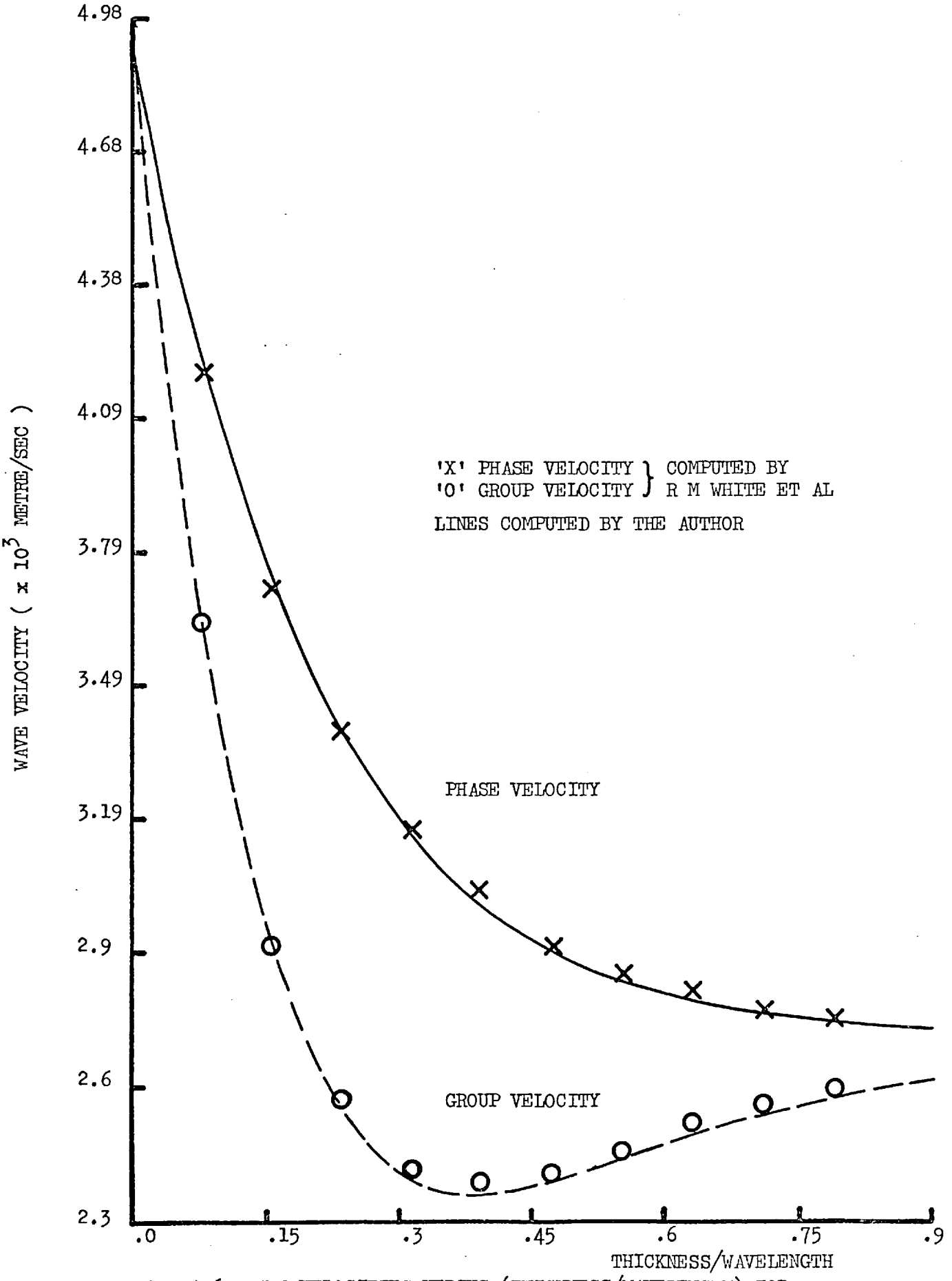

Fig. 4.6 WAVE VELOCITIES VERSUS (THICKNESS/WAVELENGTH) FOR ZnO/Si SEPARATELY OBTAINED BY R M WHITE AND THE AUTHOR

presented by the author such that the free surface of the layer was affected by a conducting film and in the second condition, the film was removed. This implies that whatever is the conductivity of the silicon substrate, the dispersion characteristic of the wave velocity should fall within the two extreme boundaries. As far as the curves and points in Figs. 4.7 and 4.8 are concerned, the agreement is not at all unexpected. Secondly, there is a conjecture on the issue as to whether there should be a 'bump' on the group velocity curve towards the larger Λ ratio. The 'bump' is not shown on the group velocity points calculated by White. It would therefore appear that if the third experimental point from the velocity axis is to be rejected absolutely on the grounds of the usually probable experimental error, the group velocity points would be in excellent agreement with his experimental points. However, the above assumption is in serious conflict with the fact that the wave velocity of $LiNbO_3$ is 3769.0 m s^{-1} which is found independently by Campbell & Jones, 1968, and the author, to be the correct value. If the aforesaid is true, the fourth experimental point should be re-examined rather than its precedent point. In a recent communication from White the aforementioned discrepancy has been explained fairly satisfactorily.

4.3 Coupling Efficiencies of CdS/Si and $LiNbO_3$/Si

If the Figs. 4.9, 4.10 and 4.12 are examined, it is obvious that in the CdS/Si combination, the coupling efficiency (i.e. $\Delta V/V$, where V is the actual velocity; see Eq. 2.8) becomes zero at some values of the Λ ratio. This tendency is not observed for the $LiNbO_3$/Si combination. The 'zero points' on the axis of the Λ ratio indicate

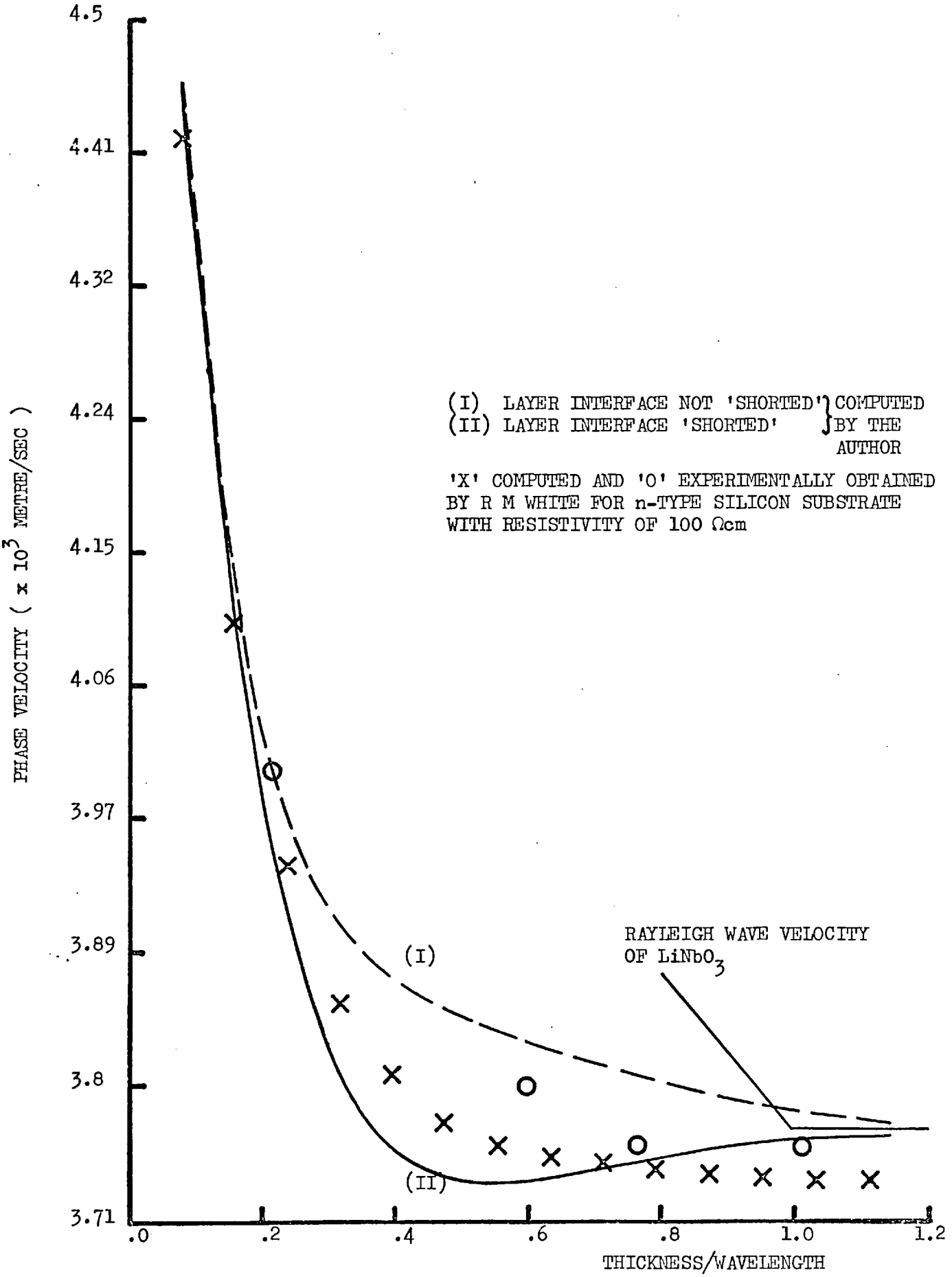

Fig. 4.7 PHASE VELOCITY VERSUS (THICKNESS/WAVELENGTH) FOR $LiNbO_3$/Si SEPARATELY OBTAINED BY R M WHITE ET AL AND THE AUTHOR

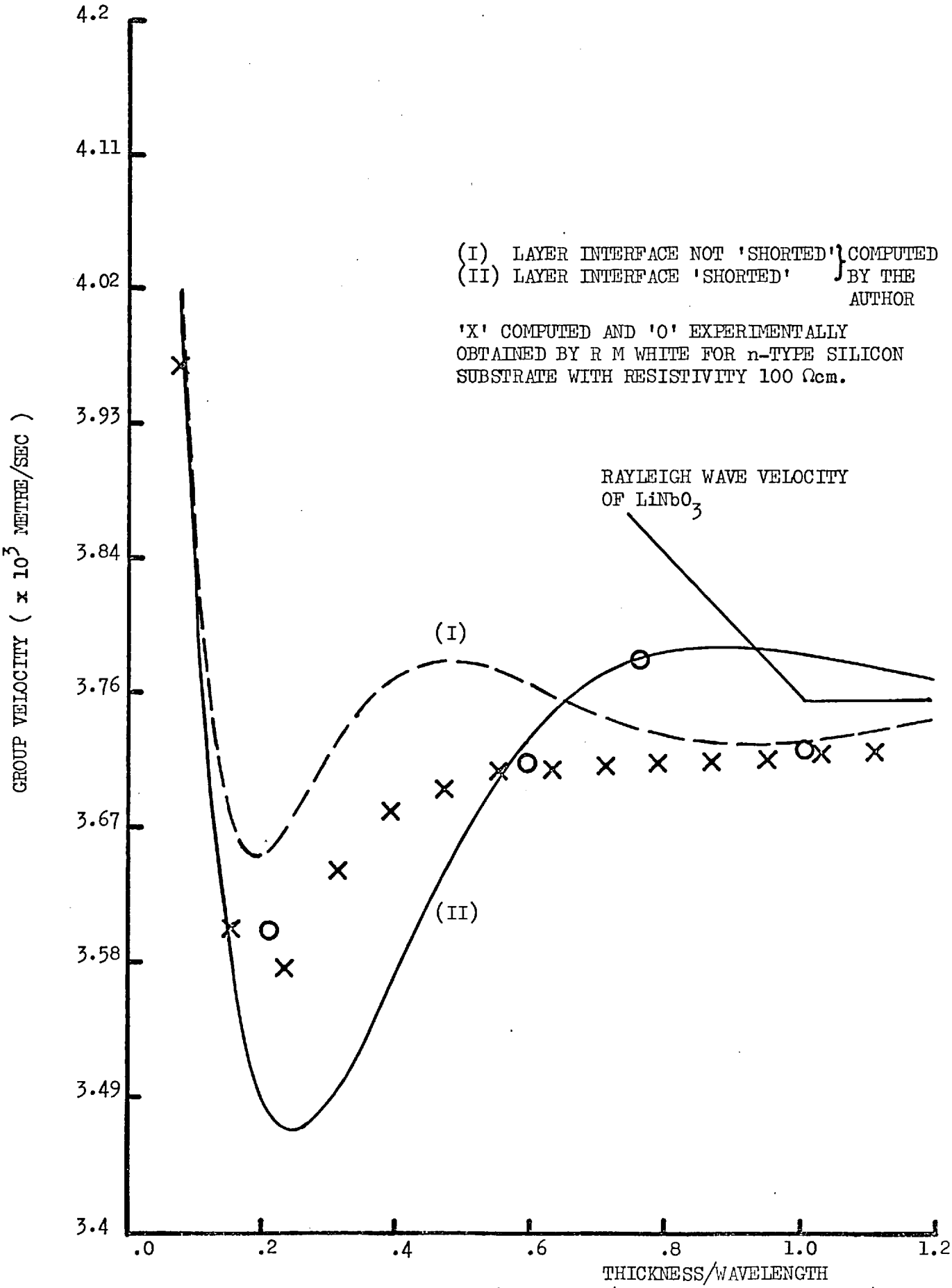

Fig. 4.8 GROUP VELOCITY VERSUS (THICKNESS/WAVELENGTH) FOR $LiNbO_3$/Si SEPARATELY OBTAINED BY R M WHITE AND THE AUTHOR

that excitation of surface wave at those values of (thickness/wavelength) is impossible. For the latter combination, the efficiency of exciting surface wave is fairly good when the layer thickness is above 0.1 of the wavelength. Basically, the coupling efficiency of a layered media is deduced from the two interdigital electrode formats. The first of the two formats is to lay the interdigital electrodes at the plane interface of the layered media and the second, the electrodes are placed directly on top of the layer. Having had the interdigital electrodes on the two surfaces, a conducting film is brought on the opposite surface to induce a change via piezoelectricity to the coupling efficiency. In both CdS/Si and $LiNbO_3$/Si the coupling efficiency is relatively high in the range of the Λ ratio between 0.15 and 0.9 irrespective to the presence of the conducting film. However, it is interesting to notice that on average, the efficiency reaches a maximum at the range of the Λ ratio between 0.3 and 0.5. As the ratio increases from 0.5, the efficiency gradually decreases and finally reaches a 'terminal' value. It may be reasonable to assume the declination continues as the wave energy at high frequency would tend to propagate on the free surface of the layered media. It would then be reasonable to accept the 'terminal' value is determined by the piezoelectric properties of the layer. Apart from the effect of the conducting film, the coupling efficiency is within the values of 10^{-4} and 10^{-2}. In general, the efficiency is one order in magnitude higher for the interface format than the free surface format. When the conducting film is introduced, one of the two distinct features is that the secondary peaks of the coupling efficiency are induced and/or enhanced. The second feature is that the peaks tend to shift

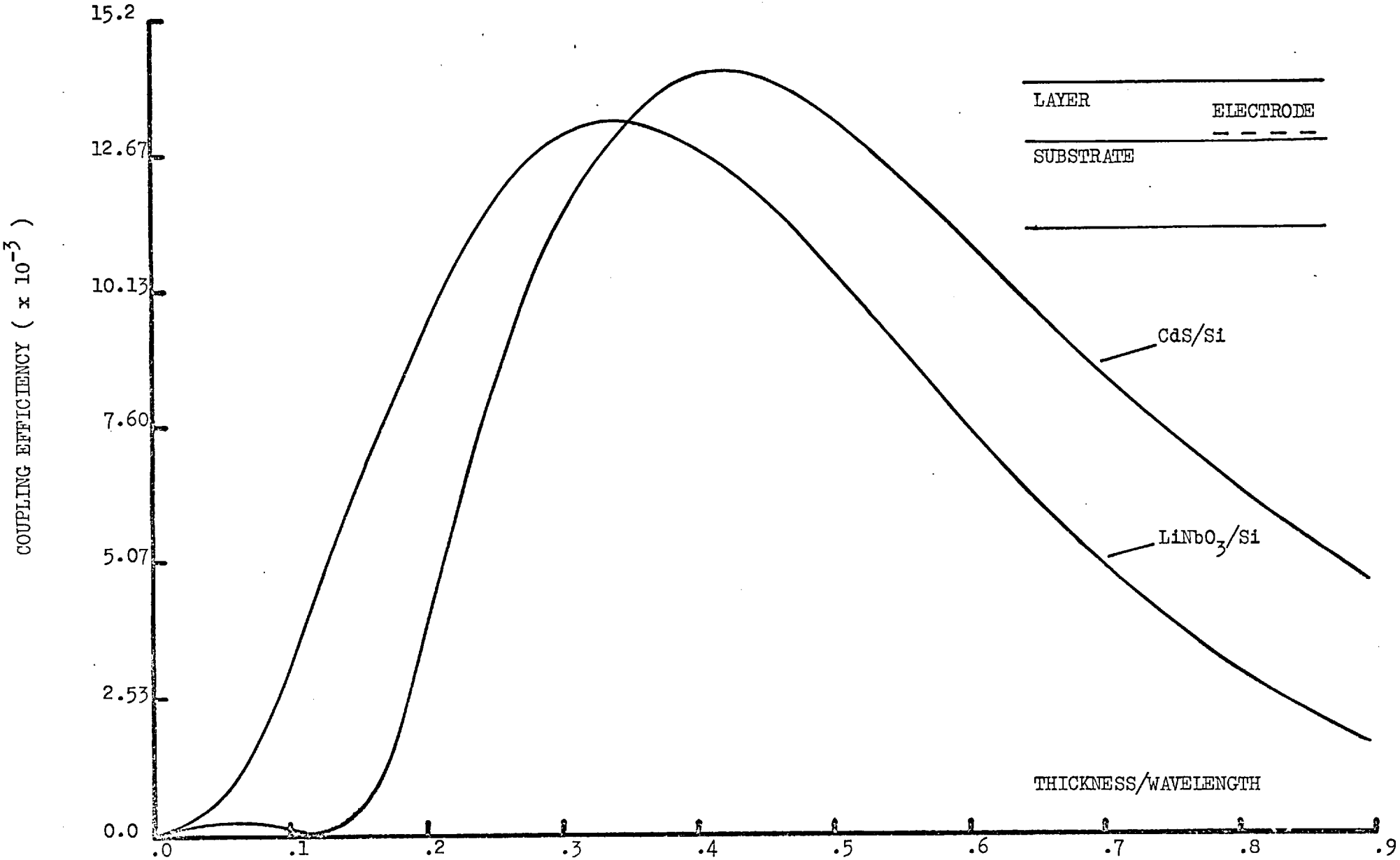

Fig. 4.9 COUPLING EFFICIENCY FOR VARIOUS (THICKNESS/WAVELENGTH) AS WAVE PROPAGATING AT INTERFACE WITH 'UNSHORTED' FREE SURFACE IN CdS/Si AND $LiNbO_3$/Si

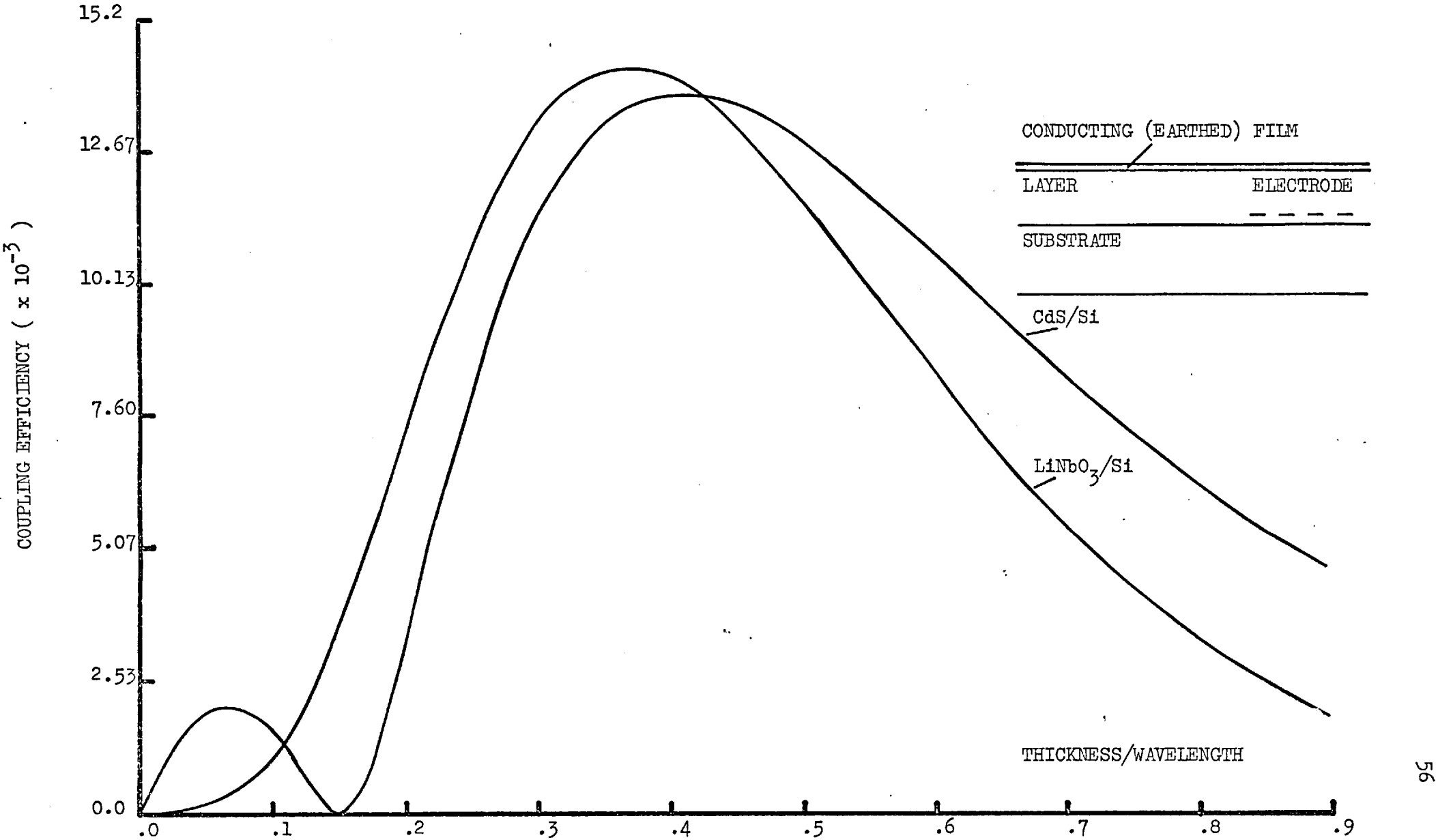

Fig. 4.10 COUPLING EFFICIENCY FOR VARIOUS (THICKNESS/WAVELENGTH) AS WAVE PROPAGATING AT INTERFACE WITH 'SHORTED' FREE SURFACE IN CdS/Si AND $LiNbO_3$/Si

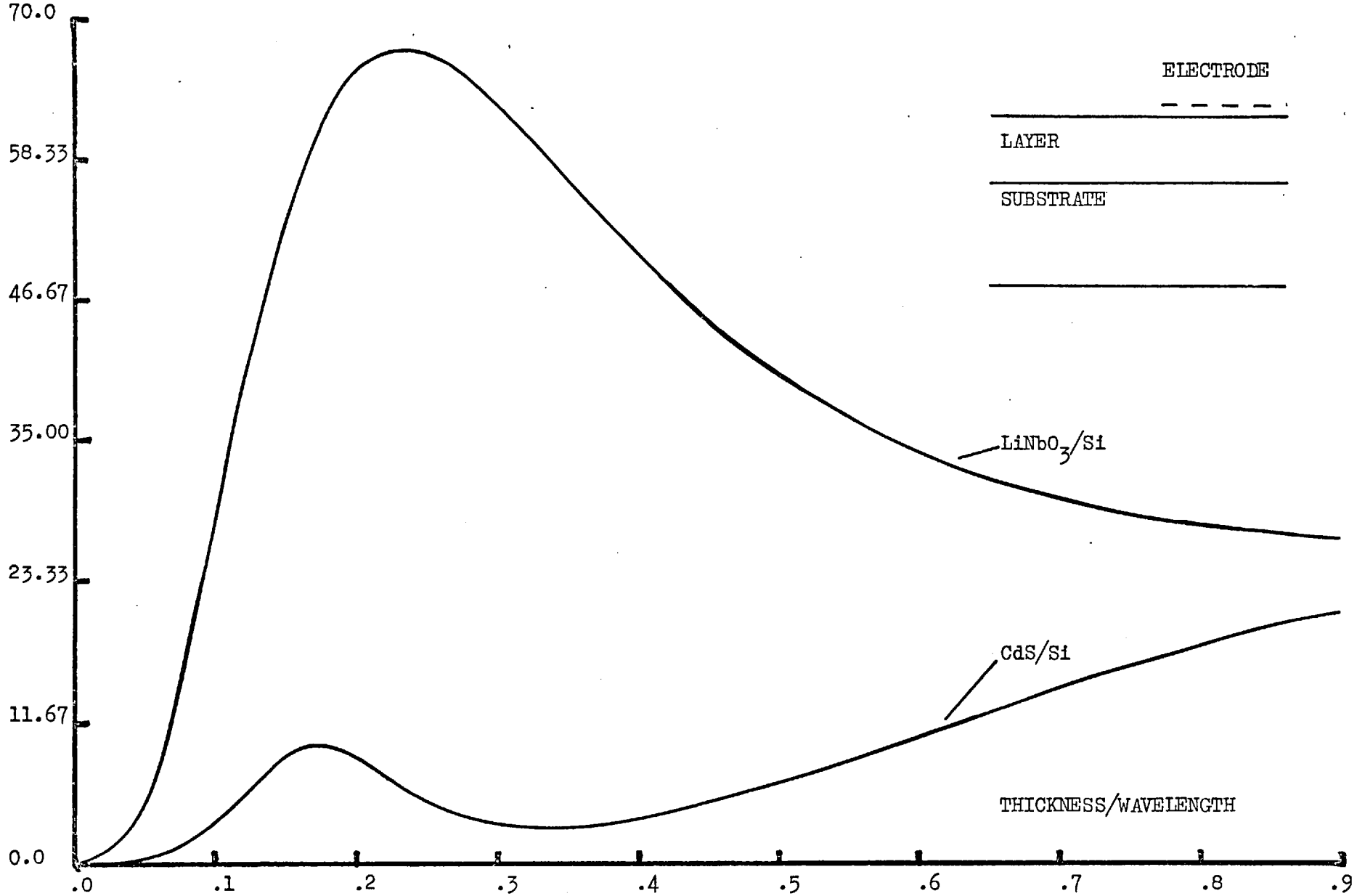

Fig. 4.11 COUPLING EFFICIENCY FOR VARIOUS (THICKNESS/WAVELENGTH) AS WAVE PROPAGATING AT FREE SURFACE WITH 'UNSHORTED' INTERFACE IN CdS/Si AND $LiNbO_3$/Si

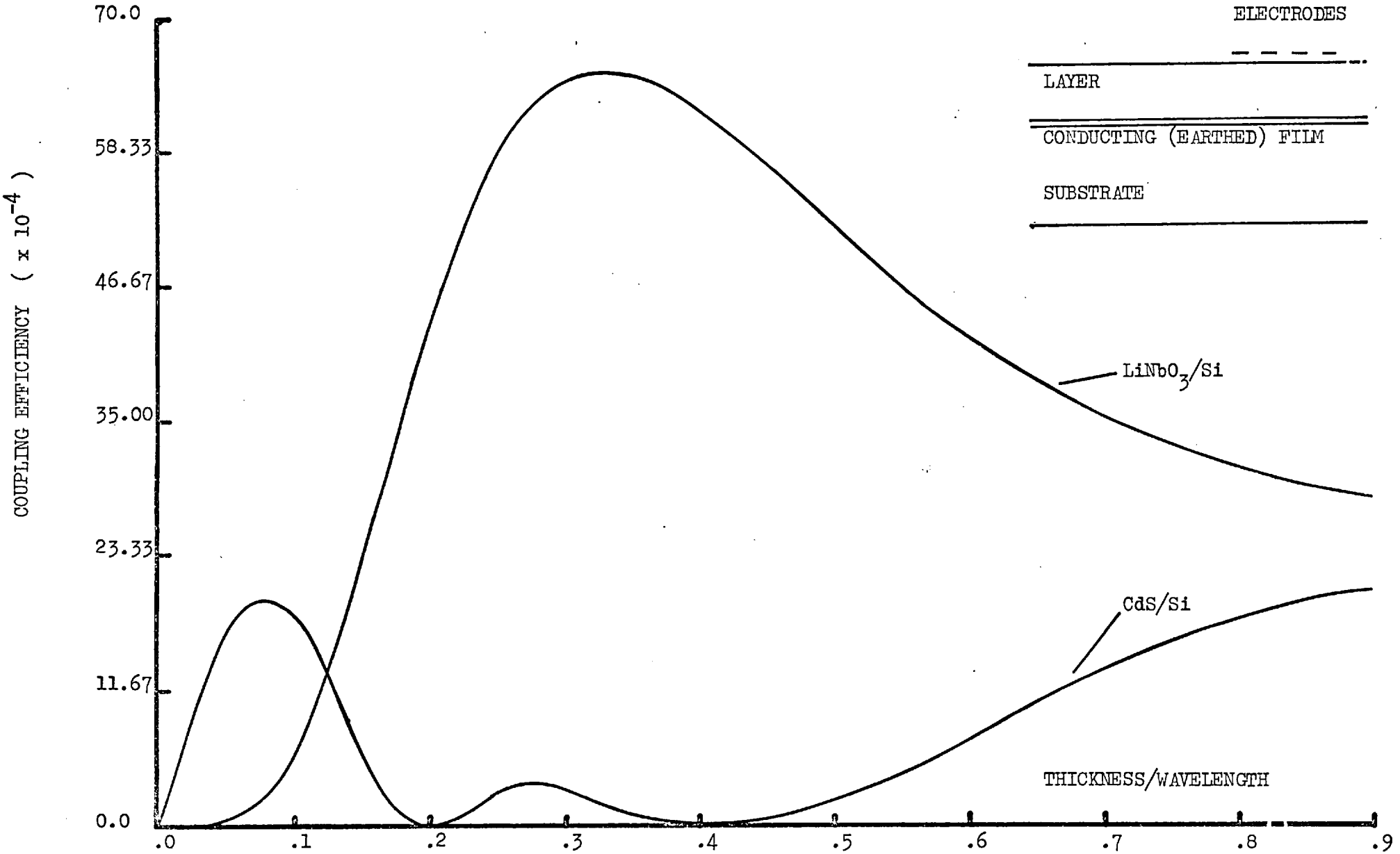

Fig. 4.12 COUPLING EFFICIENCY FOR VARIOUS (THICKNESS/WAVELENGTH) AS WAVE PROPAGATING AT FREE SURFACE WITH 'SHORTED' INTERFACE IN CdS/Si AND $LiNbO_3$/Si

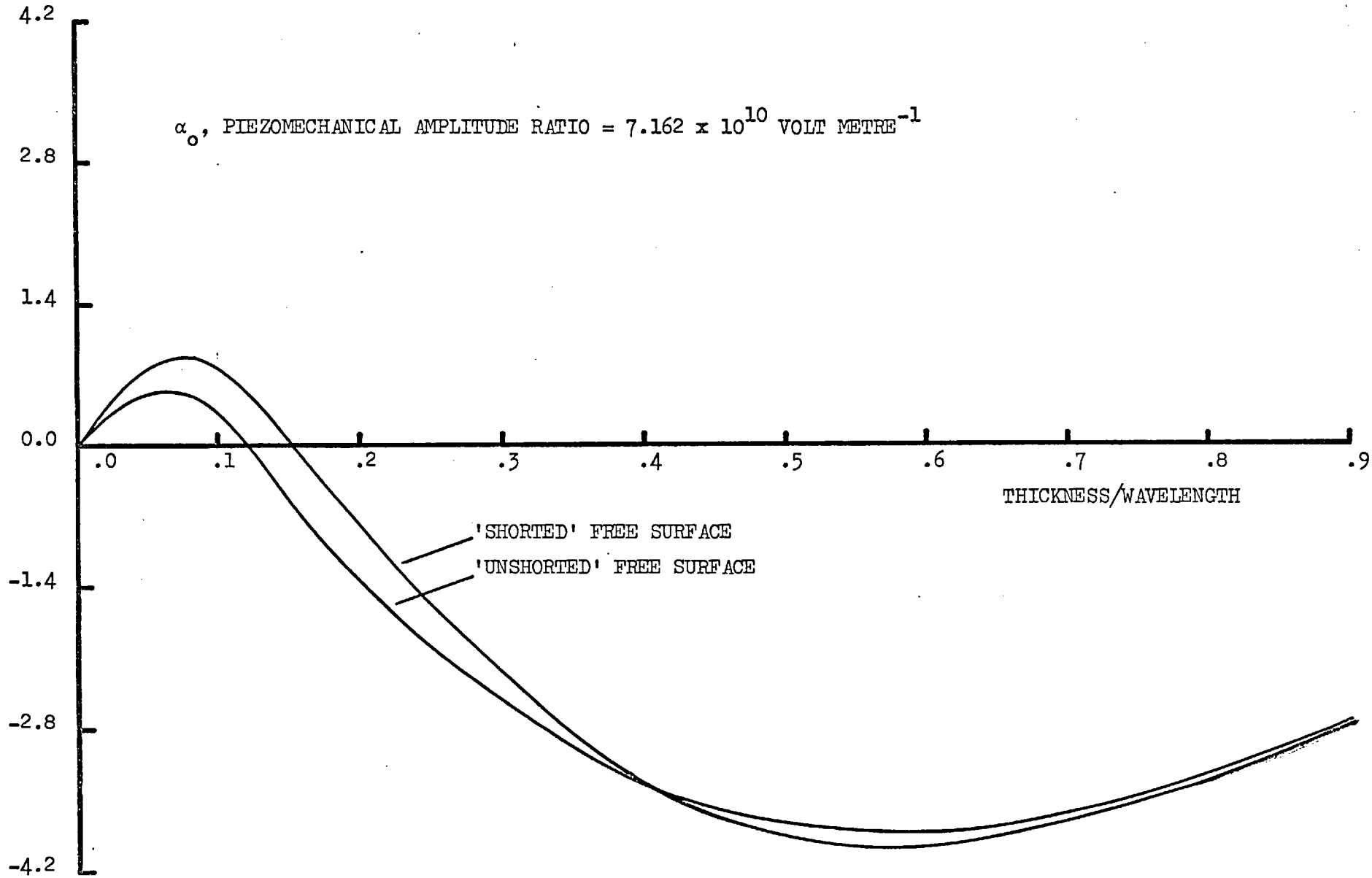

Fig. 4.13 ASSOCIATED ELECTRIC POTENTIAL AS A FUNCTION OF (THICKNESS/WAVELENGTH) WHEN WAVE PROPAGATING AT INTERFACE OF CdS/Si

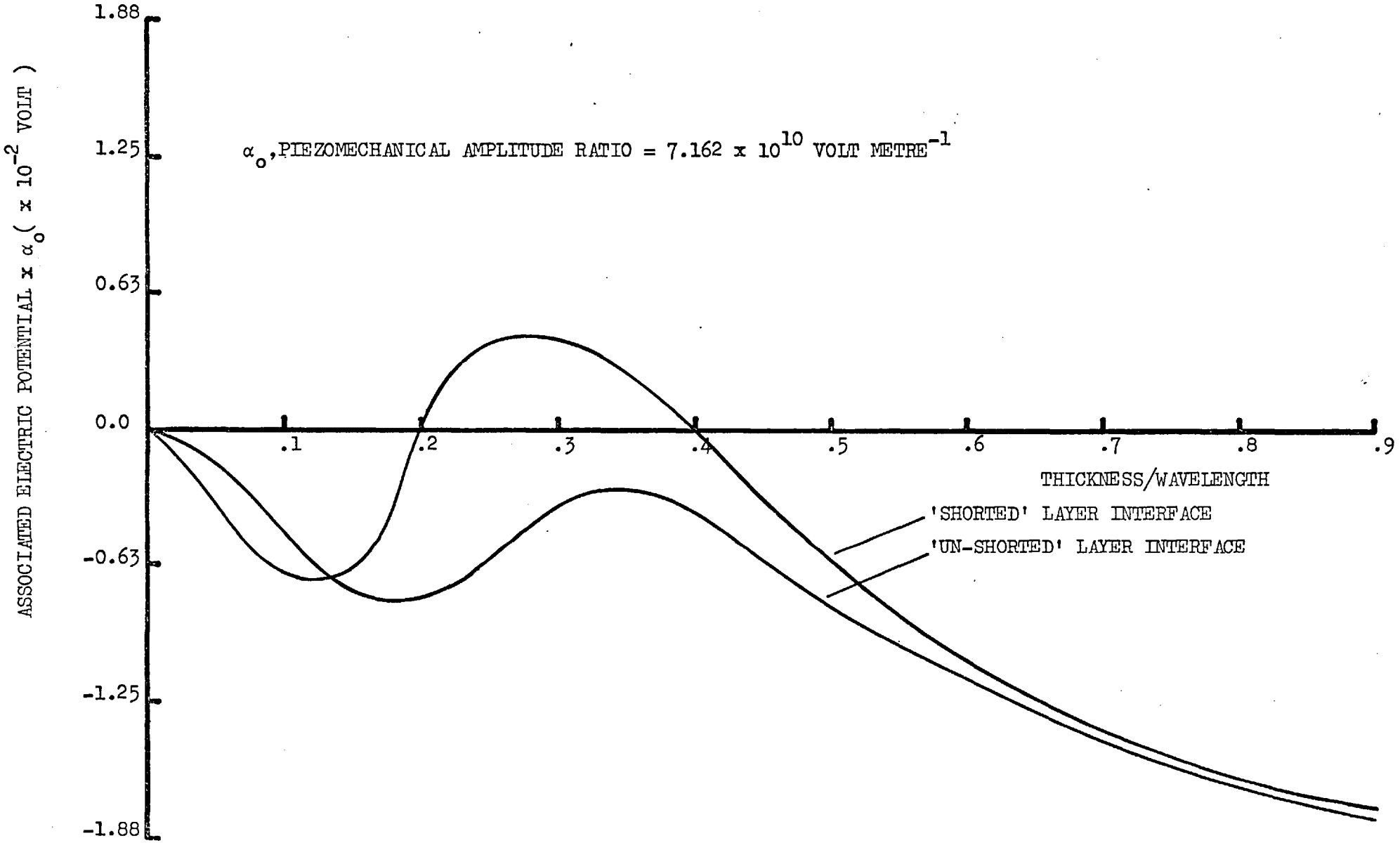

Fig. 4.14 ASSOCIATED ELECTRIC POTENTIAL AS A FUNCTION OF (THICKNESS/WAVELENGTH) WHEN WAVE PROPAGATING ON FREE SURFACE OF CdS/Si

towards the higher value of the Λ ratio and along that axis. These effects may have useful practical applications.

4.4 Associated Electric Potential in CdS/Si

Figs. 4.13 and 4.14 show the corresponding behaviour of the associated electric potential in the CdS layer under the aforesaid physical conditions. The profile of the associated electric potential bears a close resemblance to the variation of the coupling efficiency with the Λ ratio. It may be necessary to mention that by numerical analysis (see Appendix A 2), the electromechanical amplitude ratio for CdS is evaluated to be 7.162×10^{10} volt metre^{-1}. This conversion factor is particularly useful in conjunction with the coupling efficiency if the radiated acoustic power in wave propagation is the primary interest of an experiment. For completeness in this section of discussion, it is also necessary to mention that the range of useful coupling efficiency in layered media should coincide with that of the group delay time and the frequency response of the interdigital transducer used in the dispersive delay line. Another important point is that the amplification of the layer wave would not be uniform throughout a range of frequency needed for certain applications.

4.5 Comparison of Coupling Efficiencies of $ZnO/LiNbO_3$, $LiNbO_3/Si$ and $PbTe/LiNbO_3$

If influence or interactions are to be established between the wave energy and an additional electric field, it is relevant to localize the distribution of the wave energy. Fig. 4.15 is a plot of the normalized wave energy against the Λ ratio. Three combinations such

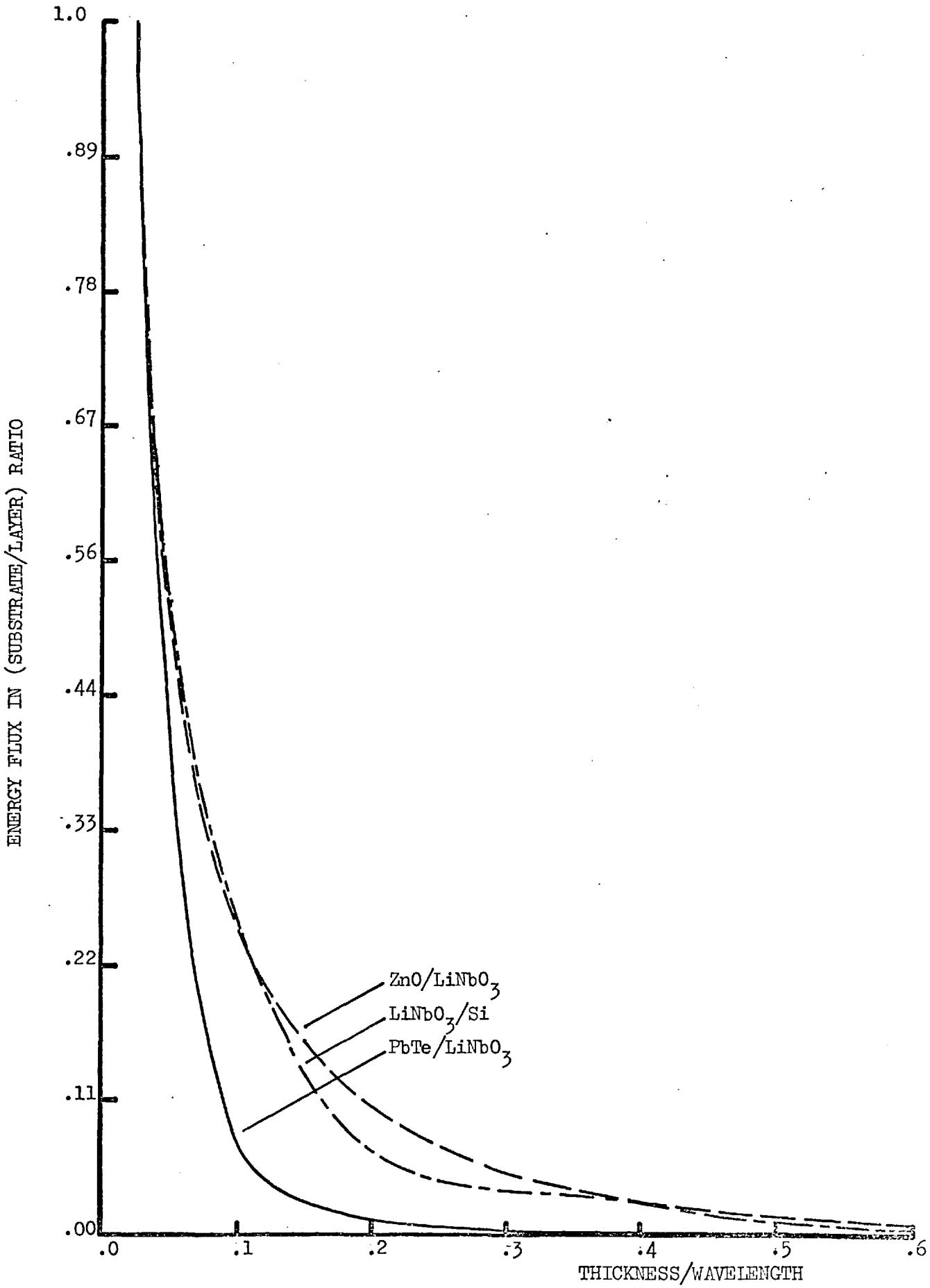

Fig. 4.15 ENERGY FLUX DISTRIBUTION AS A FUNCTION OF (THICKNESS/WAVELENGTH) IN VARIOUS LAYERED MEDIA; WAVE ENERGIES NORMALIZED AT 0.025 OF (THICKNESS/WAVELENGTH)

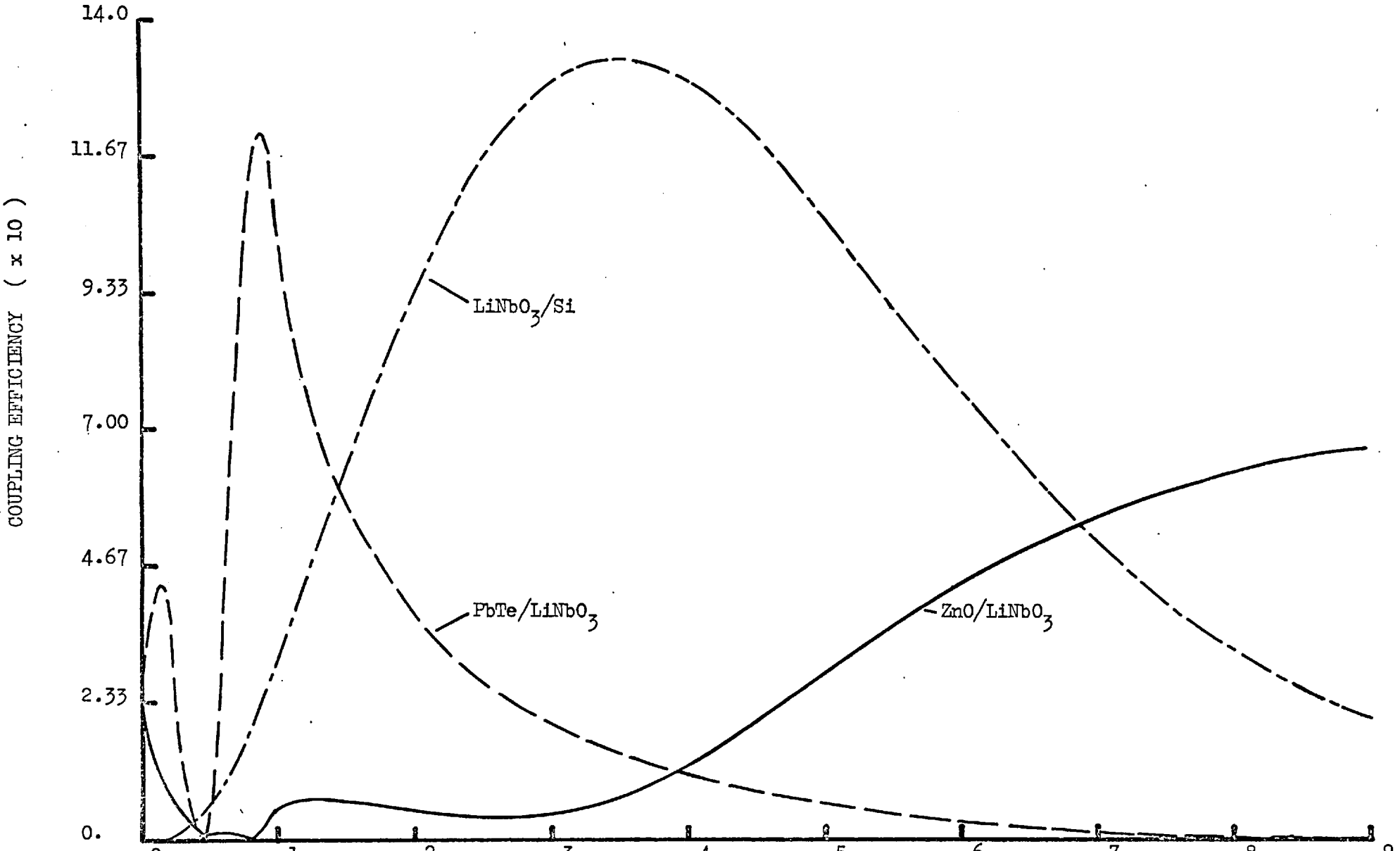

Fig. 4.16 COUPLING EFFICIENCIES VERSUS (THICKNESS/WAVELENGTH) FOR $ZnO/LiNbO_3$, $LiNbO_3/Si$ AND $PbTe/LiNbO_3$

as $ZnO/LiNbO_3$, $LiNbO_3/Si$ and $PbTe/LiNbO_3$ are arbitrarily chosen. The wave energies are propagated in the substrate and are normalized for unity at 0.025 of the ratio. As the wavelength decreases, the wave energy tends to travel along the free surface of the layer rather than to remain at the substrate and vice versa. At about 0.2 of the ratio, the wave energies of the three different material combinations fall below 12% of the initial amount. This indicates that a large amount of the energy is in the layer. The energy is continuously concentrated nearer to the free surface of the layer with increasing frequency. At this point of the energy distribution, it would not be possible for an interactive field, which is introduced on the substrate in a direction parallel to the interface, to have strong influence on the wave energy in the layer. Perhaps the energy distribution may become the prime issue in the design of a low-loss dispersive delay line. In addition to a consideration of the energy distribution, the coupling efficiency for the three two-material combinations are very different in profile (see Fig. 4.16). The typical features may be generally described as:

1. For a piezoelectric layered media, it is expected that the profile is relatively uniform with the 'terminal' values to have the same values as the two separate media.
2. For a piezoelectric layer overlay on an elastic substrate, it is expected that the profile will initially start from zero and terminate at the value of the piezoelectric layer.
3. For an elastic layer deposited on a piezoelectric substrate, the profile is expected to have an initial value of the piezoelectric substrate and fall-off to a zero value.

The above generalized features are described without consideration of

ary piezomechanical polarization based on the relative orientation of the combined crystals. It is seen in Fig. 4.16 that for a low-loss dispersive delay line, it may be better to have a strong piezoelectric layer and a moderate piezoelectric substrate. The purpose is to increase the coupling efficiency as the Λ ratio increases such that the signal amplitude could be kept approximately constant at the receiving transducer which is situated with the transmitting transducer on the plane interface of the layered media. To reduce the total insertion loss, it would be always advisable to amplify the transmitted signal by choosing a proper semiconductor material for the layer and also a good semiconductor substrate. Materials with piezoelectric and semiconductor properties are particularly useful for making solid state microsound devices with substantially large dynamic range for operation.

The associated electric potential of the above mentioned combinations can be seen in Figs. 4.17, 4.22 and 4.27. As has been illustrated before, the profiles of the corresponding electric potential are in good resemblance to those of the coupling efficiency in Fig. 4.16.

4.6 Particle Displacements of the Mechanical Surface Waves in $PbTe/SiO_2$, $PbTe/LiNbO_3$, $LiNbO_3/Si$ and $ZnO/LiNbO_3$

So far, the discussions are on the wave velocity, the coupling efficiency and the associated electric potential of the surface wave in layered media. Behind these parameters is the particle motion which defines the conclusive characteristics of the wave propagation. By the present standing of the numerical approach, the particle displacements in the reference co-ordinates are considered to couple

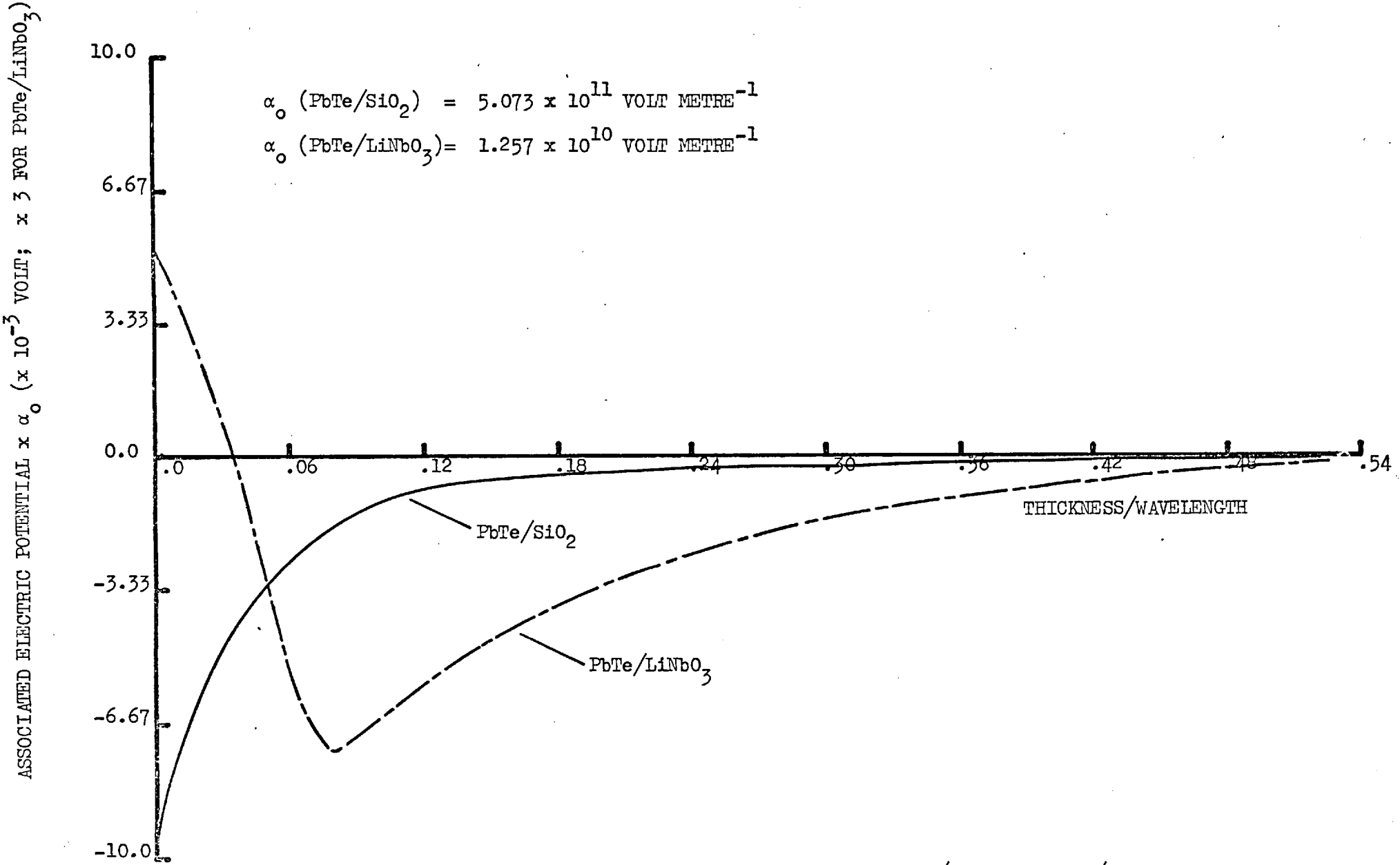

Fig. 4.17 ASSOCIATED ELECTRIC POTENTIAL AT LAYER INTERFACE OF PbTe/SiO_2 AND PbTe/$LiNbO_3$

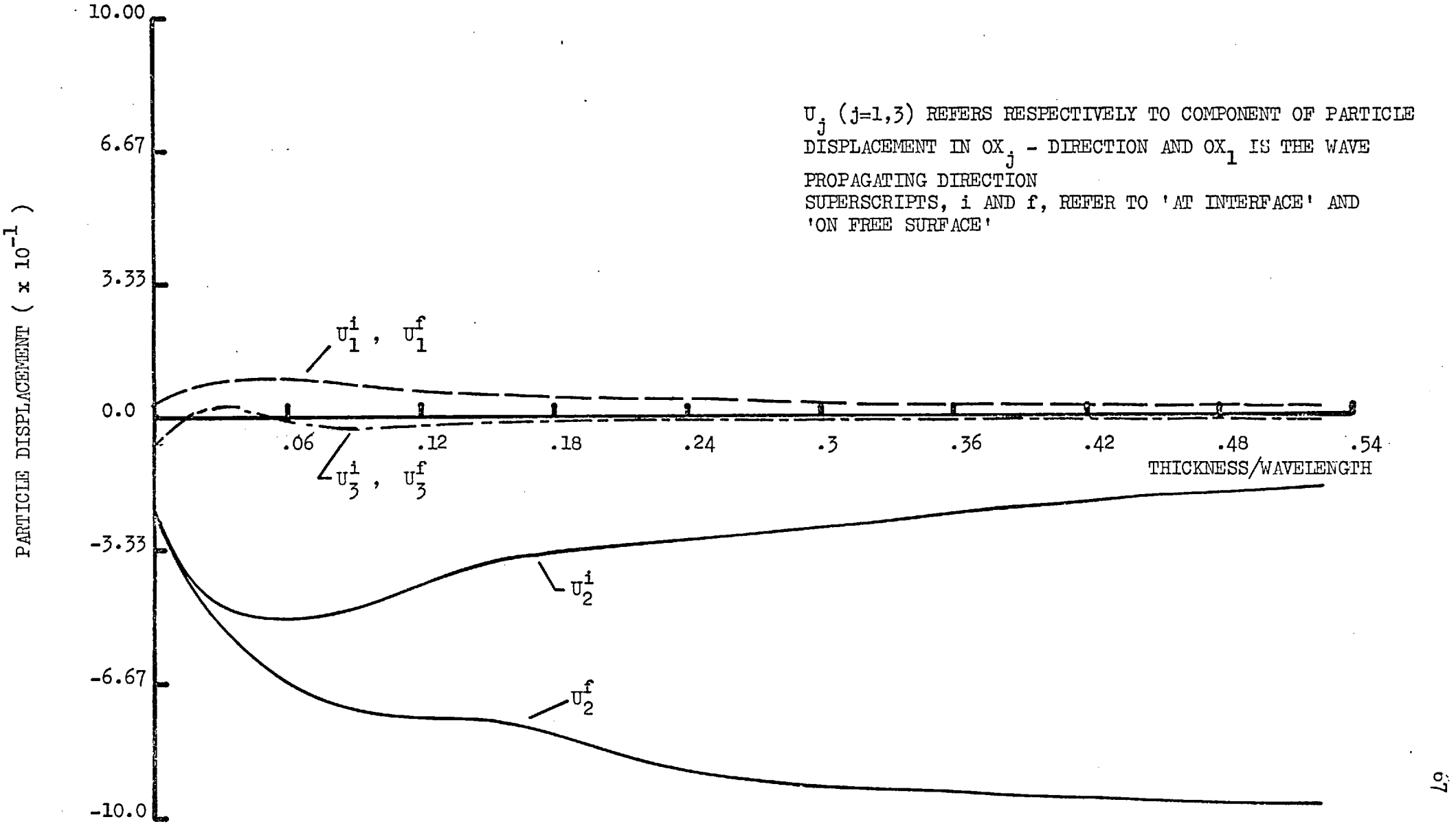

Fig. 4.18 PARTICLE DISPLACEMENTS WITHOUT CONDUCTING (EARTHED) FILM AT LAYER INTERFACE OF $PbTe/SiO_2$

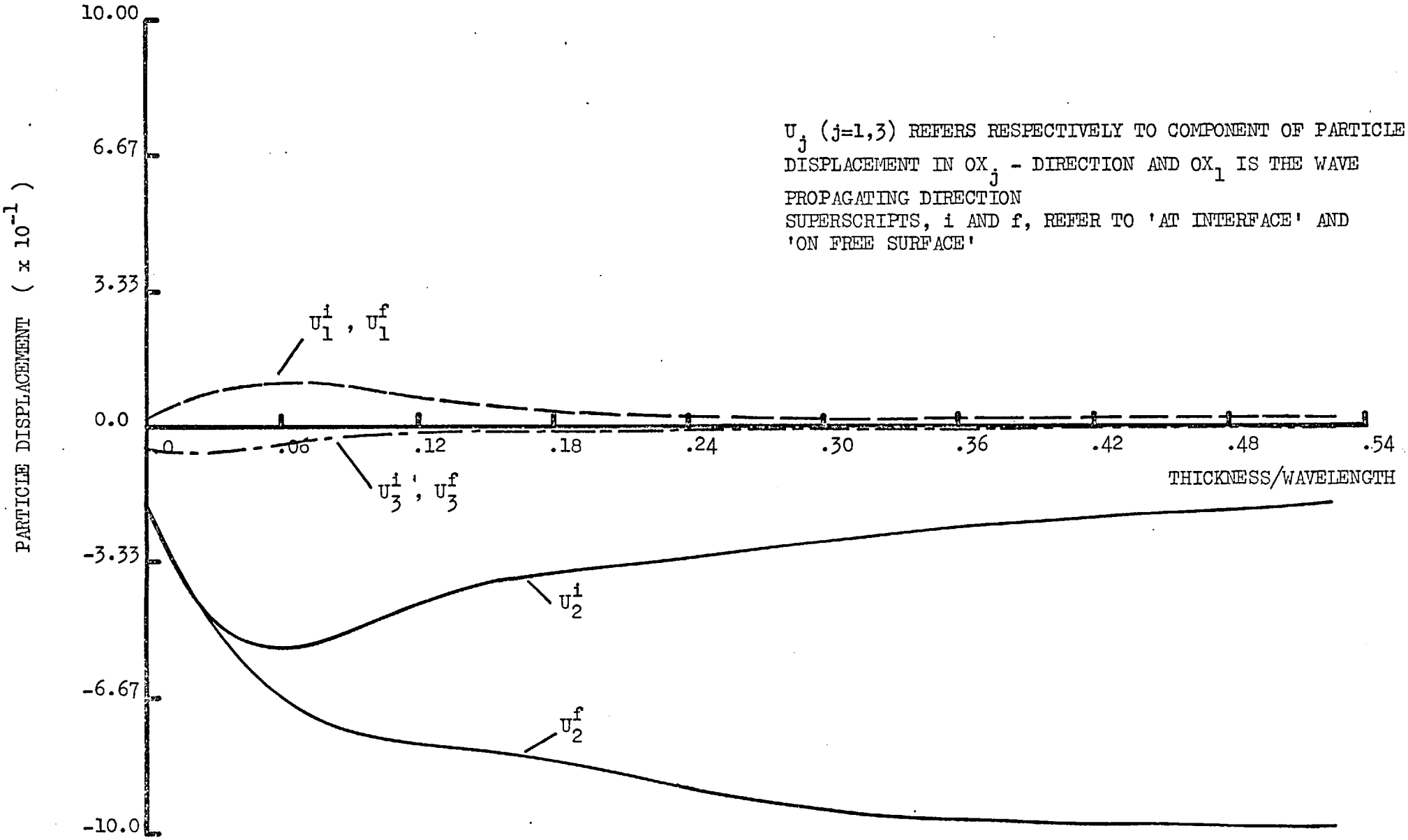

Fig. 4.19 PARTICLE DISPLACEMENTS WITH CONDUCTING (EARTHED) FILM AT LAYER INTERFACE OF $PbTe/SiO_2$

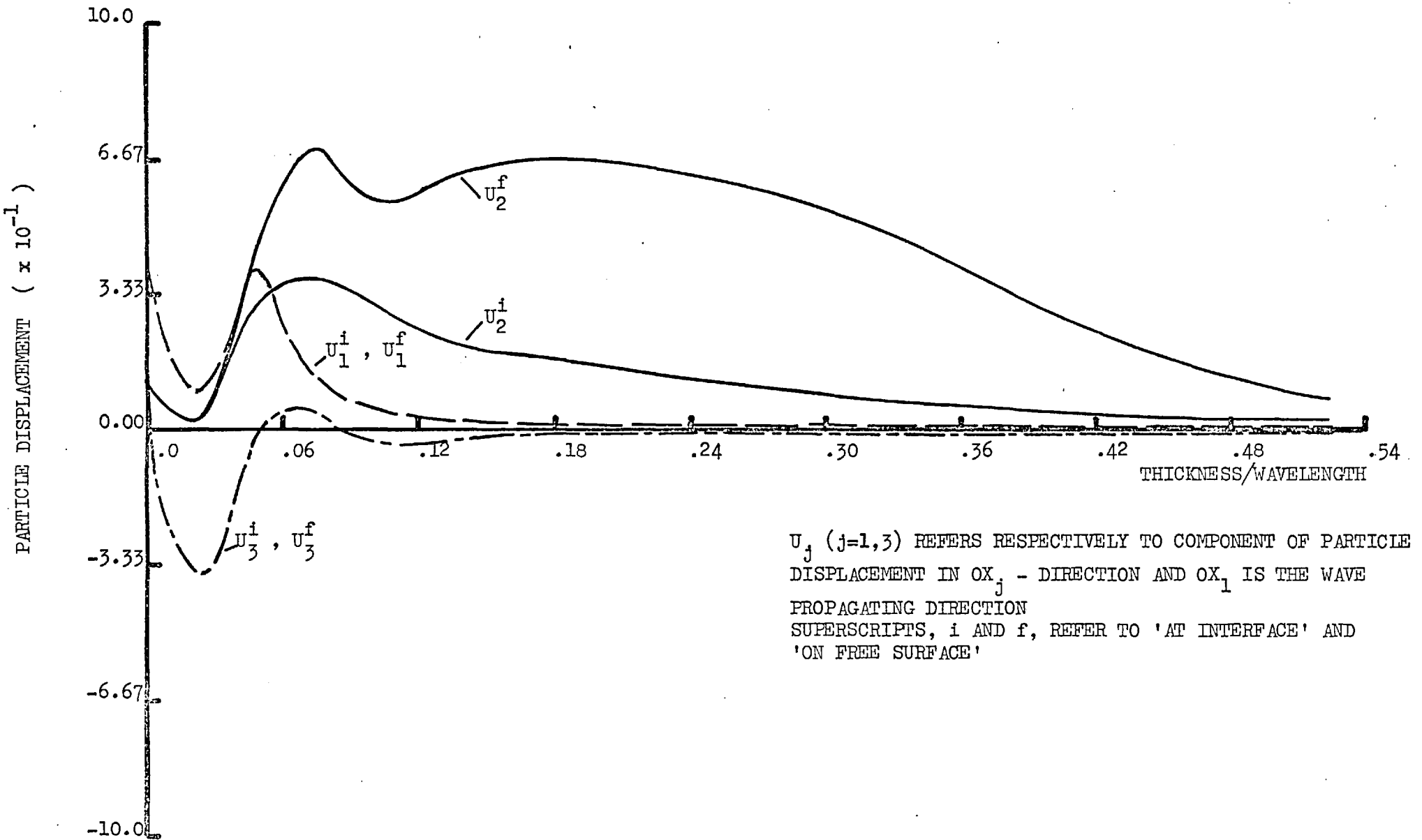

Fig. 4.20 PARTICLE DISPLACEMENTS WITHOUT CONDUCTING (EARTHED) FILM AT LAYER INTERFACE OF PbTe/$LiNbO_3$

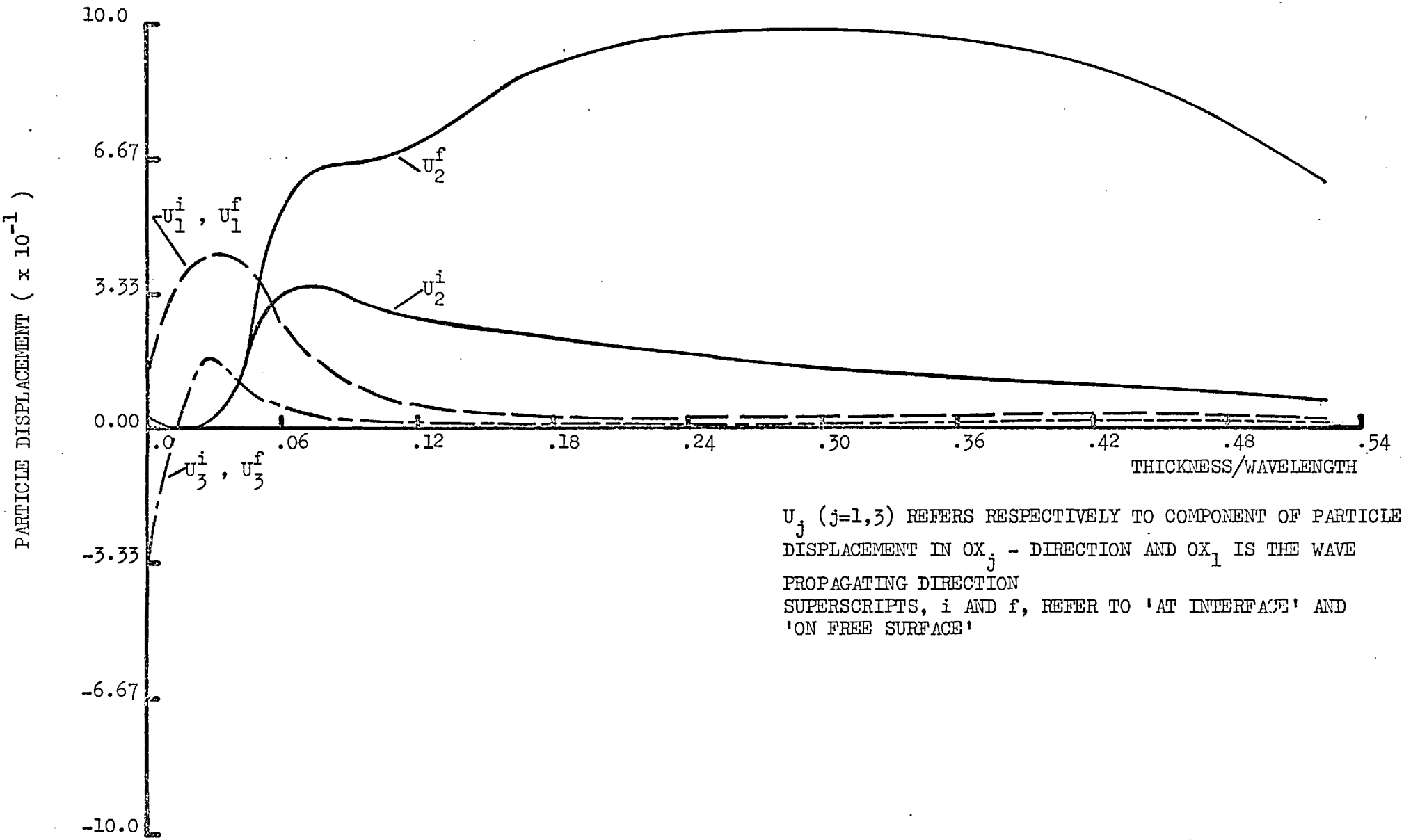

Fig. 4.21 PARTICLE DISPLACEMENTS WITH CONDUCTING (EARTHED) FILM AT LAYER INTERFACE OF PbTe/$LiNbO_3$

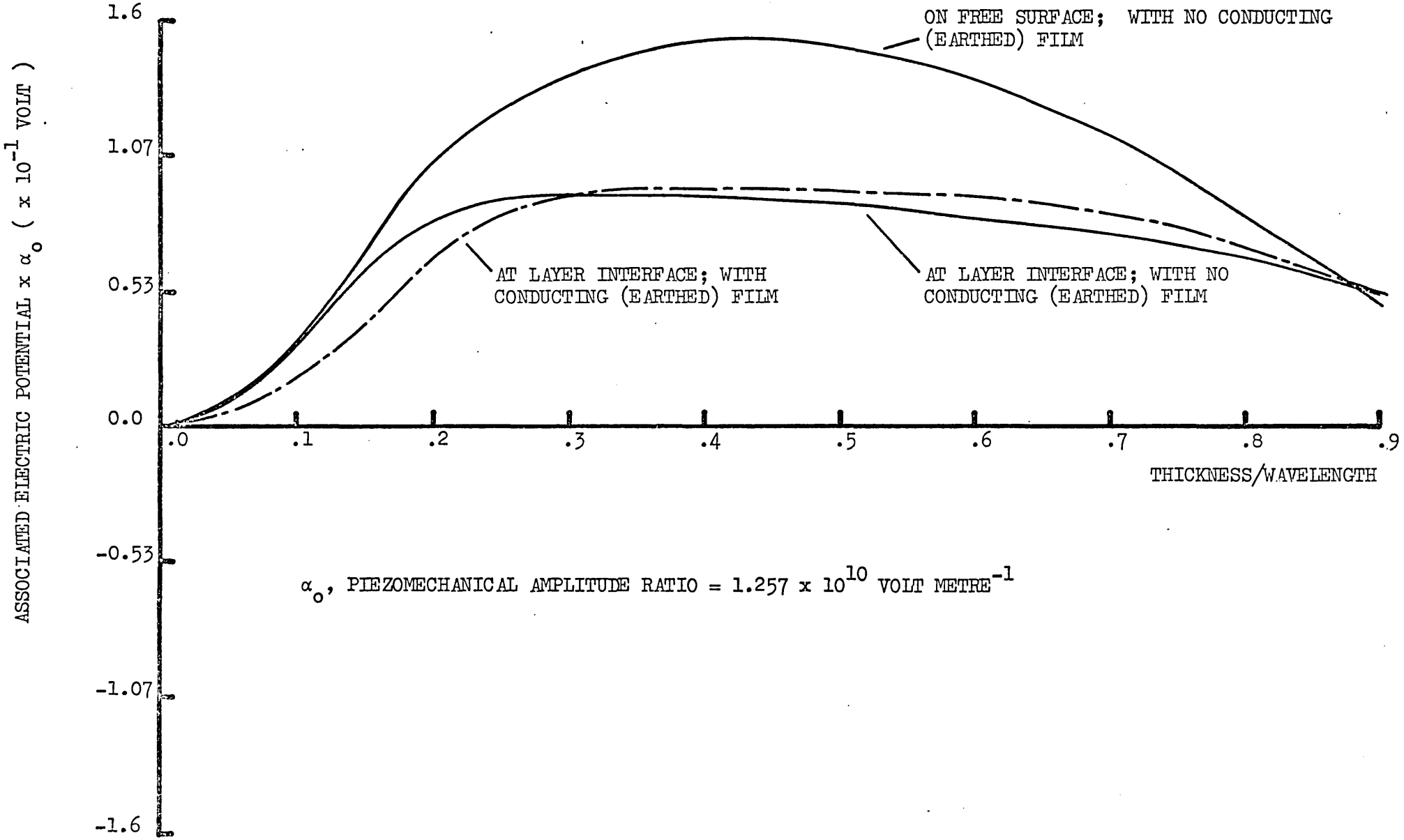

Fig. 4.22 ASSOCIATED ELECTRIC POTENTIAL AT LAYER INTERFACE AND ON FREE SURFACE OF $LiNbO_3$/Si

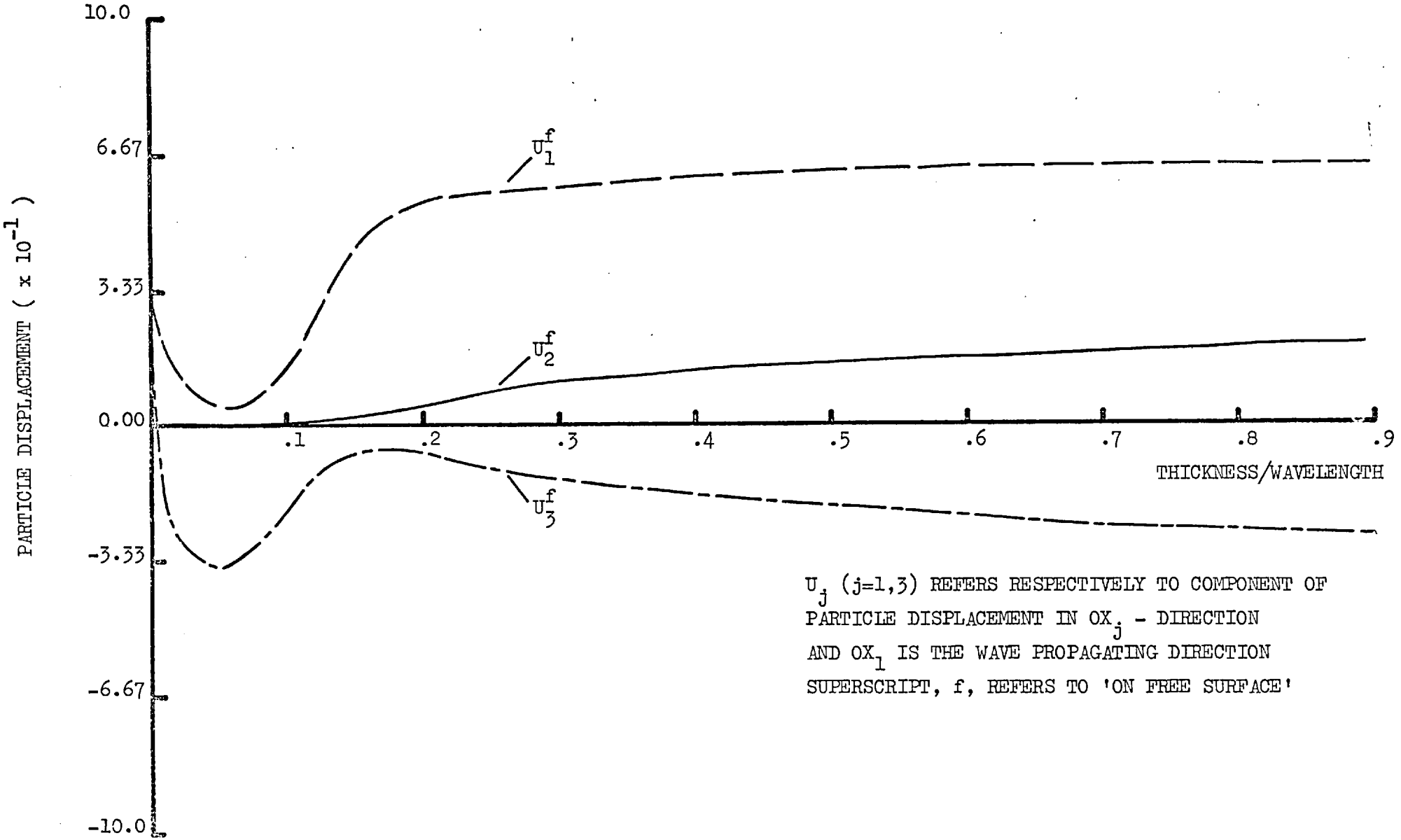

Fig. 4.23 PARTICLE DISPLACEMENTS AT FREE SURFACE (WITHOUT CONDUCTING (EARTHED) FILM AT LAYER INTERFACE) OF $LiNbO_3/Si$

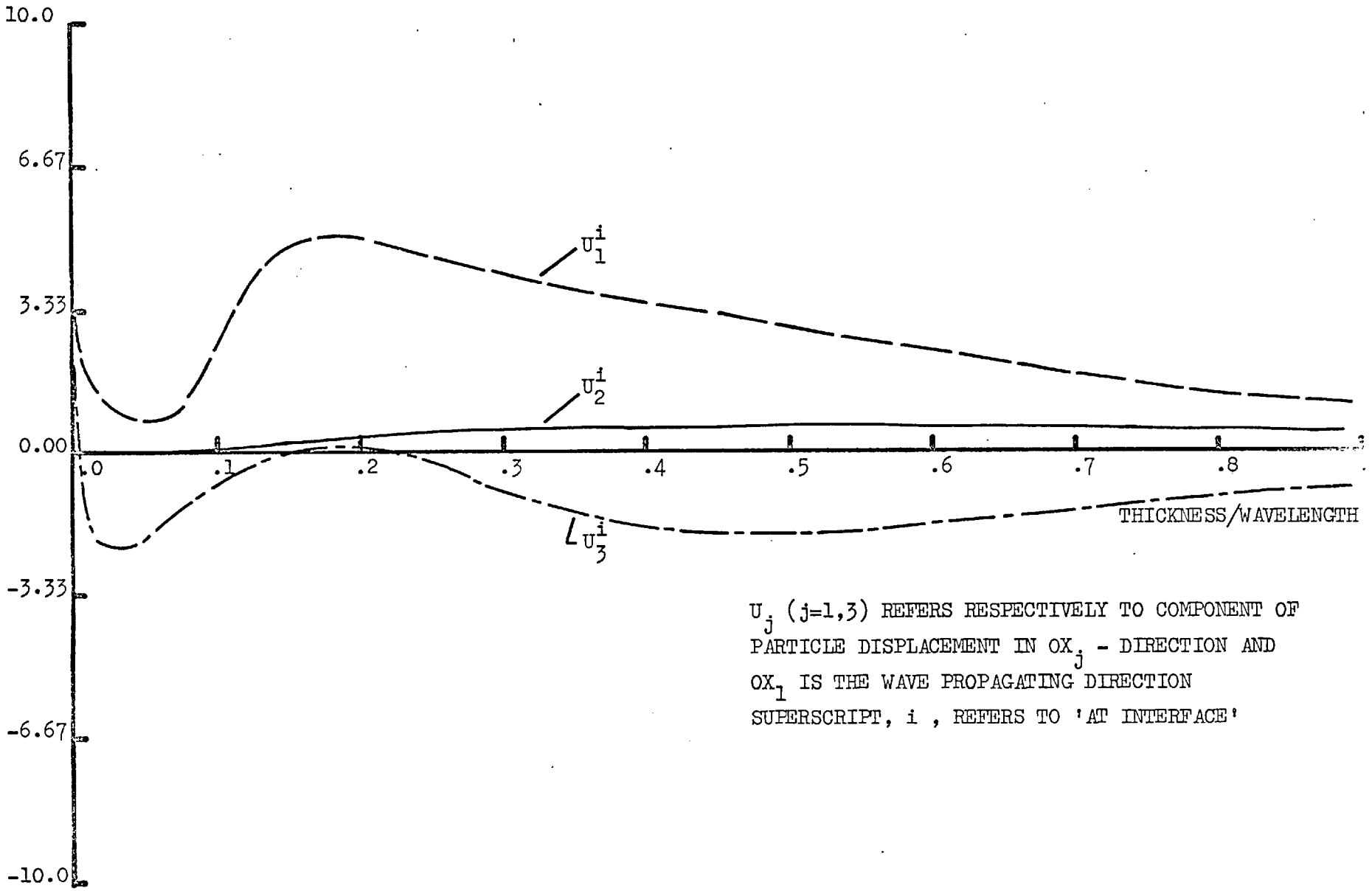

Fig. 4.24 PARTICLE DISPLACEMENTS AT LAYER INTERFACE (WITHOUT CONDUCTING (EARTHED) FILM ON THAT SURFACE) OF $LiNbO_3/Si$

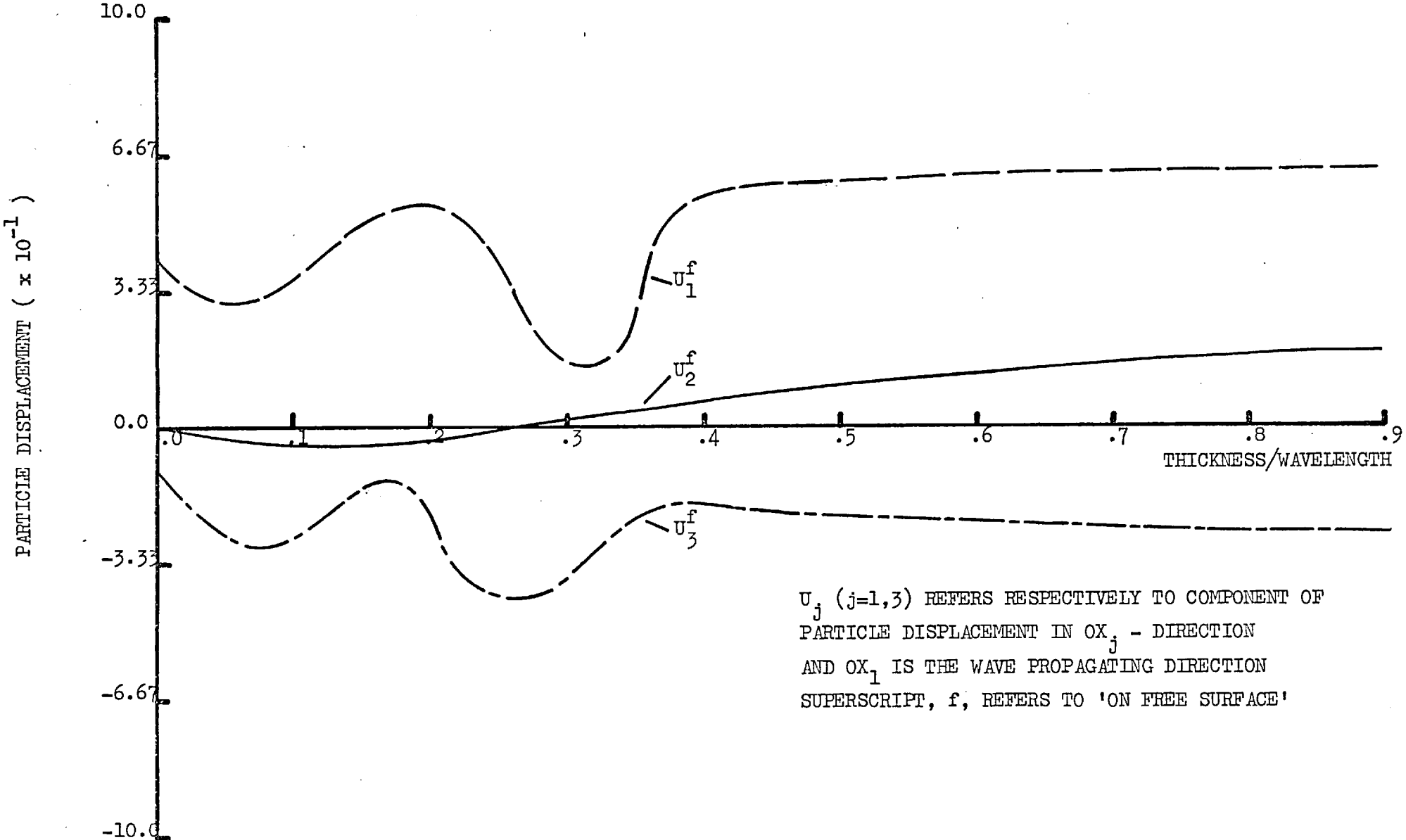

Fig. 4.25 PARTICLE DISPLACEMENTS AT FREE SURFACE (WITH CONDUCTING (EARTHED) FILM ON THAT SURFACE) OF $LiNbO_3$/Si

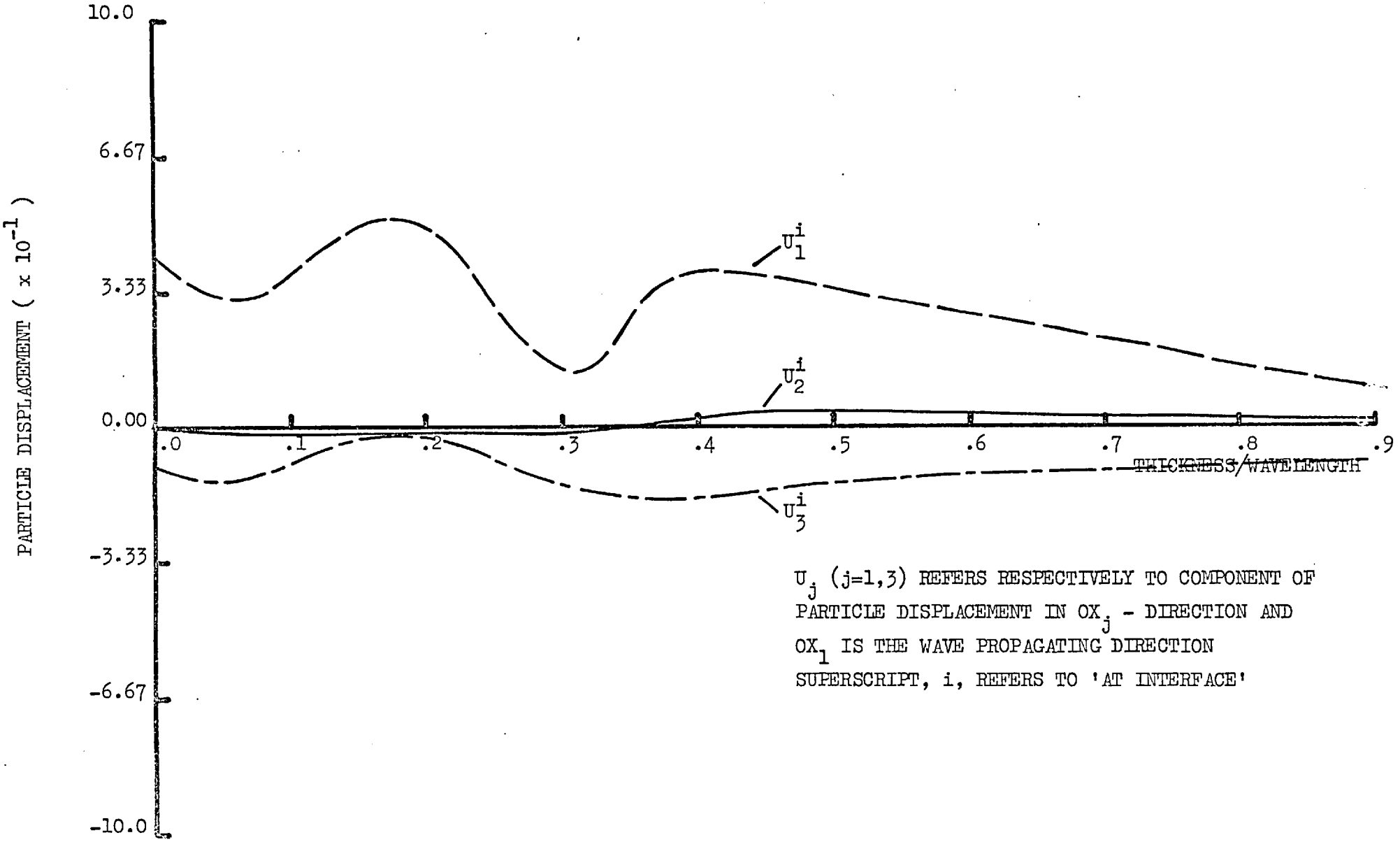

Fig. 4.26 PARTICLE DISPLACEMENTS AT LAYER INTERFACE (WITH CONDUCTING (EARTHED) FILM ON FREE SURFACE) OF $LiNbO_3/Si$

together. After the individual partial wave is evaluated, the contributory particle displacements are selected and used in the determinant of the boundary conditions. For both $PbTe/SiO_2$ and $PbTe/LiNbO_3$ as shown in Figs. 4.18/21, the predominant particle displacements are U_2^i and U_2^f where the superscripts, i and f refer to 'at interface' and 'on free surface' and the subscript 2 refers to the component in the X_2-direction. Although the other components along X_1 - and X_2 - direction are preserved, it is obvious that these two components decrease at the higher values of the Λ ratio. Especially after the Λ ratio of 0.12, it appears that in both cases (see Figs. 4.18/21) the generalized Rayleigh wave degenerates into the generalized Love wave irrespective of the presence of the conducting film. It is seen that the particle displacements of the wave fall rapidly at the interface but those on the free surface grow in magnitude. It indicates that the Love wave energy tends to move into the layer at an earlier stage of the wave propagation. The only obvious feature derived from the interface of the conducting film on the particle displacement via the associated electric potential, is that the particle motion of $PbTe/LiNbO_3$ seem to have more variation in the Λ ratio range between 0.0 and 0.06. This 'activity' of the particle motion,at low values of Λ ratio, is also observed for the other combinations, e.g. $LiNbO_3/Si$ and $ZnO/LiNbO_3$. It is also interesting to point out that in Figs. 4.22 and 4.27 the associated electric potential (like the particle motion) of those two-material combinations exhibit the similar characteristics under the influence of the conducting film. The 'activity' of the layer wave is seen to be moved along the Λ ratio axis towards its higher values. In the case of $LiNbO_3/Si$,

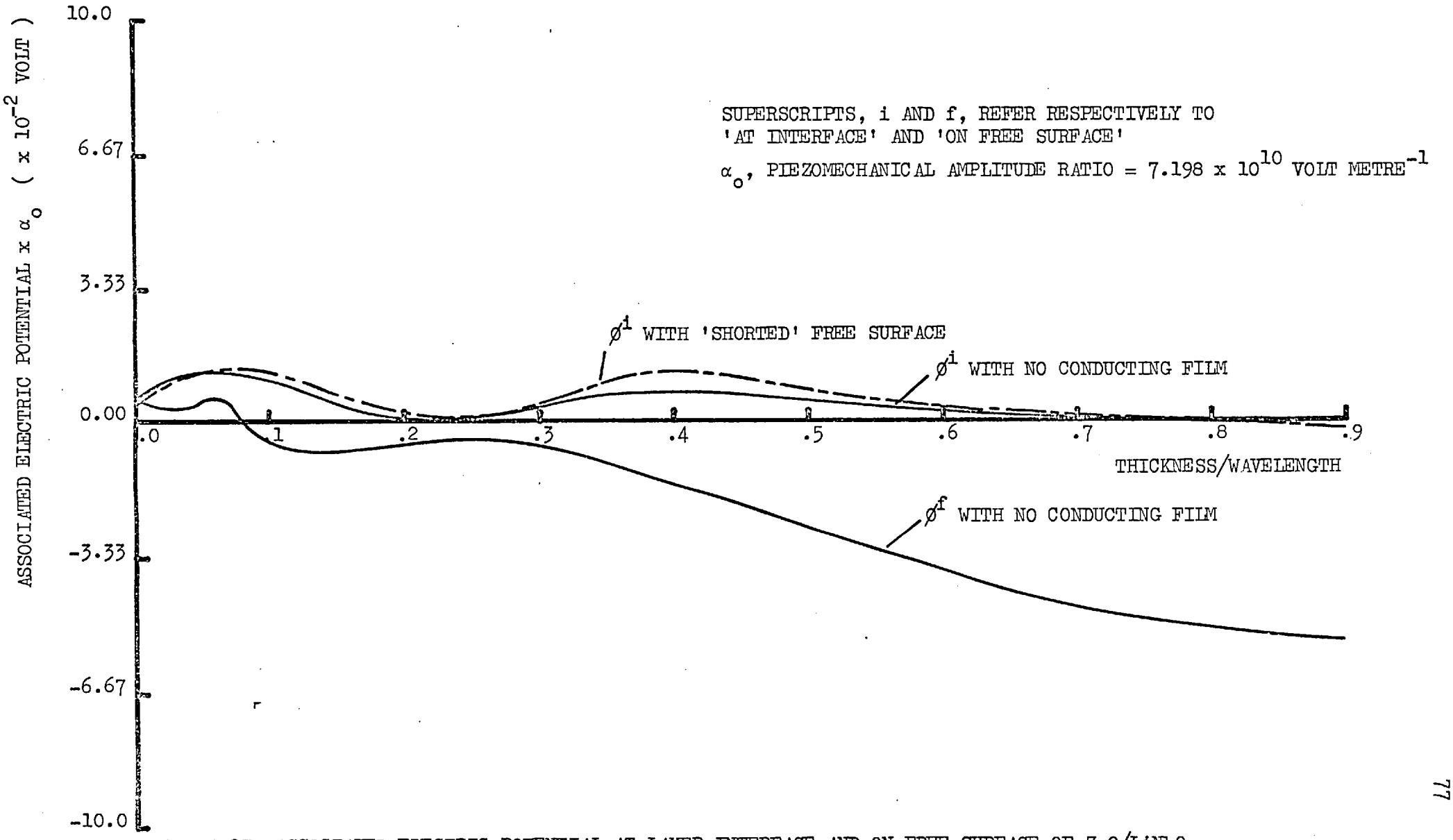

Fig. 4.27 ASSOCIATED ELECTRIC POTENTIAL AT LAYER INTERFACE AND ON FREE SURFACE OF $ZnO/LiNbO_3$

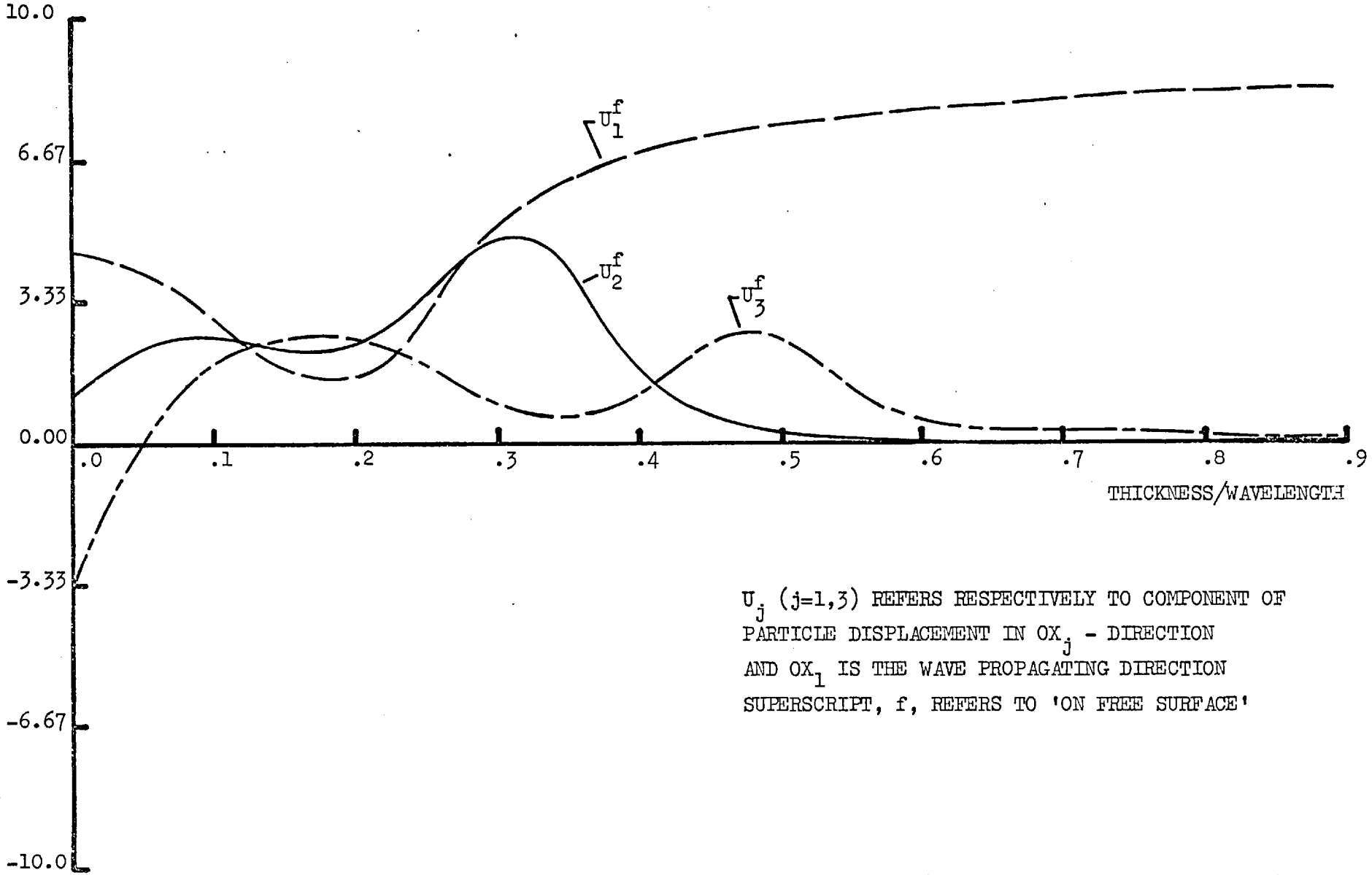

U_j (j=1,3) REFERS RESPECTIVELY TO COMPONENT OF PARTICLE DISPLACEMENT IN OX_j - DIRECTION AND OX_1 IS THE WAVE PROPAGATING DIRECTION
SUPERSCRIPT, f, REFERS TO 'ON FREE SURFACE'

Fig. 4.28 PARTICLE DISPLACEMENTS AT FREE SURFACE (WITHOUT CONDUCTING (EARTHED) FILM ON THAT SURFACE) OF $ZnO/LiNbO_3$

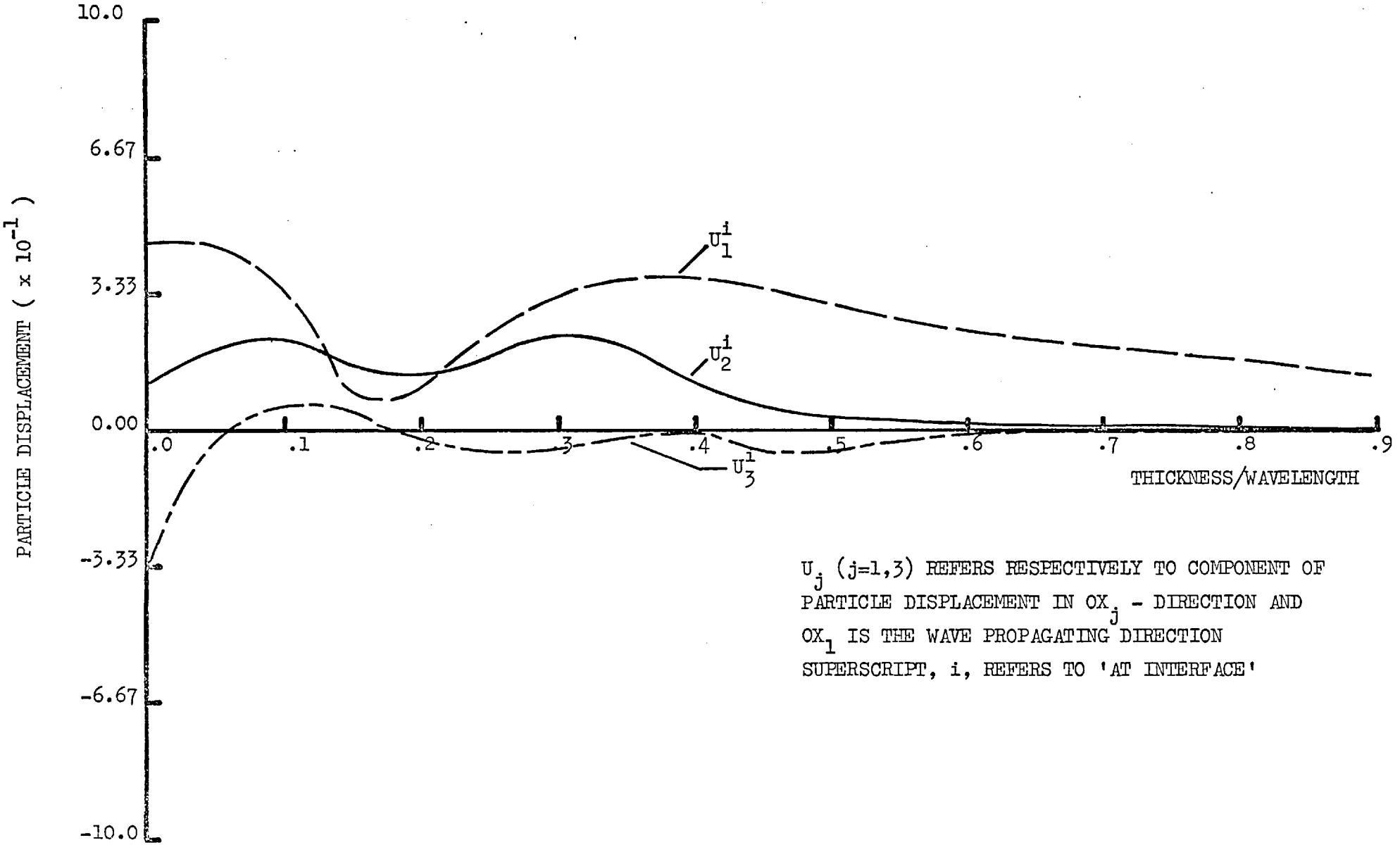

Fig. 4.29 PARTICLE DISPLACEMENT AT LAYER INTERFACE (WITHOUT CONDUCTING (EARTHED) FILM ON FREE SURFACE) OF ZnO/$LiNbO_3$

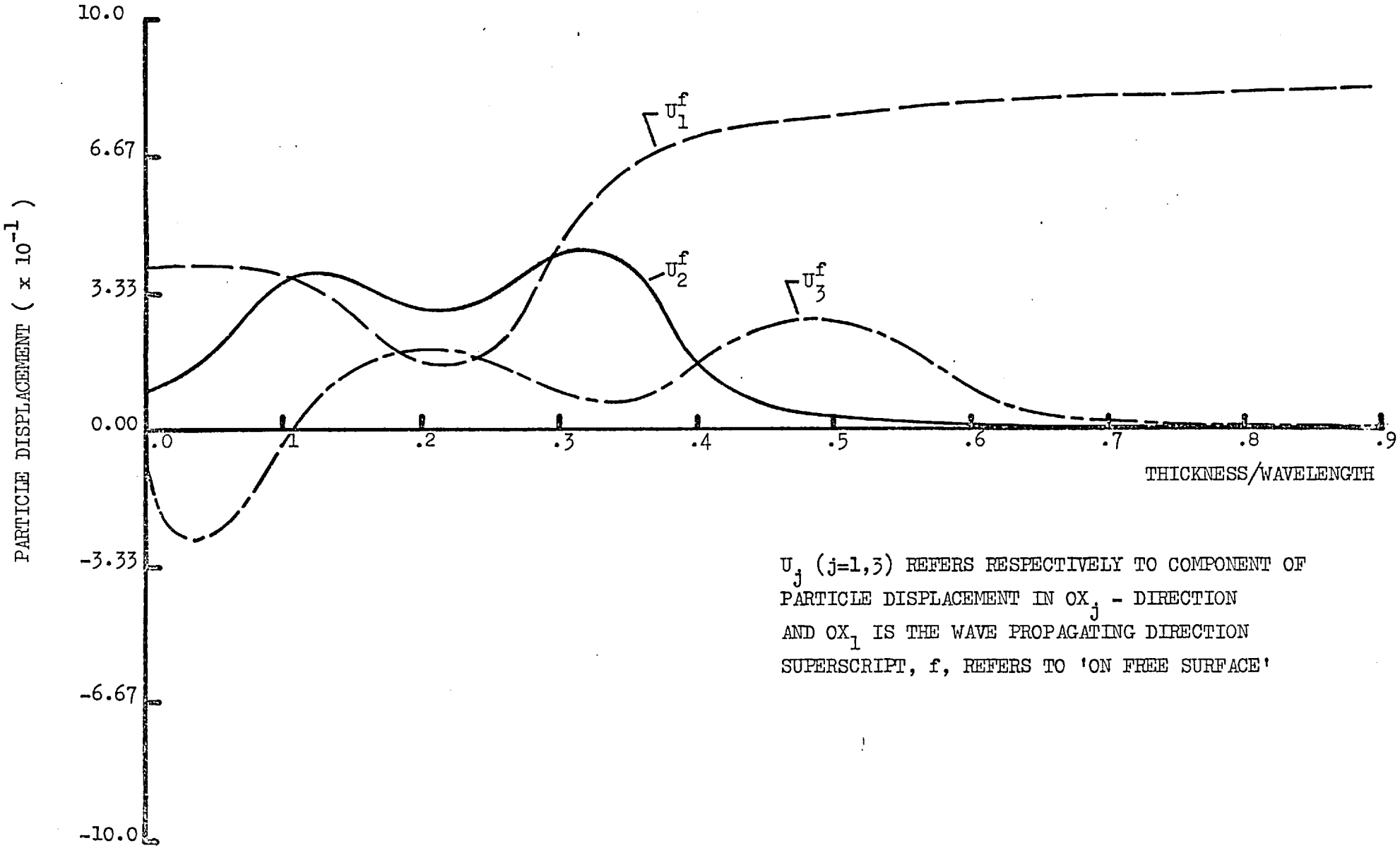

Fig. 4.30 PARTICLE DISPLACEMENTS AT FREE SURFACE (WITH CONDUCTING (EARTHED) FILM ON FREE SURFACE) OF $ZnO/LiNbO_3$

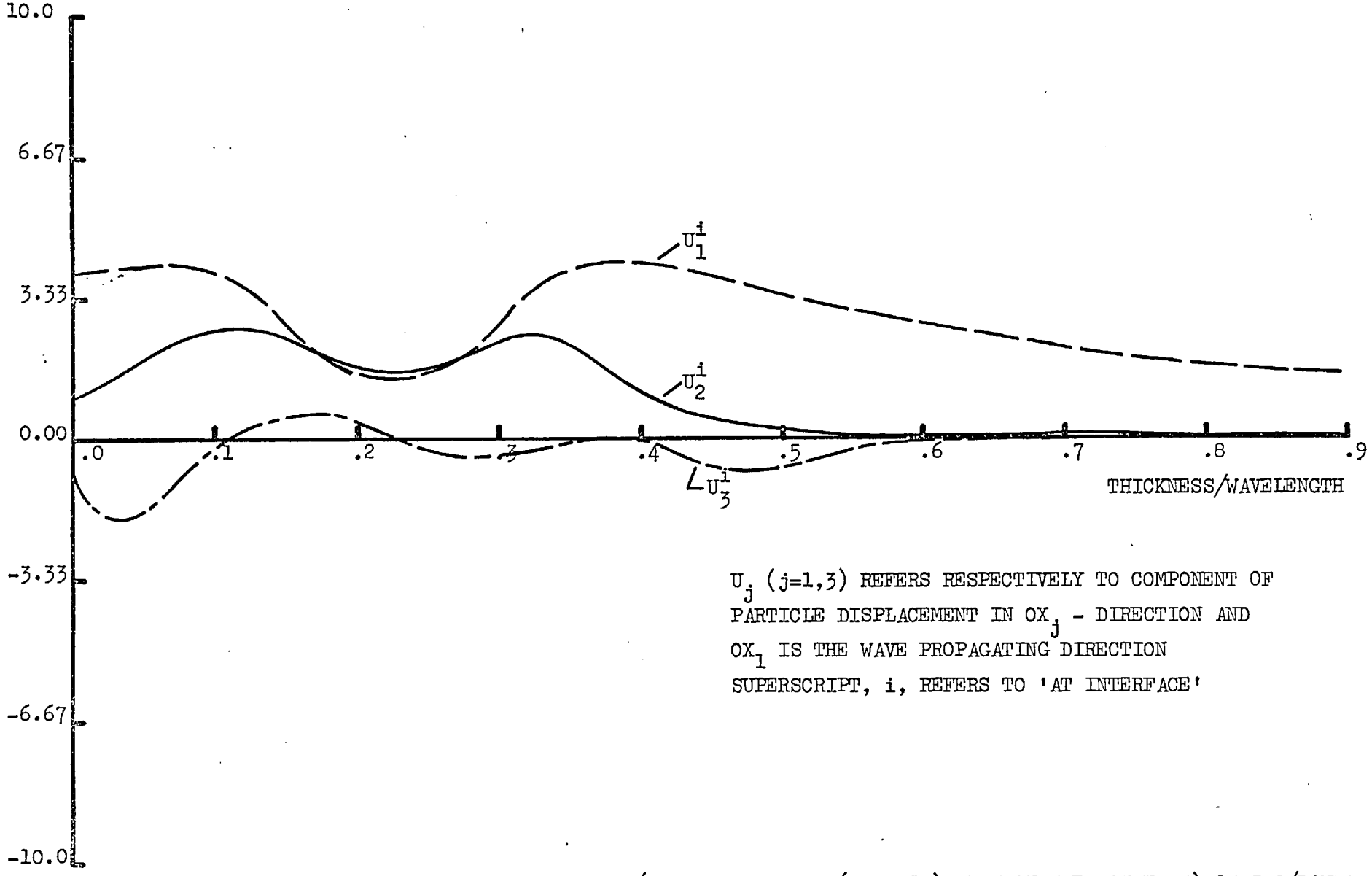

Fig. 4.31 PARTICLE DISPLACEMENTS AT INTERFACE (WITH CONDUCTING (EARTHED) FILM ON FREE SURFACE) OF $ZnO/LiNbO_3$

the particle motion is essentially that of the generalized Rayleigh wave propagating from the substrate onto the layer when the wavelength becomes smaller. Without exception, the interface particle displacements decrease and those on the free surface increase in magnitude as shown in Figs. 4.23/26. The similar tendency also appears in the case of ZnO/liNbO$_3$ as shown in Figs. 4.28/31. The mode in which the wave energy propagates in ZnO/LiNbO$_3$ uniquely differs from that of the preceding two-material combinations whereby the particle displacements, U_1^f and U_1^i are predominant at the interface of the ZnO/LiNbO$_3$. The wave motion is basically longitudinal akin to the longitude bulk wave propagating collinearly in the wave propagation direction. This kind of layer wave parallel to the plane boundary may be proved useful in regards to the amplification of acoustic wave with interaction of the electrons drifted along the same direction.

4.7 Comments

The main points which emerge from this chapter, dealing with a layer and substrate, are as follows:

1) The curves of velocity-frequency dispersion have been shown to have a negative gradient which corresponds to a positive gradient on the t_g v.(H/λ) curve, where t_g and H are respectively the group delay time and the thickness of the layer. If V_2 and V_1 are respectively the velocities of the layer and the substrate, with f_2 and f_1 the corresponding frequencies, then $(V_2 - V_1)/(f_2 - f_1)$ is an approximate measure of the dispersion. If V_2 is less than V_1, the gradient of the group delay time curve is positive, but the gradient is negative if V_2 is greater

than V_1. The positive gradient refers to a compressive pulse with a finite bandwidth and the negative gradient to an expansion of the pulse into one having a larger bandwidth. Since the one is complementary to the other, any particular form of variation of group delay time, t_g with the frequency, can be obtained by suitable 'velocity tailoring' of the layered structure.

2) A conducting (earthed) film deposited on a single piezoelectric layer can produce an appreciable but limited change in the $(t_g \cdot \Delta f)$ product, where Δf is the frequency bandwidth. The magnitude of this change depends on $\Delta t_g = t_{g2} - t_{g1}$, where 2 and 1 subscripts refer respectively to the layer and the substrate. Since the separate delay times, t_{g2} and t_{g1}, are affected by the presence of the conducting film, a change in any of the delay times would be contributory to the time-bandwidth product. Change in delay time is due to a change in the wave velocity and it is to be expected that the actual change in delay time is related to the piezoelectric coupling constant.

3) The coupling efficiency of the piezoelectric layered substrate is non-uniform throughout the investigated range of H/λ ratio. The profile of the coupling efficiency, varying with H/λ ratio, is dependent on:

   a. The position of the plane containing the interdigital electrodes,

   b. The position of the plane of the conducting film,

   c. The intrinsic nature of the layer and the substrate being piezoelectric or purely elastic, and

   d. The orientation of the piezomechanical polarization in the layer and the substrate.

Although the item (d) was not discussed, it is to be expected that the combined value of the associated electric potentials in the separate media, can be enhanced or reduced by the boundary matching.

4. It is important to refer the associated electric potential and the coupling efficiency as the overall effects due to the combined nature of the piezoelectric property of the layer and the substrate. It has been shown that in bulk wave propagation, the associated electric potential distribution reveals the affect of anisotropy. In a layered substrate there is an additional geometrical factor arising from the differing electric potentials at the various interfaces. It is therefore important to point out that the profile of either the electric potential or the coupling efficiency can be modified by selecting different crystalline planes and/or applying various electric potentials at the plane interfaces.

5. As the H/λ ratio increases from near zero, the wave energy resides more and more in the layer and finally becomes concentrated near the surface. Correspondingly it implies that the particle motion changes from the generalized Rayleigh wave at the substrate into other layer modes. In the lower range of H/λ ratio, the layer is effectively an elastic skin on the substrate and hence the particle motions on both surfaces of the layer are in phase with each other. At the higher values of H/λ ratio, the particle displacements on the free surface are more dominant than those at the substrate interface. The variation of the particle motion from the lower to the higher (H/λ) ratio, occurs approximately between the values 0.2 and 0.6. If wave propagation in the layer

is considered as arising from multi-reflections and lateral displacements along the parallel surfaces, the layer might be regarded as a quarter-wavelength plate rigidly attached to the substrate. This conjecture is supported by the appropriate curves of the particle displacements of the various two-material combinations (Sec. 4.6).

CHAPTER 5

EXPERIMENTAL PROCEDURE

5.1 Thin Film Deposition by Radio Frequency Sputtering

As a simple means of introducing R.F. sputtering, let us consider a pair of metal electrodes immersed in a low pressure gas. If a high d.c. voltage is applied to the electrodes, the gas is ionized and a gaseous discharge occurs between the electrodes. Basically, the gaseous discharge consists of a Crooke's dark space at which the d.c. potential drop largely occurs and a plasma region where there are many ion collisions. Ions are accelerated across the Crooke's dark space and their momenta are finally transferred to the surface of the cathode. As a result, the material of the cathode is released (or sputtered) and the greater portion is deposited on the anode. This process is described as d.c. sputtering.

If a R.F. alternating voltage is applied to the electrodes, ionization will still take place between them. However, the gaseous discharge is symmetrical with respect to the plasma because identical gaseous discharge occurs alternately at each electrode during every half-cycle. If an electrode is covered by a sheet of dielectric material and a d.c. potential is applied, the gaseous discharge ceases because of an accumulation of positive charge at the surface of the dielectric after the first ionic bombardment. This effect can be offset by applying a R.F. voltage to the electrodes and the gaseous discharge is restored. This phenomena can be explained by the fact (H S Butler, 1963) that the positively charged surface is neutralized by electron bombardment before the next ionic bombardment takes place. The surface of the dielectric is self-

biassed negatively with respect to the plasma during a larger part of each cycle, because the mobility of the electrons is much higher than that of the ions. In this situation the prescribed symmetry in discharge is altered as the dielectric surface becomes relatively more negative than the metal surface. This effect may be explained by the fact that the electrical impedance with respect to the plasma is lower at the electrode having the dielectric material cover. Hence, there is a larger Crooke's dark space at the cathode (i.e. the electrode with a dielectric sheet) and a small one at the anode. The d.c. potential between the electrodes will have the profile as shown in Fig. 5.1.

It may be important to note that the plasma potential relative to the anode may be as high as over 100 volt. With this field across the smaller dark space to the anode, the energies of ions reaching the anode surface may well be above 10 eV which is sufficient to damage the surface structure of a deposited thin film at the anode. Another feature in R.F. sputtering is that if the frequency of the applied voltage is lower than the order of 10 MHz, the d.c. potential distribution as indicated above may not be possible because there will be insufficient ions reaching the cathode and neutralize the negative surface charge. At higher frequencies, an increased field arises across the dark space as fewer ions are able to reach the cathode. As the rate of the impinging ions decreases, the deposition rate of the dielectric onto the anode will be lowered. There is thus no advantage in operating the R.F. sputtering process at the higher frequencies. Finally, it may be necessary to point out that the energy distribution of the sputtered particles is dependent upon the d.c.

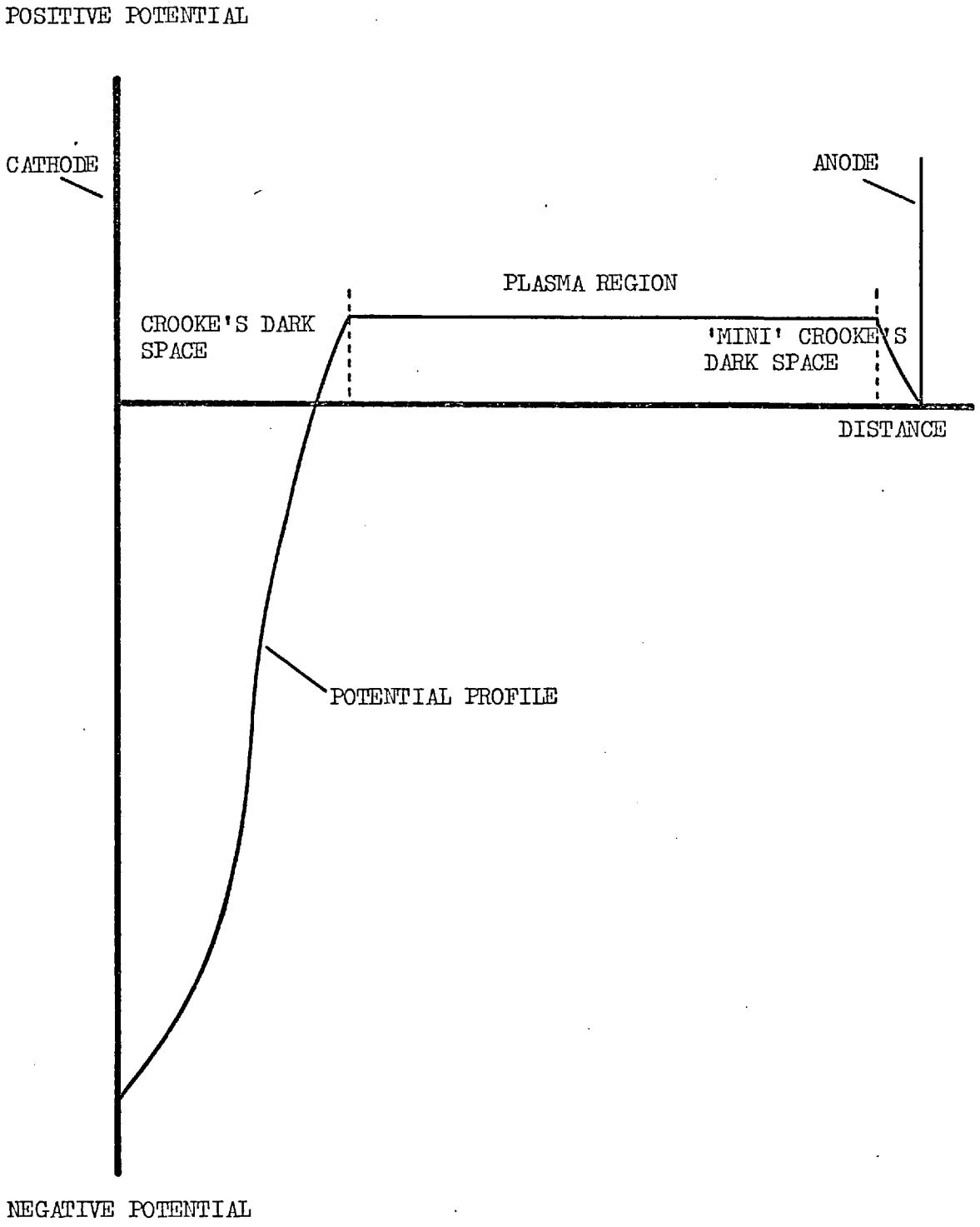

Fig. 5.1 TYPICAL PROFILE OF d.c. POTENTIAL BETWEEN CATHODE AND ANODE DURING R.F. DISCHARGE

offset voltage between the two electrodes. The d.c. offset voltage may be defined as the required voltage to sustain a gaseous discharge for a given gas pressure. Normally, the energy range lies within 10^{-1} and 10^{4} eV for a d.c. offset voltage of approximately 4.0 kV. Majority of the sputtered particles will have energy of about 50 eV which is considerably higher than the 1 eV of the thermally ejected particles.

The block diagram in Fig. 5.2 gives details of the experimental arrangement for depositing a dielectric film. The sputtering unit was commercially purchased from Material Research Corporation, U.S.A. It consists of two material targets, an etching platform and a heating table which is capable of providing a maximum temperature of 500°C. The available R.F. power can be delivered up to a maximum value of 2 kW at 13.95 MHz which is within the free radio-band. By using the matching unit, the R.F. power is either transferred directly to the material target alone or partially channelled to give a biassed sputtering at the specimen situated on the etching platform. The background pressure of the sputtering chamber is attainable at approximately 0.5×10^{-6} μ ($1\ \mu = 10^{-3}$ torr) with the aid of the liquid nitrogen trap. The partially fabricated specimen (i.e. the thermally oxidized silicon substrate with deposited interdigital electrodes) is cleaned in the vapour degreased chamber and then placed on the heating table to be preheated at a low pressure. In all depositions, the specimens were heated overnight and maintained at 200°C for approximately 12 hours in order to evaporate any volatile chemical. Before deposition, the material target was presputtered to remove any possible unwanted material on the surface of

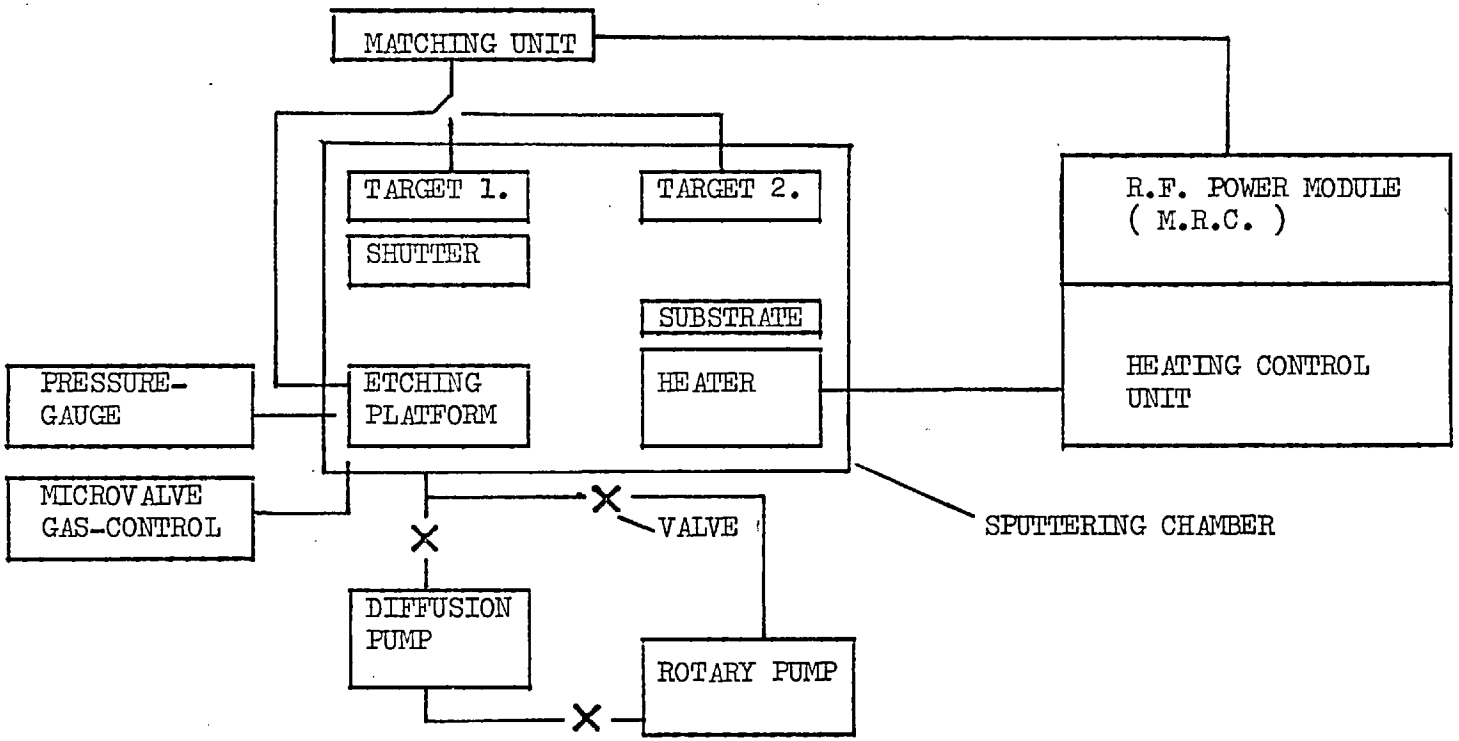

Fig. 5.2 BLOCK DIAGRAM OF R.F. SPUTTERING UNIT

the material target. The specimen is then moved into position below the target of the sputtering material.

The technical notes on the sputtering of piezoelectric materials are given in Table 5.1. The same conditions were applied to CdS and ZnO, expect that only pure argon gas was used for CdS deposition. The 10% oxygen in mixture with 90% argon was used to provide an oxygen-rich atmosphere in the sputtering chamber and to compensate any possible loss of oxygen atoms during their release. It was found that the ZnO film was relatively more stable than the CdS film in the sense that the film did not disintegrate after deposition on the substrate. This may be attributed to the result of reactive sputtering, whereby chemical reaction takes place during deposition. However, a slower deposition rate and/or a higher elevated substrate temperature was found to be useful means for obtaining good quality film. The quality of the sputtered films of ZnO and CdS on Si and Ge respectively are found to be crystalline and highly oriented. The electron diffraction pattern of these films are revealed in Figs. 5.3a and 5.3b. It is seen that the c-axis of the hexagonal crystal of ZnO and CdS is parallel to the surface of the substrate, and confirmed for all depositions. This phenomena may be well demonstrated by the article written by J C. Anderson et al, 1970, in 'Structure and Growth of Oriented Tellurium Thin Film'. Lastly, it must be added that the crystalline films were found to have high resistivity in the typical region of 10^6 ohm measured directly at the interdigital transducer having 12 finger pairs with 5.93 μm separation. Since it was thought that transducer with that value of resistivity was sufficient to excite the surface waves, no elaborate measurement of resistivity of the film was made in a more accurate way.

TABLE 5.1

TECHNICAL NOTE ON R.F. SPUTTERING

Target material	CdS, ZnO
Substrate material	Ge, Si
Vacuum pressure	1.0 10^{-6} torr
Argon pressure	4.0 10^{-3} torr (10% oxygen 90% argon for ZnO)
Substrate temperature	200°C
Electrode voltage	2.0 kV
R.F. power	260 Watt
Deposition rate	1.2 μm/hour for CdS 0.6 μm/hour ZnO

Note: In both situations, the substrate is placed in vacuum and heated at 200°C for over 12 hours before deposition.

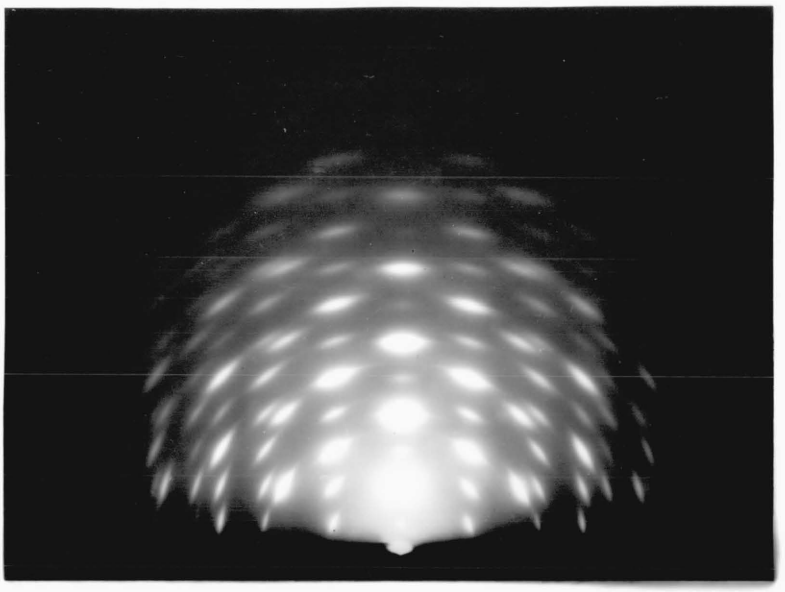

(a) c-AXIS OF ZnO FILM IS IN THE PLANE OF Si SUBSTRATE

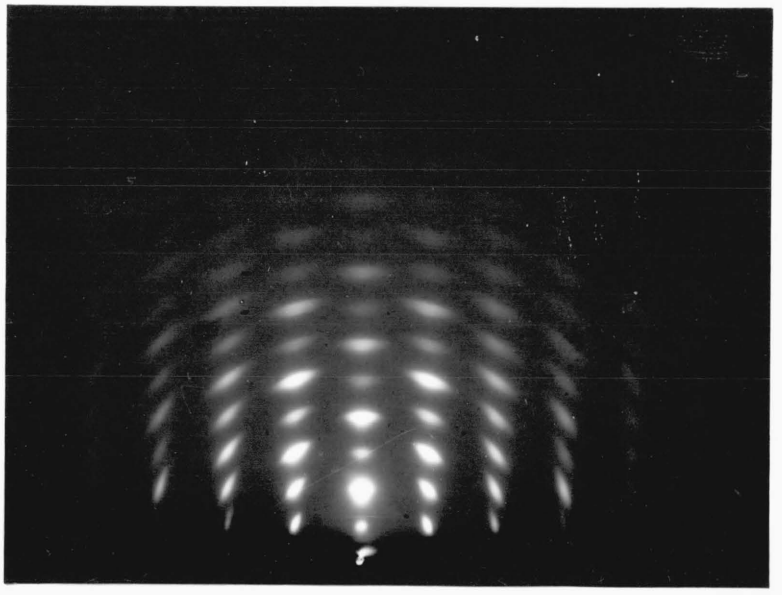

(b) c-AXIS OF CdS FILM IS IN THE PLANE OF Ge SUBSTRATE

Fig. 5.3 ELECTRON DIFFRACTION PATTERNS OF ZnO AND CdS CRYSTALLINE FILMS SEPARATELY DEPOSITED ON Si AND Ge SUBSTRATES

5.2 Fabrication of Interdigital Transducer

Several sets of interdigital masks were made with 2" x 2" Kodak high resolution plates and the original art work was drawn and cut on Rubylith film. The required pattern was obtained by removing one of the two layers of the Rubylith film. Figs. 5.4 and 5.5 show the patterns of the interdigital electrodes. The physical dimension of the pattern was initially estimated and calculated from the actual size intended for the interdigital electrodes. The total reduction was carried out in stages after evaluation from special instruments made by D.W. Mann Company, U.S.A. A ten-fold reduction was made with the Mann-Type 1003 camera followed by second and third reductions of ten- or three-fold by the Mann-Type 1080 photorepeater. To ensure interdigital electrodes with long finger and extremely narrow separation, the art pattern in Fig. 5.5 was used. The various parts (a,b and c) were accurately laid out such that their relative separations were precisely known. At the second reduction, the various parts were carefully manipulated into the desired positions. With multi-exposures of those parts, the required interdigital pattern was formed. By trial and inspection, the mask such as that for 12 finger pairs was achieved with extreme good definition for 2.45 μm separation in 1.5mm length. The different masks for the interdigital electrodes are shown in Table 5.2. The suitable mask for the zinc oxide overlay silicon, in view of 100 MHz as the operating frequency, was that with 5.93 μm separation. On each specimen of ZnO/Si structure,(see Fig. 5.8b), there are four transducers equally spaced at an interval of 0.5mm.

In Figs. 5.6a and 5.6b, the photographs show the top view of the

TABLE 5.2

A LIST OF PHOTOGRAPHIC MASKS

Size	Finger separation (μm)		Finger length (mm)
	dark-line	bright-line	
large	7.28	8.94	5.0
medium	5.93	5.93	1.0
small	4.99	4.57	1.4
smallest	2.45	2.45	1.5

Note: Separation between each adjacent interdigital pattern is 0.5 cm.

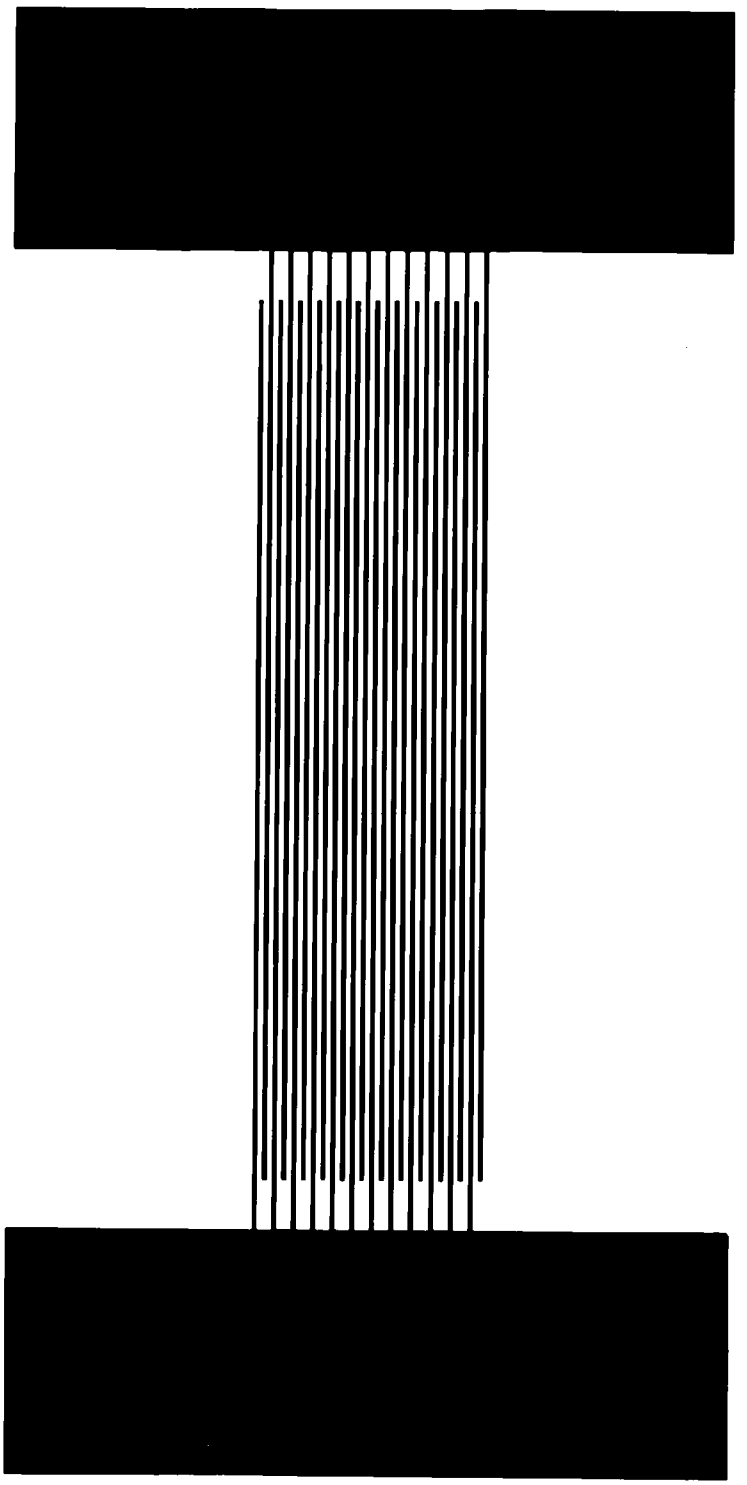

Fig. 5.4 A REDUCED COPY OF THE ORIGINAL INTERDIGITAL PATTERN

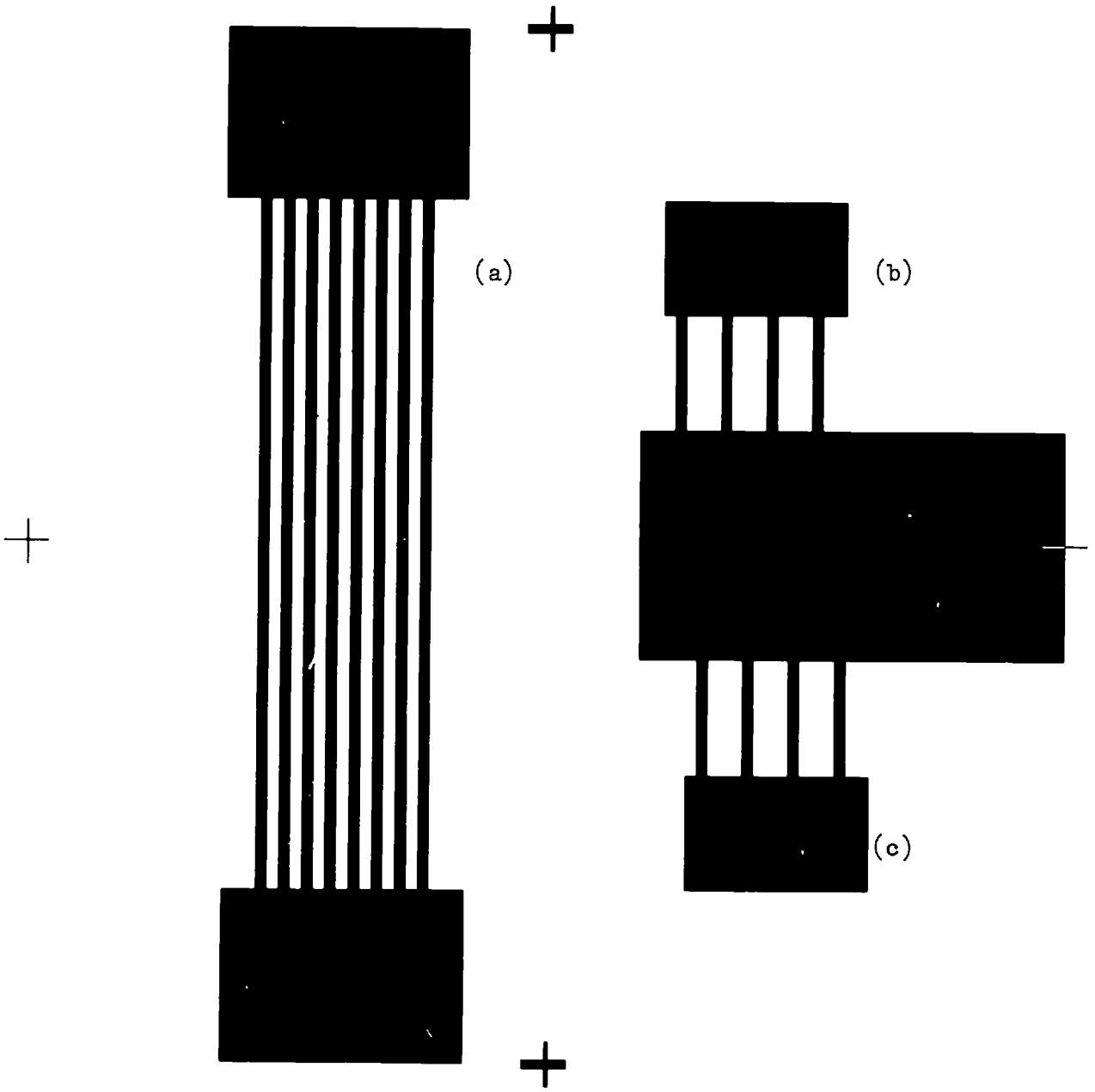

Fig. 5.5 A REDUCED COPY OF THE ORIGINAL INTERDIGITAL PATTERN WHICH IS DIVIDED INTO THREE SECTIONS a, b AND c

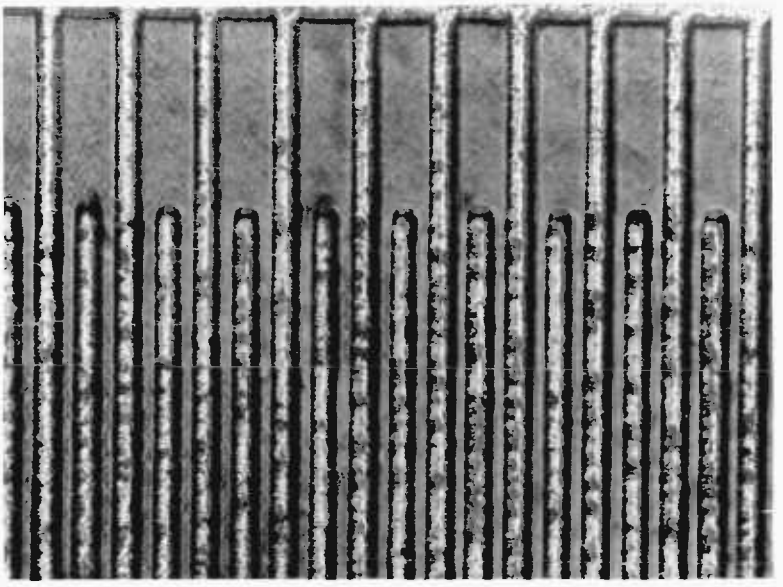

(a) INTERDIGITAL TRANSDUCER WITH 5.93 μm ALUMINIUM ELECTRODES DEPOSITED AT THE INTERFACE OF ZnO CRYSTALLINE LAYER AND Si OXIDIZED SURFACE

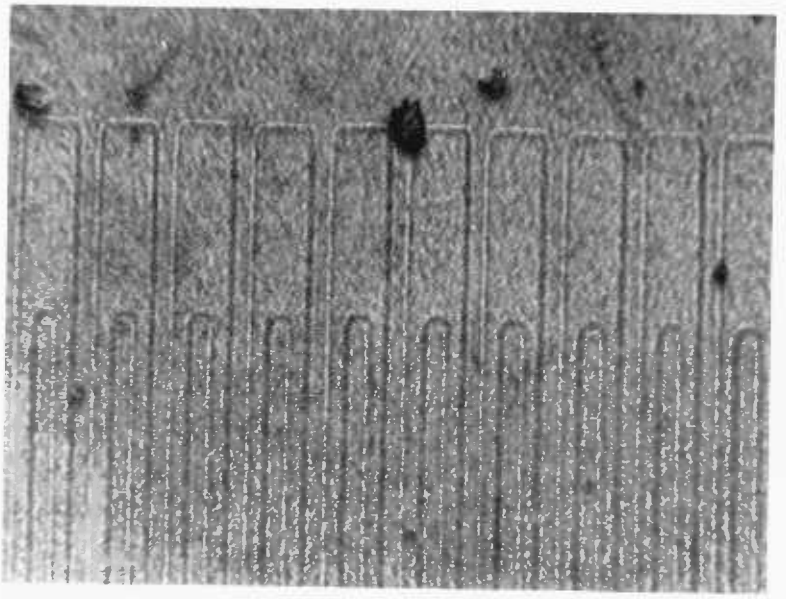

(b) SILICON (n-TYPE) INTERDIGITAL TRANSDUCER WITH 5.93 μm FINGER WIDTH OBTAINED BY THERMAL DIFFUSION INTO p-TYPE SILICON SUBSTRATE WITH ZnO CRYSTALLINE LAYER

Fig. 5.6 TOP VIEWS OF THE TWO DIFFERENT INTERDIGITAL TRANSDUCERS

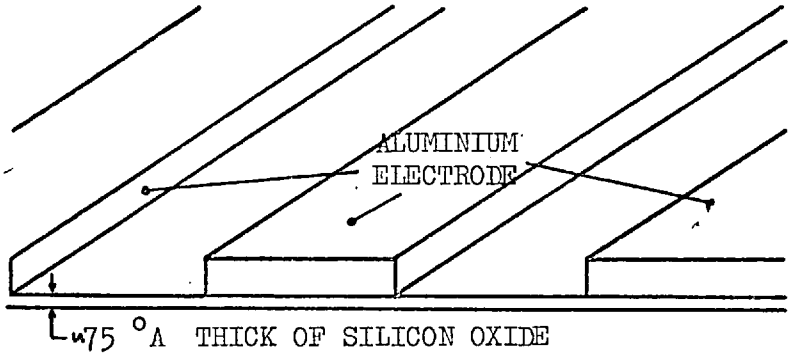

(a) INTERDIGITAL ALUMINIUM ELECTRODES DEPOSITED ON SILICON OXIDE SURFACE

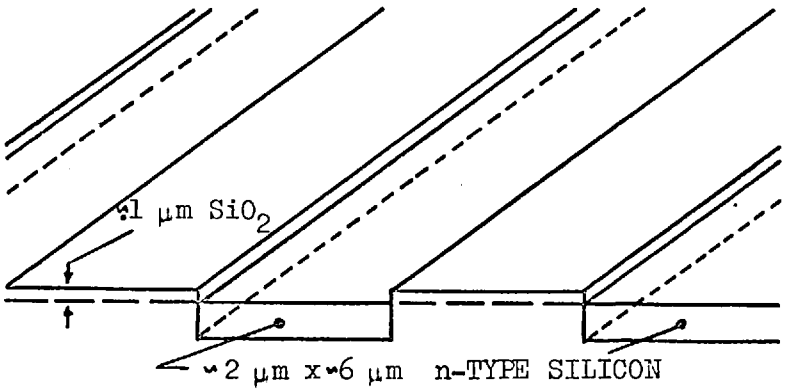

(b) INTERDIGITAL n-TYPE SILICON ELECTRODES ON p-TYPE SILICON SUBSTRATE

Fig. 5.7 SCHEMATIC PRESENTATION OF TWO INTERDIGITAL TRANSDUCERS FOR SURFACE ACOUSTIC WAVES

aluminium and n-type electrodes covered by a layer of ZnO. The difference between the two configurations is shown in Figs. 5.7a and 5.7b. In one case, aluminium electrodes were directly deposited on the thermally oxidized silicon film and in the other, the electrodes were actually n-type silicon interdigital fingers. The low resistive n-type electrodes were obtained through standard chemical diffusion process on the p-type silicon wafer which was commonly used for fabricating other microelectric components. H_2O and $POCl_3$ were used respectively as the dopants for the oxidized layer and n-type electrodes.

In order to increase the yield of the SAW (i.e. surface acoustic wave) device, a (6 x 6) matrix of the interdigital electrodes was made on each silicon wafer (see Fig. 5.8a). At each appropriate step in the fabricating process, the SAW device was carefully examined to eliminate any serious defect. It was found useful to inspect the aluminium electrodes at intervals during chemical etching, since the deposited thickness of aluminium was slightly different on different silicon wafers. At the same time, the unwanted aluminium in-between the electrodes could be detected and removed by further etching. It may be worthy of note that the etchant for aluminium consisted of Ortho-phosphoric acid (80 ml.), Nitric acid (4 ml.) and deionized water (18 ml.). To reduce the viscosity of the etchant, it was used at the elevated temperature of $30^{\circ}C$. If the photoresist (e.g. Shipley AZ-1350H) was properly applied for masking the aluminium electrodes, three or four inspection intervals could be done without damaging the photoresist layer. From experience the author found that it was essential to carry out the device fab-

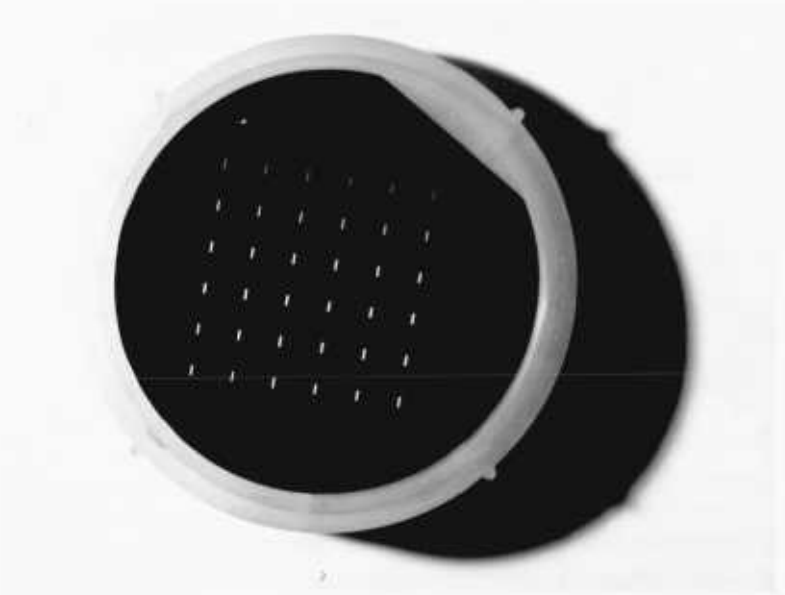

(a) A (6x6) MATRIX OF INTERDIGITAL ALUMINIUM ELECTRODES DEPOSITED ON SILICON WAFER

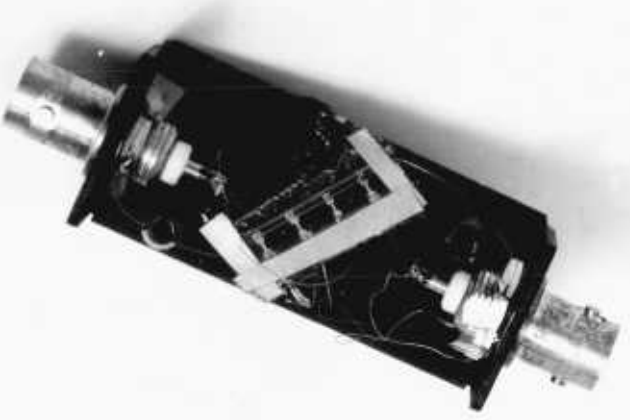

(b) A VIEW OF THE SAW DEVICE WITH FOUR INTERDIGITAL TRANSDUCERS EQUALLY SPACED AT 0.5 cm

Fig. 5.8 DISPERSIVE SAW DEVICE

rication in dust-free surroundings, because the sizes of the dust were normally larger than that of the electrode spacings.

5.3 Insertion Loss of the SAW Transducer

In the experimental work, main effort was directed especially to the fabrication and testing of the two aforementioned interdigital transducers. Two different patches of specimens were deposited with ZnO film under the same physical conditions and later the devices were tested with the experimental arrangement as indicated in Figs. 5.8b and 5.9. It should be mentioned that the author failed to excite any surface wave on those specimens with the n-type silicon electrodes, but wave transmitted by the aluminium electrode was easily detectable when operating frequency of the R.F. pulse generator was scanned over a frequency range near resonant-frequency of the transducer. The insertion loss of the transducer in the frequency range near self-resonance is deduced from Fig. 5.10 and the results are plotted in Fig. 5.11. The minimum loss is approximately 70 dB. This loss was also found to be typical for all transducers and by Hickernell, 1971, on ZnO transducers. The characteristics of the transducer are not modified by any external component.

A simple equivalent circuit for the transducer, as shown in Fig. 5.12, is considered to consist of a 'static' capacitance in parallel with a series RCL resonant circuit. The resistance is regarded to have two parts in parallel: a d.c. resistor and a radiation resistor. The latter delivers the radiated acoustic power. Using the equivalent circuit, it may be shown that the magnitude of the radiation resistor is that on the resistance-curve at resonant frequency. Off the region of the self-resonance, the capacitance-curve determines

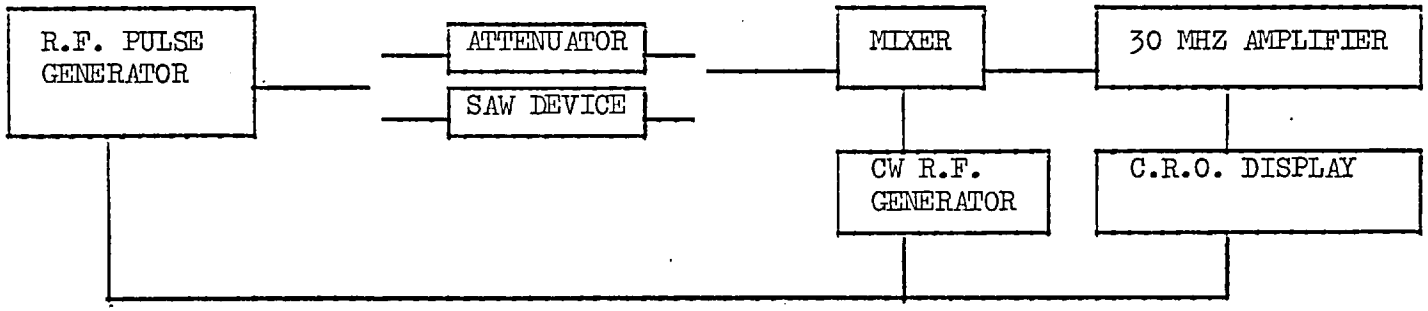

Fig. 5.9 BLOCK DIAGRAM OF EXPERIMENTAL MEASUREMENT ON SAW DEVICE

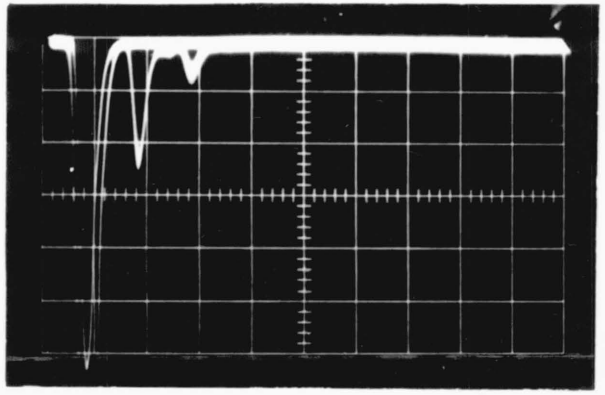

Freq. = 122 MHz ; Ref. pulse = -80 dB

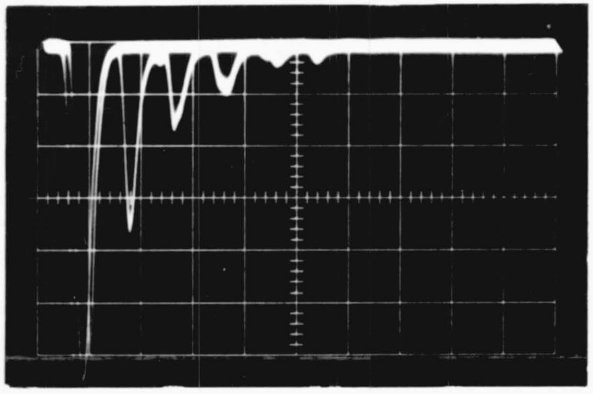

Freq. = 126 MHz ; Ref. pulse = -74 dB

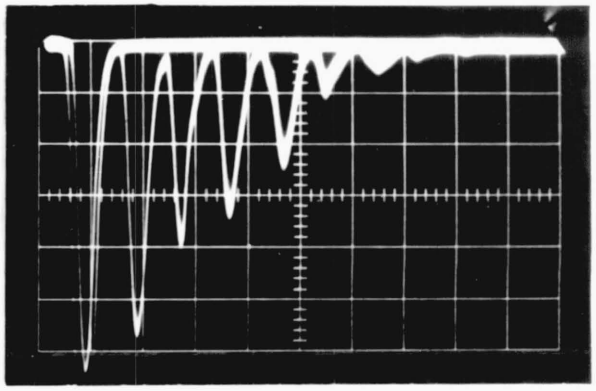

Freq. = 130 MHz ; Ref. pulse = -73 dB

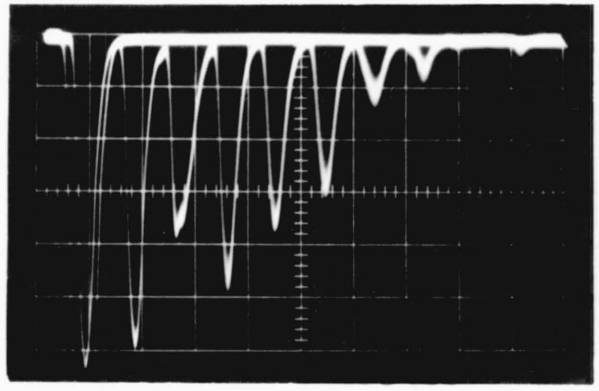

Freq. = 134 MHz ; Ref. pulse = -72 dB

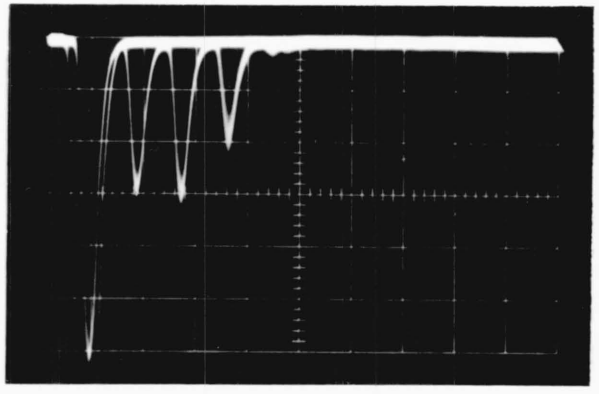

Freq. = 138 MHz ; Ref. pulse = -72 dB

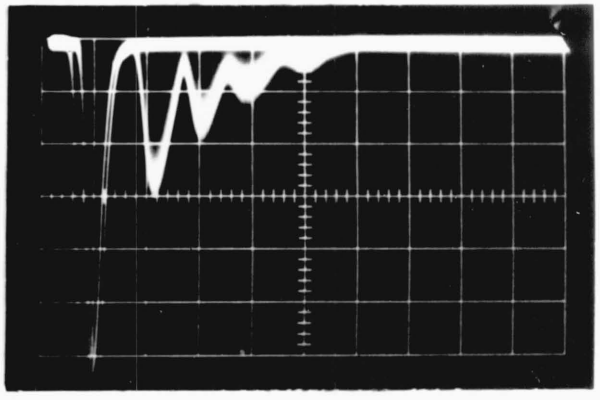

Freq. = 142 MHz ; Ref. pulse = -70 dB

Fig. 5.10 FREQUENCY RESPONSE OF A SAW TRANSDUCER WITH INTERDIGITAL ALUMINIUM ELECTRODES DEPOSITED AT THE INTERFACE OF ZnO LAYER AND OXIDIZED SILICON SUBSTRATE

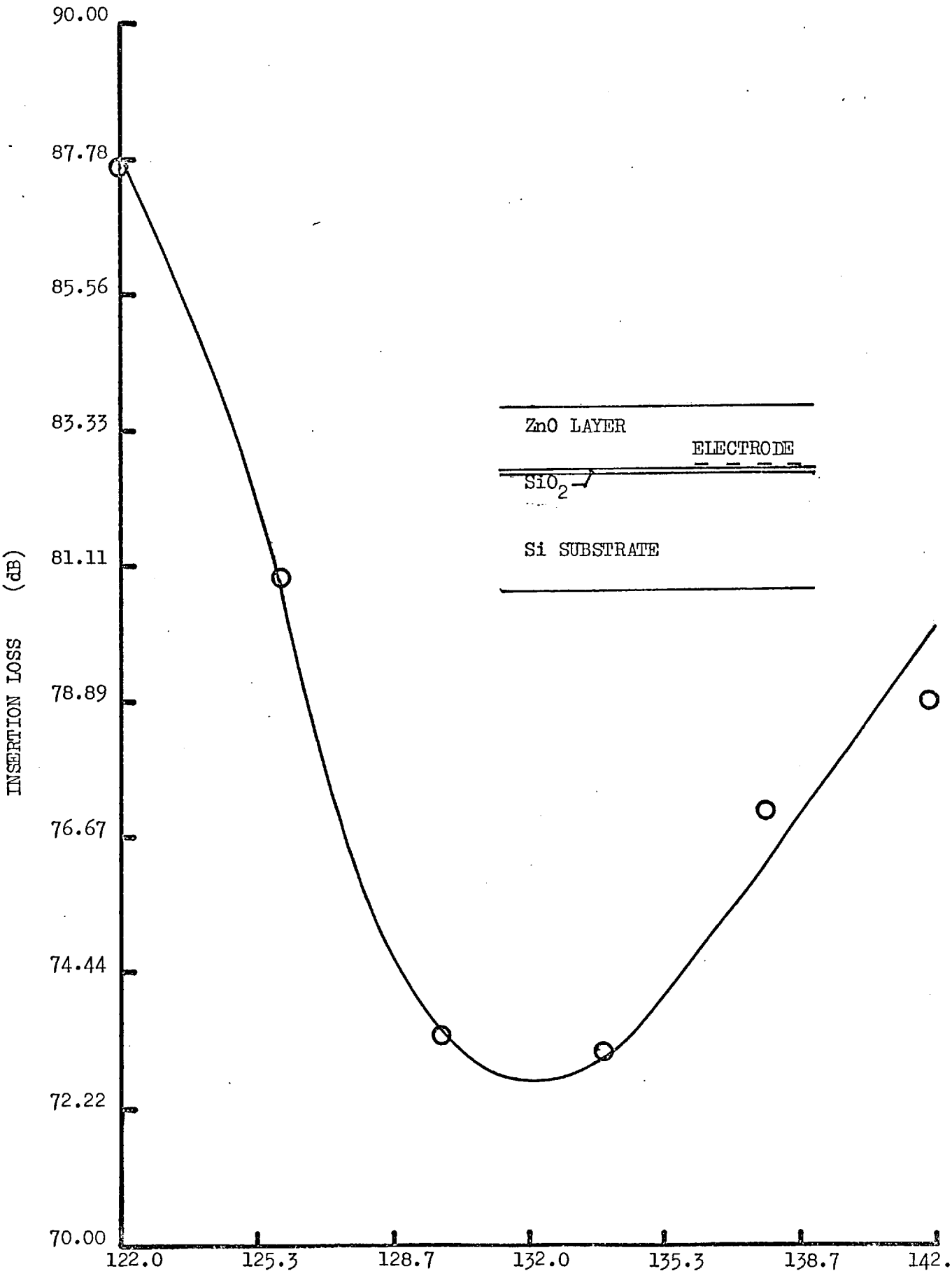

Fig. 5.11 INSERTION LOSS OF A SAW TRANSDUCER IN A FREQUENCY RANGE NEAR SELF-RESONANCE

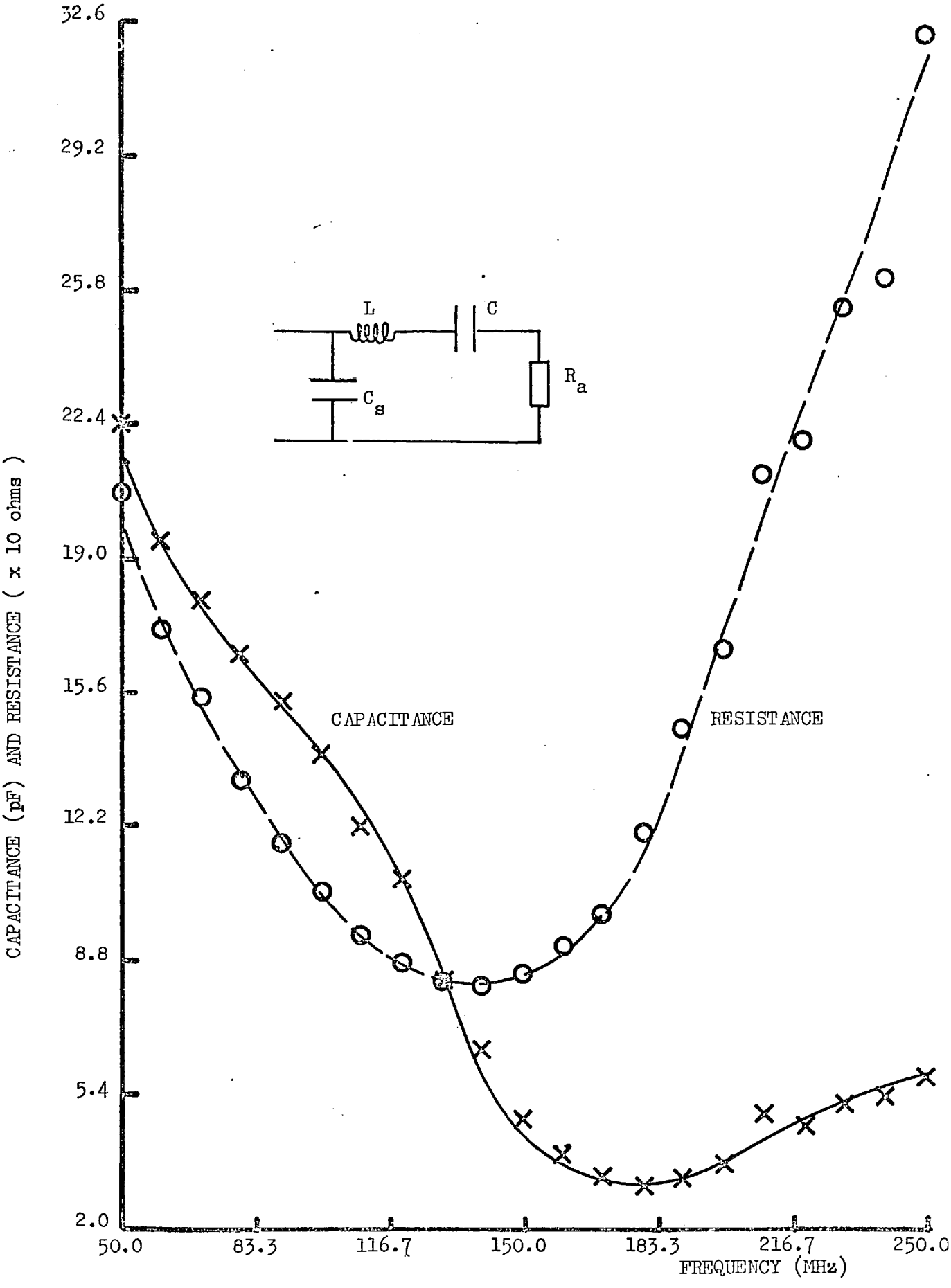

Fig. 5.12 ADMITTANCE OF A SAW TRANSDUCER IN A FREQUENCY RANGE NEAR SELF-RESONANCE

the 'static' capacitance due to the interdigital electrode. Hence, knowing the number of the periodic pairs of the electrodes, it is possible to calculate the electromechanical coupling constant, K_p, of the transducer. If the following expression is taken to be accurate (W R Smith et al, 1969):

$$K_p^2 = 1/ (8 f_o R_a C_s N)$$

where f_o = the resonant frequency of the transducer,

R_a = the radiation resistance at resonant frequency,

C_s = the capacitance of the interdigital electrodes and

N = the number of periodic pairs of the electrodes,

the coupling constant is estimated to be equal to 0.124 for 0.25 (H/λ). The coupling constant experimentally obtained by Hickernell, 1971, 1972, was between 0.005 and 0.025 within the ratio, H/λ, of 0.01 and 0.35. From the above estimation of the electromechanical coupling and with the view that the ZnO crystalline film is highly oriented, it may be said that little modification could be made to improve the quality of the ZnO film by varying the R.F. sputtering conditions. If that is the case, other improvements should be made with an analysis of the transducer layout with the aid of a better electrical equivalent circuit.

5.4 Comments

The experience gained from the experimental procedures described have suggested ideas for improvement of experimental techniques. The features of significance are the thin film deposition, the electrode efficiency and the frequency bandwidth of the surface wave transducer:

1. The use of a 'catalysing' layer is to promote a suitable angle

of deposition of the film with respect to the substrate so as to obtain a desired film orientation (M Nagao, 1966; N F Foster, 1965 & 1969). A knowledge of the orientation enables the mode of the layer wave to be predicted.

2. In order to obtain better pattern definition of the interdigital electrodes, it is proposed that 'sputter-etching' be employed instead of chemical etching. This procedure avoids 'under-cutting' of the deposited electrodes and possible erosion of the substrate surface, but care has to be exercised in avoiding the decomposition of the photoresist layer in the presence of the discharge plasma.

3. The reason for the non-existence of a detectable surface wave when using n-type silicon electrodes on p-type low resistive silicon substrate, has been thought to arise from a low value of the substrate/layer resistivities and the consequent liability of leakage currents. This hazard may be eliminated by the use of dielectric insulator between the layer electrode and the substrate.

4. In order to reduce the undesirable R.F. coupling between the electrodes and the substrate, it is desirable to obtain a thicker silicon oxide layer directly beneath the electrodes. However, the oxide layer is kept thin in the wave-path between electrodes so as to permit stronger coupling between wave in piezoelectric layer and drift electrons on substrate when the latter is d.c. biassed.

5. From section 5.3, it is clear that at self-resonance an acoustic transducer can simply be regarded as a 'static' capacitance in parallel with a radiation resistance. In order to deliver or extract electrical power at radio frequency, the electrical impedance of the transducer should be matched with the other connected electrical systems. Since maximum transfer of electrical power requires conjugate impedance matching between any two systems, it is therefore necessary to match the resistive part of the transducer impedance with that of the system. A tunnel diode with suitable d.c. biassing provides negative resistance (W J Getsinger, 1963; J O Scanlan et al, 1964 & 1965). This resistance can be used in parallel with the transducer resistance to give a 50 ohm terminal impedance if all reactive components are cancelled with their counterparts which are externally added to the transducer.

6. Reactance compensation methods may be used to increase the electric tuning range of a solid state oscillator and it is similarly possible to extend the frequency bandwidth of a transmitting transducer and also to improve the gain-bandwidth product of receiving transducer when both transducers are incorporated with tunnel diodes (R M Fano, 1950; B L Humphreys, 1964; K Kurokawa, 1969). It should be noted that a tunnel diode is suggested because it is easy to use as a device and only requires d.c. supply source.

CONCLUSION

Since an exact description of wave propagation in the layered system is not possible, an analytical numerical method (see chapter 3) is used. The present approach treats a mechanical surface wave as one having three particle displacements. In order to include the piezoelectric property, a relation is established between the strain amplitude and the associated potential amplitude (see Appendix A 2).

The present computer programme is not able to give a full analysis for attenuated waves because only the wave vector normal to the plane interface is regarded as complex. By using a multi-search method for three complex wave vectors of an attenuated surface wave, the computer programme can easily be changed for studying an attenuated surface wave. The other feature is that in all calculations, the required information only involves the physical constants of the crystal, the specified wave propagation direction and the wave-depth penetration.

An attempt is made to use low resistive silicon electrodes for the excitation of surface waves and a reason is given in chapter 5 comments for failing to detect any surface wave. The insertion loss is also very high for aluminium electrodes on a silicon oxide surface, and thus no further measurements were carried out for this layered system. However, an improvement for reducing this insertion loss is also given in the chapter 5 comments. Apart from the electrode lay-out giving rise to high insertion loss, the quality of the ZnO crystalline film is good. The author, on reflection, feels that more time should have been given to improving the acoustic surface wave device.

As for the theoretical studies, the numerical approach has proved to be useful for giving a fair understanding of the layer problem. Since it is shown that wave propagation is affected by a conducting (earthed) film deposited on the piezoelectric free surface or layer interface, the author feels that further studies in theory and experiment can be focussed on the change of wave propagation behaviour when the conducting film is biassed at different values of electric potential.

In looking ahead there are other possibilities of acoustoelectric interactions:

1) The surface wave amplication by charge carriers in layered piezoelectric semiconductors.
2) The convolution or correlation integral of signals in a layered system.

APPENDIX A 1

PIEZOELECTRICALLY STIFFENED ELASTIC CONSTANTS

From the necessary Eqs. 2.4, 2.5 and 2.9 /13, for the piezoelectric crystal, the following two expressions are obtained:

$$\rho V^2 \alpha_j = C_{ijkl}\, \alpha_k\, l_i l_l + e_{nij}\, \alpha_4\, l_i l_n \; ; \; i,j,k,l,m,n,p,q = 1,2,3$$

$$0 = e_{mkl}\, \alpha_k\, l_m l_l - \varepsilon_{pq}\, \alpha_4\, l_p l_q$$

By combining them, they become:

$$\rho V^2 \alpha_j = \left(C_{ijkl} + \frac{e_{nij}\, l_n\, e_{mkl}\, l_m}{\varepsilon_{pq}\, l_p l_q} \right) l_i l_l\, \alpha_k$$

$$= C'_{ijkl}\, l_i l_l\, \alpha_k$$

$$\text{Thus } C'_{ijkl} = C_{ijkl} + \frac{e_{nij}\, e_{mkl}\, l_n l_m}{\varepsilon_{pq}\, l_p l_q}$$

APPENDIX A 2

PHYSICAL SIGNIFICANCE OF ELECTROMECHANICAL AMPLITUDE RATIO

In a piezoelectric crystal, the crystalline stresses, T_{ij}, and the electric displacements, D_i, can be produced by applied strain and electric fields in a direct manner through the material constants as indicated in the linear piezoelectric constitutive relations (Eqs. 2.12 and 2.13). If the totality of the contributory charges and the crystalline stresses in an elementary volume of crystal is conserved and considered to have zero value, the equations of electrostatic charge and stress motion can be respectively expressed as:

$$D_{i,i} = 0 \quad \text{and} \quad T_{ij,i} = 0 \quad ; \quad i,j = 1,2,3$$

Within the context of the above proposition, the physical state of the crystal can be described strictly as electrically static and mechanically unstrained. In a slow process the free-energy of the crystal interchangeable between the strain and electric fields is conservative and independent of time.

In the present approach, the amplitude of the electric potential, α_4, is considered as a scalar quantity. The electric polarization obtainable in the crystal merely depends on the effective piezoelectric coupling. From the Eqs. 2.12 and 2.13, and with the above two assumptions, the following expression is obtained:

$$\begin{bmatrix} C_{ijkl}\, l_l l_i & , & e_{kij}\, l_k l_i \\ e_{lij}\, l_l l_i & , & -\varepsilon_{ik}\, l_k l_i \end{bmatrix} \begin{bmatrix} \alpha_k \\ \alpha_4 \end{bmatrix} = 0 \quad ; \quad i,j,k,l = 1,2,3$$

where C_{ijkl}, e_{kij} and ε_{ik} are the material constants, l's, the direction cosines and α_k and α_4 are respectively the mechanical and potential

amplitudes. It is well known that crystalline stresses can be induced in the piezoelectric crystal, not only through applied strain field but also by applied electric field. An estimate of the partial stress contribution by the electric field can be obtained, if there is a conversion factor for the two fields. At this juncture, it is obvious that the conversion factor would be a ratio of the separate normalizing factors for the variable amplitudes α_k and α_4. Following the same line of thought, the electric field, E_k can be generally expressed in a power series of strain, S_{kl}, as given below:

$$E_k = c_l S_{kl} + c_{lm} S_{kl} S_{km} + \text{HIGHER POWER TERMS}$$

where c's, the various coefficients of strain can be regarded as the constants of characterization between the electric field E_k and the mechanical strain S_{kl}.

For infinitely small amplitudes in E_k and S_{kl}, the first term of the power series is only of consequence. Therefore, let us consider merely the following relation:

$$E_k = c_l S_{kl}$$

By substituting the Eqs. 2.10 and 2.2 into the above expression, we have:

$$-\phi_{,k} = \tfrac{1}{2} c_l \left(U_{k,l} + U_{l,k} \right)$$

Due to crystal symmetry, k and l are interchangeable. Subsequently, by substituting in Eqs. 2.9 and 2.5, we have:

$$-\alpha_4 = c_k \alpha_k \quad ; \quad k = 1,2,3$$

Apart from squaring both sides of the above expression, let us assume

that c_1, c_2 and c_3 are all equal to a constant, α_o. This assumption is justifiable in a situation whereby the electric polarizability in the piezoelectric crystal is linearly related to the particle displacement of any mechanical deformation. In what follows, the electromechanical amplitude ratio, α_o, is therefore defined in a simple form such as:

$$\alpha_o = \frac{|\alpha_k|}{|\alpha_4|}$$

where $|\alpha_k|$ and $|\alpha_4|$ are respectively the normalising factors for the strain and electric fields. The magnitudes of α_k and α_4 are determined by the material constants as previously indicated in the matrix.

APPENDIX A 3

CONCEPT OF COMPLEX PLANE WAVE

The term, 'complex' is inferred from the fact that the wave vector, $\bar{k}$, and the angular frequency, ω, of a wave can become complex quantities. In any case, the wave would propagate with a variation in amplitude and phase which are dependent upon the imposed boundary constraints of the physical system. In the present studies of mechanical surface waves, it implies an inhomogeneous plane wave propagating with a complex wave vector. The components of the wave vector can be represented by the wave number and the respective direction cosines with reference to the co-ordinate axes. The angle of the direction cosine is equal to an angle plus a so-called 'phase' angle. Therefore, the direction cosines can be expressed as:

$$\bar{l}_1 = l_1^* + l_1^+ \quad , \quad \bar{l}_2 = l_2^* + l_2^+ \quad \text{and} \quad \bar{l}_3 = l_3^* + l_3^+$$

where the asterisk and the cross indicate respectively the real and imaginery parts of the direction cosine. If the wave vector is explicitly defined by the two angles θ and φ, as shown in Fig. 3.3, the direction cosines become:

$$l_1^* = \cos\theta \sin\varphi' \cosh\varphi'' \; ; \; l_1^+ = \cos\theta \cos\varphi' \sinh\varphi''$$

$$l_2^* = \sin\theta \sin\varphi' \cosh\varphi'' \; ; \; l_2^+ = \sin\theta \cos\varphi' \sinh\varphi''$$

$$l_3^* = \cos\varphi' \cosh\varphi'' \; ; \; l_3^+ = -\sin\varphi' \sinh\varphi''$$

where $\varphi = \varphi' + i\varphi''$ and θ remains as real number.

Let us consider the following expression for the mechanical displacement of a plane harmonic wave which contains the co-ordinate axes

denoted by x_i and with the time varying term indicated by t:

$$A = A(\omega) \exp ik (l_i x_i - Vt)$$

where $A(\omega)$ = wave amplitude depending on angular frequency,

k = wave number and

V = wave velocity.

Using the previously defined direction cosines, the plane wave solution takes the form:

$$A = A(\omega) \exp ik (l_i^+ x_i) \exp ik (l_i^* x_i - Vt)$$

This describes a wave which propagates in the direction specified by l_i^*, with a varying amplitude ruled by l_i^+. Moreover, the planes of equal amplitude and those of equal phase can be expressed by the two equations as:

$$l_i^+ = b_1 \quad \text{and} \quad l_i^* = b_2 \quad ; \quad i = 1,2,3$$

where b_1 and b_2 are constants. Since $l_i^2 = 1$, there exists a relation such as:

$$l_i^+ l_i^* = 0$$

This expression indicates the two families of planes of equal amplitude and equal phase are mutually orthogonal. From the above description, it is quite apparent that an inhomogeneous plane wave is relatively a more general form of the ordinary homogeneous plane wave. Hence, it is appropriate to mention that a complex plane wave is the generalized form of any plane wave.

To have further understanding of the wave with the complex direction cosines, let us look into an ideal case of the mechanical surface wave. The complex direction cosines can be defined as below:

$$l_1^* = \cos\theta \quad ; \quad l_1^+ = \cos\theta \cot\varphi' \tanh\varphi''$$

$$l_2^* = \sin\theta \quad ; \quad l_2^+ = \sin\theta \cot\varphi' \tanh\varphi''$$

$$l_3^* = \cot\varphi' \quad ; \quad l_3^+ = -\tanh\varphi''$$

As is easily seen, l_1^+ and l_2^+ are both dependent on $\bar{l}_3$ which is itself a function of the complex angle, φ. If φ' is only equal to 90° and φ'' is non-zero, the mechanical surface wave can be inherently described as:

(1) A wave that propagates on the plane $\{\cos\theta, \sin\theta, 0\}$, is totally undamped in amplitude except along the perpendicular direction to the plane.

(2) The wave propagation constant is equal to $-\tanh\varphi''$ which lies within the values of 0 and -1.

(3) The wave velocity, i.e. $V / \cosh\varphi''$, is always less than the velocity of propagation of an ordinary plane wave, V.

In general, l_1^+ and l_2^+ are not necessarily equal to zero unless φ'' is zero. The pseudo surface wave (H Engan et al, 1967; T C Lim, 1968) is a good illustration as in that case, all three direction cosines are complex. l_1^+ and l_2^+ are found to be extremely small in magnitude and hence there is a substantial amount of energy in the pseudo surface wave propagating near to the boundary interface. It is an unstable mode of the mechanical surface wave since the wave energy of the pseudo surface wave is not confined to the interface.

APPENDIX A 4

VARIOUS BOUNDARY CONDITIONS FOR DIFFERENT COMBINED CRYSTALS IN LAYERED STRUCTURE

In the present consideration of the mechanical wave propagation, the crystal can be considered as purely elastic, piezoelectrically stiffened or piezoelectric. Between the first two kinds, there is no difference in the number of boundary conditions, because the effect of piezoelectricity can be quantitatively included in the purely elastic constants giving the piezoelectrically stiffened constants. Basically, there are four areas of the different variations in crystals. Let us classify the various layered structures as below:

Type A : Piezoelectric Layer on Piezoelectric substrate,

Type B : Piezoelectric Layer on Elastic (or piezoelectrically stiffened) Substrate,

Type C : Elastic (or piezoelectrically stiffened) Layer on Piezoelectric Substrate and

Type D : Elastic (or piezoelectrically stiffened) Layer on Elastic (or piezoelectrically stiffened) Substrate.

Before proposing the respective sets of the boundary conditions for the above classification, it is essential to describe the 'characteristic' matrix which represents the required boundary condition equations. One may visualize the matrix with the following properties:

1. Each element in the matrix represents one component of a governing parameter (e.g. T_{ij}, D_i, U_j and ϕ) for the wave propagation.

2. Except for the zero elements, all other elements in each n column associate with a different Γ_3^n value and also for a different C^n, the weighting factors on the partial waves.

3. Each row represents a boundary condition equation. The number of the equations is equal to that of the Γ_3^n roots for the physical system.

4. To avoid repeatedly writing the equations for the classified types, it is necessary as references for understanding the various characteristic matrices, to have the information given in Tables A 4.1 and A 4.2.

5. In Type A and Type B, the order of the matrices can be reduced respectively to (12x12) and (11x11) in the situation whereby the conducting film is brought onto the free surface of the piezoelectric layer. This implies that all the elements of the last column and the last row would have zero value.

Finally, the various characteristic matrices for the different combined crystals in layered structure are given in the following pages which are respectively indicated by Types A,B, C and D.

TABLE A 4.1

LIST OF BOUNDARY CONDITIONS

Descriptions of Boundary Conditions	Basic Equations
Mechanical Stresses at Layer/Substrate	$_2T_{ij} = {}_1T_{ij}$
Mechanical Displacements at Layer/Substrate	$_2U_j = {}_1U_j$
Mechanical Stresses at Layer/Free Space	$_2T_{3j} = 0$
Electric Potentials at Layer/Substrate	$_2\phi = {}_1\phi$
Electric Potentials at Layer/Free Space	$_2\phi = {}_3\phi$
Electric Displacements at Layer/Substrate	$_2D_3 = {}_1D_3$
Electric Displacements at Layer/Free Space	$_2D_3 = {}_3D_3$

Note :

1. The lower left subscripts 1,2 and 3 indicate respectively the substrate, the layer and the free space above the free surface of the layer.

2. The electric potential is a scalar quantity and the electric displacement with the lower subscript, 3, infers the normal component of the electric displacement along the OX_3 direction.

TABLE A 4.2

BASIC BOUNDARY CONDITION EQUATIONS

1. Mechanical Displacements and Electric Scalar Potential in Crystal:

$$U_j = C^n \alpha_j^n \exp ik l_3^n x_3 \quad ; \qquad j = 1,2,3$$

$$\phi = C^n \alpha_4^n \exp ik l_3^n x_3$$

where n is respectively equal to 3 (or 6) and 4 (or 8) for the substrate and the layer.

2. Mechanical Stresses and Normal Electric Displacement in Crystal:

$$T_{ij} = (0.5\, C_{ijkl}\, f_1 + e_{kij}\, f_2)\, f_3 \quad ; \quad i,j,k,l = 1,2,3$$

$$D_3 = (0.5\, e_{3kl}\, f_1 - \varepsilon_{3k}\, f_2)\, f_3$$

where $f_1 = \alpha_k^n l_1^n + \alpha_1^n l_k^n$

$$f_2 = \alpha_4^n l_k^n$$

$$f_3 = C^n \exp ik l_3^n x_3$$

3. Electric Scalar Potential and Normal Electric Displacement in Free Space:

$$\phi = C_o \left(\sinh k(h - x_3) / \sinh kh\right)$$

$$D_3 = -i\, \varepsilon_o\, C_o \left(\cosh k (h - x_3) / \sinh kh\right)$$

Note: It is necessary to mention that at the plane interface between the layer and the free space, T_{ij} become T_{3j}.

TYPE A

PIEZOELECTRIC LAYER ON PIEZOELECTRIC SUBSTRATE

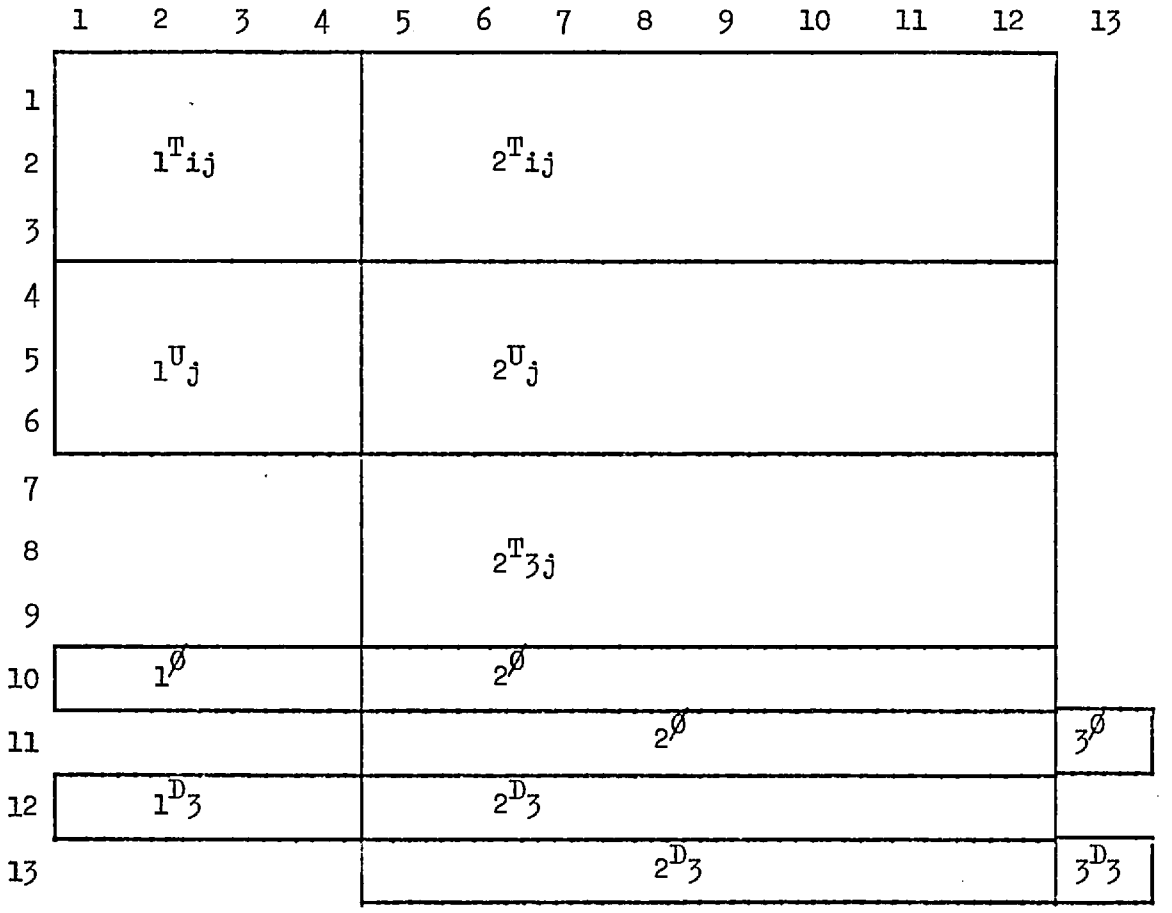

TYPE B

PIEZOELECTRIC LAYER ON ELASTIC (OR PIEZOELECTRICALLY STIFFENED) SUBSTRATE

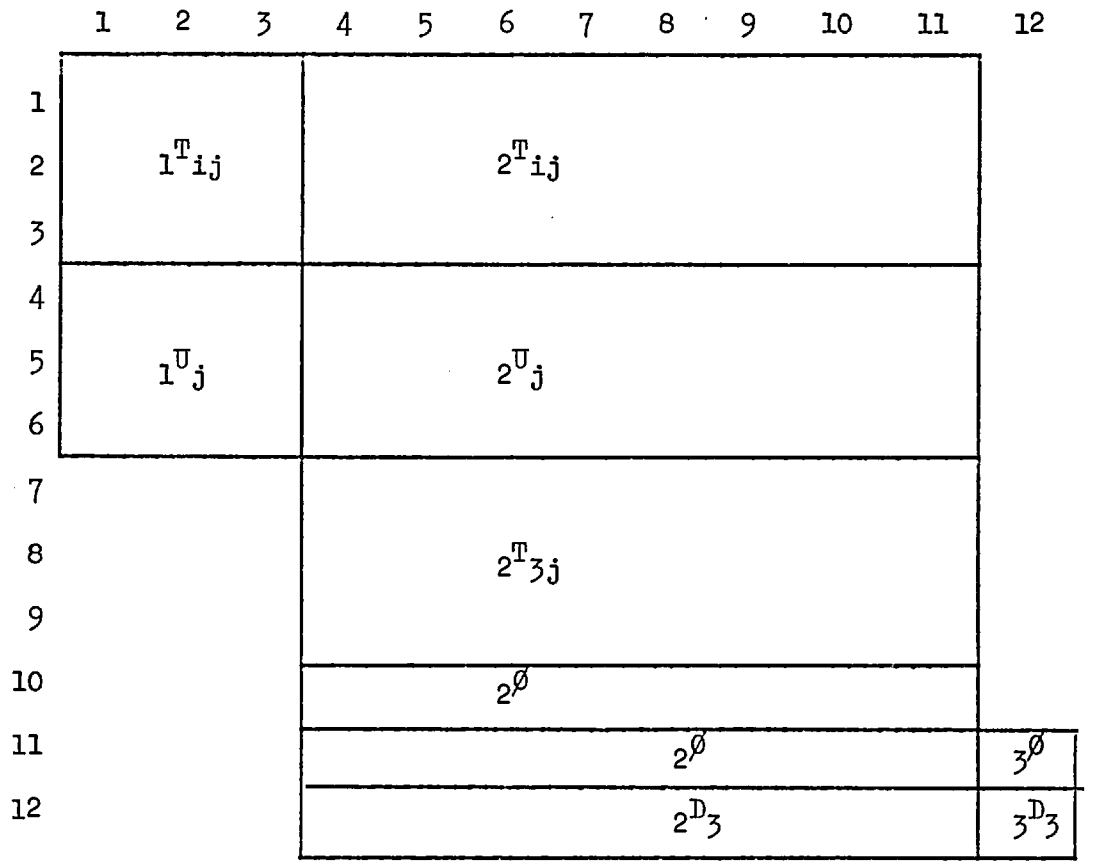

TYPE C

ELASTIC (OR PIEZOELECTRICALLY STIFFENED) LAYER ON PIEZOELECTRIC SUBSTRATE

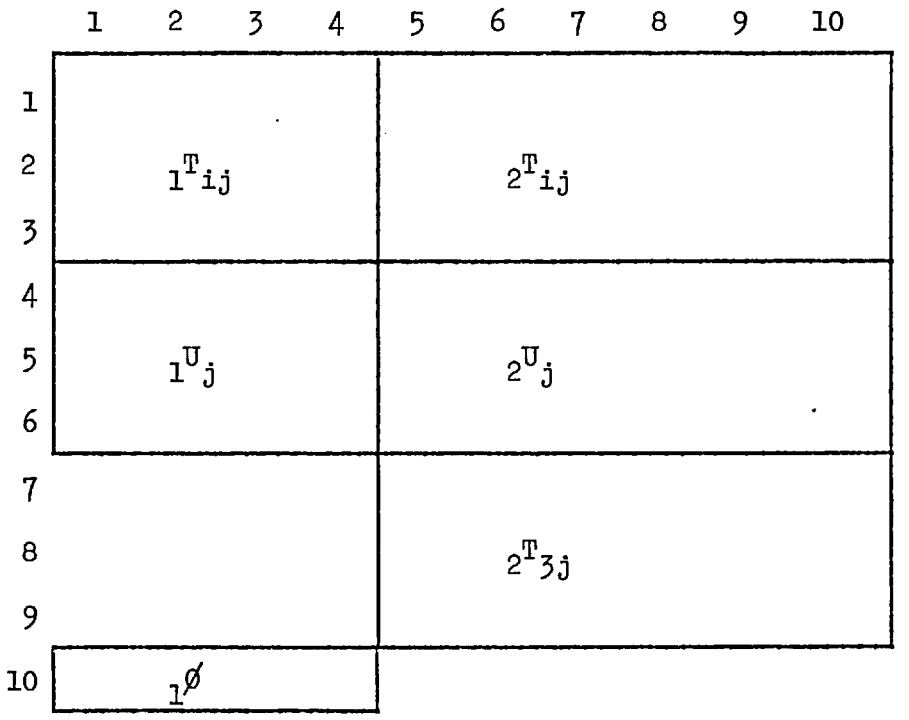

TYPE D

ELASTIC (OR PIEZOELECTRICALLY STIFFENED) LAYER ON
ELASTIC (OR PIEZOELECTRICALLY STIFFENED) SUBSTRATE

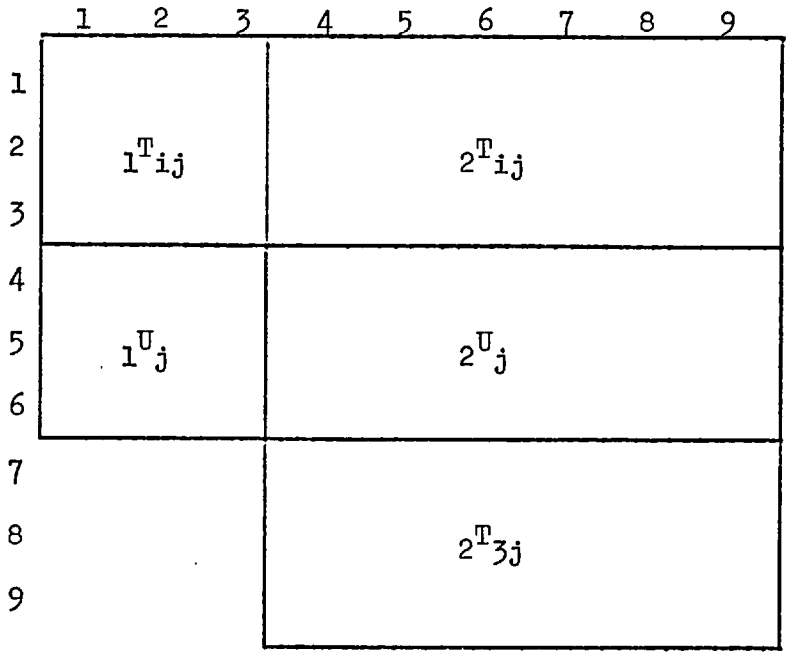

APPENDIX A 5

ELECTRIC POTENTIAL ABOVE FREE SURFACE OF PIEZOELECTRIC CRYSTAL

In this section, a plane metal earthed film is located parallel with and above the free surface of the crystal (see Fig. 3.6). In order to determine, at a given instant, the electric potential acquired by the film, we will be concerned with:

1. The region between the conducting film and the free surface.
2. The variation of the electric field along the OX_3 direction.

For simplicity the constant part of Eq. 3.5 is omitted and so it may be written as:

$$\phi = A_n \exp ik\, l_3^n\, x_3$$

where A_n are the amplitudes, the values for l_3^n are $\pm i$, and so the electric potential becomes:

$$\phi = A_1 \exp -kx_3 + A_2 \exp kx_3$$

In this case, the required boundary conditions for the electric potential are:

$$\phi = 0 \text{ for } x_3 = h \text{ and } \phi = C_o \text{ for } x_3 = 0$$

where h is the height of the conducting film above the free surface of the piezoelectric crystal and C_o is a measure of the effective electric potential at the free surface of the crystal. By applying the given boundary conditions, the following equations are obtained:

$$A_1 \exp -kh + A_2 \exp kh = 0$$

$$A_1 + A_2 = C_o$$

By combining the above equations, the two amplitudes are:

$$A_1 = (C_o \exp kh) / (2 \sinh kh)$$

$$A_2 = (-C_o \exp -kh) / (2 \sinh kh)$$

Including the omitted terms of Eq. 3.5, the final expressions for the electric scalar potential, ϕ, and also the corresponding normal electrical displacement, D_3, are:

$$\phi = C_o (\sinh k(h-x_3) / \sinh kh) \exp ik(l_1x_1 + l_2x_2 - Vt)$$

$$D_3 = -i \varepsilon_o C_o (\cosh k(h-x_3) / \sinh kh) \exp ik(l_1x_1 + l_2x_2 - Vt)$$

APPENDIX A 6

COMPUTER PROGRAMME "SNOOPY"

The programme involves six basic calculations: solving for the eigen values and eigen vectors of a complex matrix, expressing the complex matrix as a characteristic polynomial, extracting the roots of the polynomial, applying search method for a wave velocity and establishing the required determinant of the boundary-conditions.

The mathematical manipulations are carried out in more than 3000 statements in the programme "SNOOPY". The programme takes approximately 9.4 sec. to be executed by the Minnesota Fortran Compiler in the Control Data Corporation 6600 computer. To evaluate a wave velocity, approximately 0.25 sec. and 0.82 sec. are respectively required to compute for a half-space and a layered half-space. If the media are regarded as purely elastic, the computing time is relatively reduced as there are fewer roots from the polynomial to be used in the determinant of the boundary condition. Since the programme is lengthy, a listing is not included in the thesis, but a brief description is given in the following four parts:- block diagram, implementation, control instructions and data entering sequence.

BLOCK DIAGRAM OF PROGRAMME "SNOOPY"

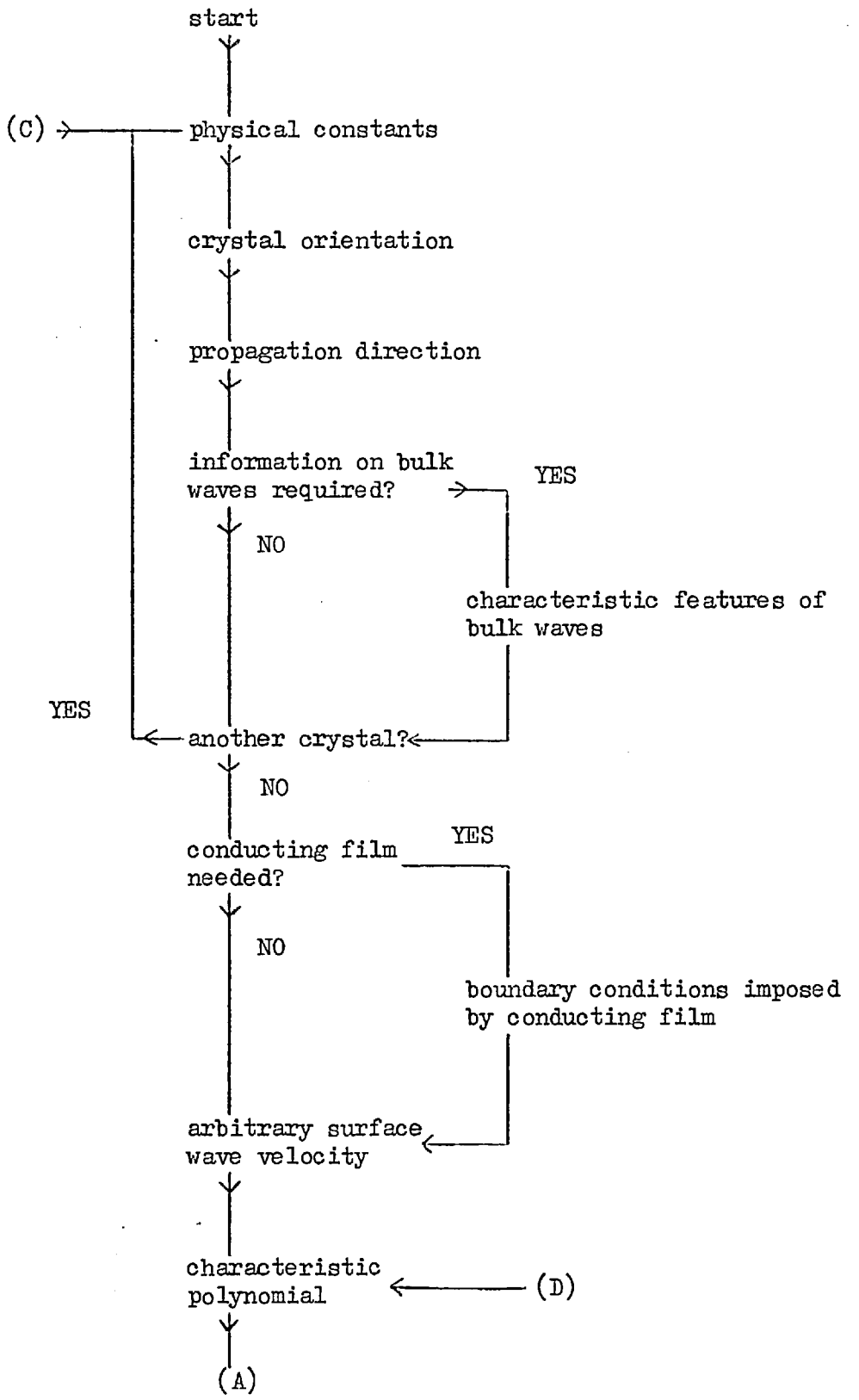

Contd....

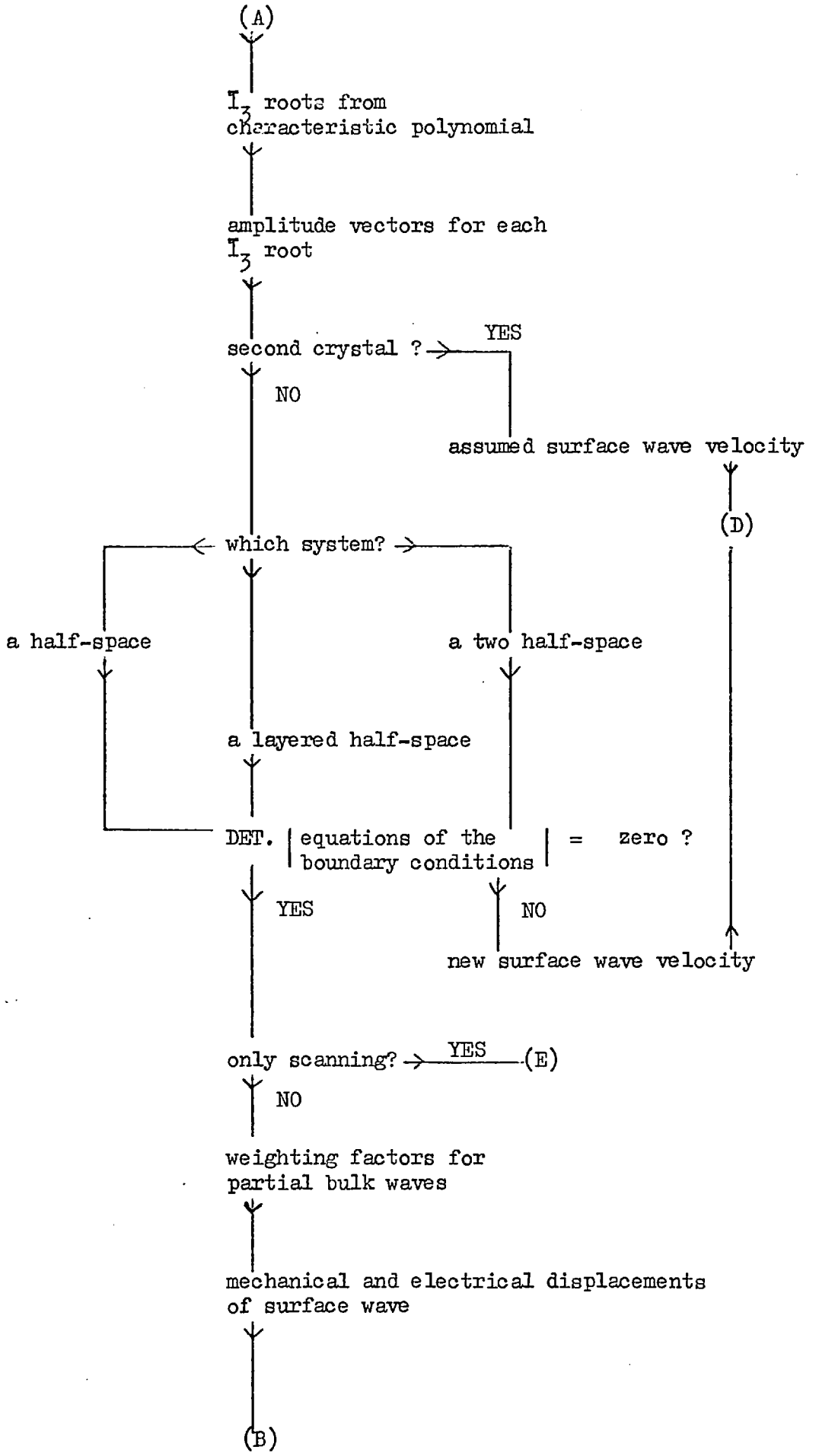
(A)
Γ_3 roots from characteristic polynomial
amplitude vectors for each Γ_3 root
second crystal ?
YES
NO
assumed surface wave velocity
(D)
which system?
a half-space
a two half-space
a layered half-space
DET. | equations of the boundary conditions | = zero ?
YES
NO
new surface wave velocity
only scanning?
YES
(E)
NO
weighting factors for partial bulk waves
mechanical and electrical displacements of surface wave
(B)

Contd....

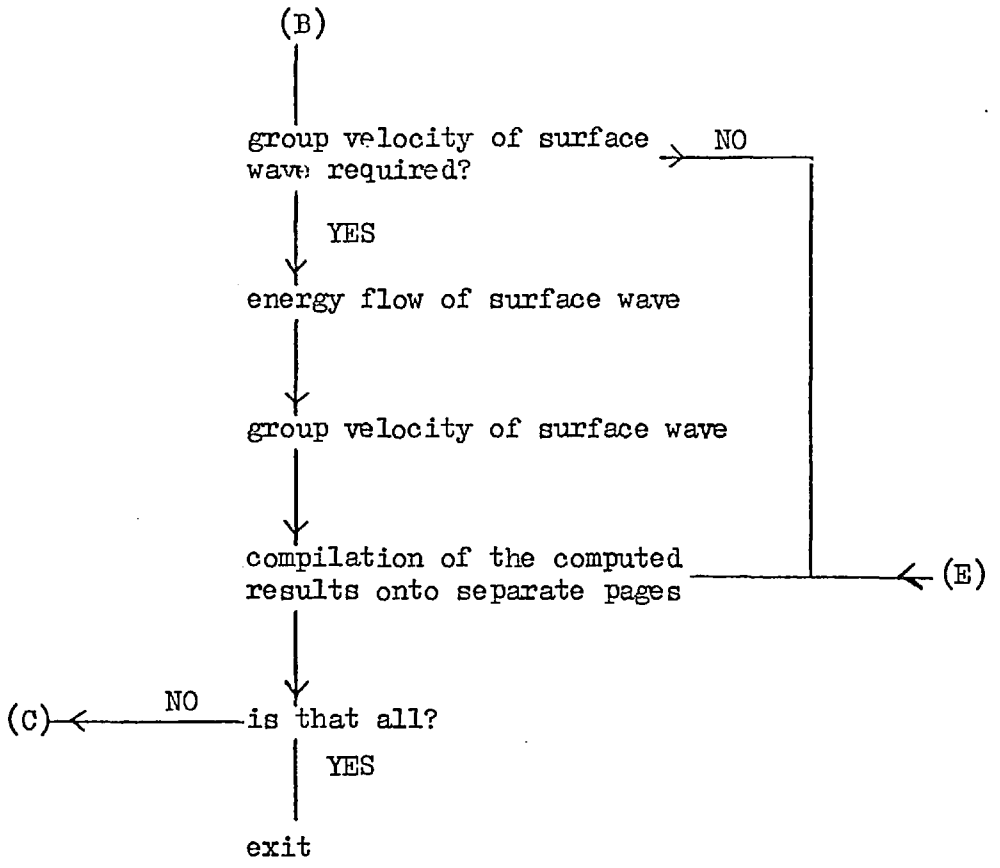
(B)
group velocity of surface wave required?
NO
YES
energy flow of surface wave
group velocity of surface wave
compilation of the computed results onto separate pages
(E)
NO
(C)
is that all?
YES
exit

Contd....

IMPLEMENTATION OF PROGRAMME "SNOOPY"

Subroutine	Function
RU730	primary part of the programme : reading control codes, controlling subroutines and interacting with FMIN through SEARCH
STORE	storing all physical constants
FMIN	secondary part of the programme : determining the modulud of characteristic matrix and controlling subroutines
RESULT	printing information obtained from the various computations into different pages
CONST	reading crystal data : mass density, name of crystal, elastic constants, piezoelectric constants, and dielectric constants
AXES	defining the angles in degrees for crystal rotation and new physical constants in specified direction
DIRN	defining the angles in degrees for wave propagation direction and (wave-depth penetration/wavelength) ratio
STIF	calculating the piezoelectrically stiffened constants
BULK	providing the characteristic features of bulk waves and the electromechanical coupling constants
RATIO	estimating the electromechanical amplitude ratio (i.e. scaling factor) in a piezoelectric crystal
FILM	specifying the (height/wavelength) ratio of the conducting film above piezoelectric crystal
SEARCH	seeking for a mechanical surface wave velocity within a given velocity range
DISPLA	calculating the mechanical and electrical displacements
ENERGY	determining energy flux and energy density of the surface wave
GROUP	calculating surface wave group velocity and propagation direction with angular deviation
GRAPH	plotting out a curve of the magnitude of the characteristic determinant against the surface wave velocity

Contd....

DETC	calculating the magnitude of a complex determinant
EIGEN	finding the eigen values and eigen vectors of a complex matrix
ORDER	sequencing a set of numbers
NORMX	normalizing a set of vectors
DCOS	defining a direction in terms of degrees from a set of displacement vectors
SUBFTN	setting the characteristic matrix from the boundary condition equations
POLY	calculating an inverse matrix and the characteristic polynomial from a complex matrix
ROOT	selecting the required $\bar{I}_3$ roots for the system
FACT	finding $\bar{I}_3$ roots from the characteristic polynomial with complex coefficients
VECT	calculating a set of vectors for each $\bar{I}_3$ root
HALF	setting boundary conditions for a half-space
THALF	setting boundary conditions for a two half-space
LAHALF	setting boundary conditions for a layered half-space
COMP	reducing a matrix into a determinant
WTF	estimating the appropriate weighting factors for the partial bulk waves

Contd....

CONTROL INSTRUCTIONS FOR PROGRAMME "SNOOPY"

Code	Coding integer	Function
NJ	0	stop
	1	a half-space (i.e. substrate)
	2	a two half-space (i.e. two substrates)
	3	a layered half-space (i.e. a layer and a substrate)
NC	bb	number of jobs for computation
NV	0	internal velocity range
	1	external velocity range
NO	bb	number of points on velocity range
NP1	0	purely elastic crystal I (i.e. CI)
	1	piezoelectrically stiffened crystal I
	2	piezoelectric crystal I
NP2	0	purely elastic crystal II (i.e. CII)
	1	piezoelectrically stiffened crystal II
	2	piezoelectric crystal II
NX1	0	crystal rotation not required for CI
	1	rotation required
NX2	0	crystal rotation not required for CII
	1	rotation required
NR1	3 or 4	number of $\bar{\Gamma}_3$ roots for CI
NR2	3,4,6, or 8	number of $\bar{\Gamma}_3$ roots for CII
NF	0	no conducting film
	1	conducting film needed
NS	0	source at free surface of layer
	1	source at interface of layer (to be implemented)
NB	0	bulk waves information not required
	1	information required
NSO	0	phase velocity scanning not required
	1	scanning required
NG	0	energy flux and group velocity not required
	1	both required

Contd....

DATA ENTERING SEQUENCE FOR PROGRAMME "SNOOPY"

No. of cards	Required data	Format on card
1	control codes	I1,2(I2,I1),1II1
1	mass density, name of crystal	E10.3,6A10
9	elastic constants	4E20.4
3	piezoelectric constants	6E10.4
3	dielectric constants	6E10.4
1	degrees for crystal rotation	3E10.2
1	degrees for propagation direction and (wave-depth penetration/wavelength)ratio	3E10.2
1	velocity range and tolerance	3E20.12
1	(height/wavelength) ratio for a conducting film	F10.4

Note:

i. For each job, the following data such as mass density, name of crystal, all the above physical constants and crystal orientation are first defined and stored in the programme.

ii. Following the above input, wave propagation direction, (wave-depth penetration/wavelength), external velocity range, velocity tolerance, and (height/wavelength) of the conducting film could be respectively varied or repeated for the specified crystal (or crystals) before processing the next set of input data in subsequent jobs.

Contd....

APPENDIX A 7

ASSOCIATED ELECTRIC ENERGY ACCOMPANYING THE MECHANICAL SURFACE WAVE IN A PIEZOELECTRIC CRYSTAL

In any piezoelectric crystal, the electric dipole field can be varied by mechanical deformation and vice versa. Hence in a mechanical vibration an oscillatory electric field is produced. It is to be expected that the induced electric field would be in phase with the associated mechanical deformation and thus accompanies the propagation of the mechanical wave. It is shown below that the fractional electric energy in the electric field is not completely insignificant when compared with the energy of the mechanical deformation.

In order to estimate the energy density ratio in the two types of fields, the following parameters have been estimated and are approximately correct in the order of magnitudes:

1. The ratio between electric and mechanical amplitude,

   (α_4 / α_i), is 10^{10}.

2. The ratio between dielectric and elastic constant,

   (ε / C), is 10^{-21}.

Hence, the energy density ratio of the electric field to the mechanical field would be given as:

$$\frac{\text{Electric Energy Density}}{\text{Mechanical Energy Density}} = \frac{\varepsilon}{C} \left(\frac{\alpha_4}{\alpha_i}\right)^2$$

$$= 10^{-21} \quad 10^{20}$$

$$= 10^{-1}$$

It should be mentioned that for most piezoelectric crystals, the fractional energy residing in the electric field is approximately 5×10^{-2}.

GLOSSARY

w	angular frequency
k	modulus of wave number
t	time coordinate
ρ	material density
V	wave velocity
T_{ij}	component of stress tensor
C_{ijkl}	component of elastic stiffness tensor
S_{kl}	component of strain tensor
U_j ; $\dot{U}_j$; $U_{k,l}$	component of mechanical particle displacement; dot and comma indicate respectively the time and space derivatives of the particle displacement
α_j	component of mechanical displacement amplitude
l_i	component of direction cosines for wave propagation
x_i	spatial coordinates of rectangular axes
Γ_{jk}	Kelvin-Christoffel stiffness
δ_{jk}	Kronecker delta
μ	eigenvalue
L_i	component of direction cosines for wave energy
L_i'	component of direction cosines for wave polarization
K_p	piezoelectric coupling factor
ε_{ik}	component of dielectric tensor
e_{kij}	component of piezoelectric tensor
ϕ	associated electric scalar potential
α_4	electric potential amplitude
E_k	component of electric field
D_i	component of electrical displacement

α_o	piezomechanical amplitude ratio
θ, φ	Eular angles
$\bar{l}_3$, l_3^+, l_3^*	complex direction cosine in OX_3 -direction; cross and asterisk indicate respectively the imaginary and real part of the complex direction cosine, $\bar{l}_3$.
C^n	weighting factor of n^{th} partial bulk wave
h	height of conducting (earthed) film
H	thickness of layer material
λ	wavelength
V_{s1} , V_{s2}	velocities of the fast and the slow shear waves
Z_m	real coefficient of m - order polynomial
$'a_j^n$	component of scaled particle amplitude of n^{th} partial bulk wave
$'a_4^n$	scaled amplitude of electric potential of n^{th} partial bulk wave
Λ	abbreviation of (layer thickness/wavelength)
P_i	component of energy flux
E_i	component of energy density
Pl_i	component of integrated energy flux
El_i	component of integrated energy density
V_g	group velocity
ZnO(YX)/Si	implying Y-cut ZnO crystalline layer overlay onto Z-cut Si crystalline substrate and the crystals are aligned with X-axes as wave propagation direction; if the crystalline layer is (Z-cut, X-propagation), the expression is simply written as ZnO/Si. This rule holds for other two-material combinations.
Rubylith film	a double (i.e. red and transparent) plastic film often used as an original art work for the photographic mask of an integrated circuit.

REFERENCES

Andrianova Z S, Keilisborok V I, Levshin A L & Neigauz M G	1967	Seismic Love Waves, Consultants Bureau, New York
Anderson J C & Weidmann E J	1971	Thin Solid Films, Vol. 7, p.265-276
Brekhovskikh L M	1960	Waves in Layered Media, Vol. 6 Academic Press, New York
Brugger K	1965	J. Appl. Phys. Vol. 36, 3, p.759-768
Borgnis F E	1955	Phys. Rev., Vol. 98, 4 p.1000-1005
Burridge R	1970	Quart. J.Mech. Appl. Math., Vol.23, p.217-224
Buchwald V T	1961	Quart. J.Mech. Appl. Math., Vol.14, p.293-317
Buchwald V T	1961	ibid., p.461-469
Bleutein J L	1968	Appl. Phys. Lett., Vol. 13,12, p.412-413
Berlincourt D A, Curran D R & Jaffe H	1964	Physical Acoustics, Vol. 1A, Academic Press, New York & London
Butler H S & Kino G S	1963	Phys. of Fluids, Vol. 6,9, p.1346-1355
Cagniard L	1962	Reflection and Refraction of Progressive Seismic Waves, McGraw-Hill, New York
Coquin G A & Tiersten F	1966	J.Acoust. Soc. Am.,Vol.41,4, p.921-939
Campbell J J & Jones W R	1968	Hughes Aircraft Company, Lab. Report TP 68-14-7
Ewing W M, Jardetzky W S & Press F	1957	Elastic Waves in Layered Media McGraw-Hill, New York
Engan H, Ingebrigtsen K A & Tonning A	1967	Appl. Phys. Lett., Vol. 10,11 p.311-313
Foster N F	1965	Proc. IEEE, Vol. 53,10, p.1400-1405
Foster N F	1969	J.Appl.Phys,Vol. 40,10, p.4202-4204
Farnell G W	1970	IEEE Trans., Vol. SU-17,4, p.229-238

Fano R M	1950	J.Franklin Inst., Vol. 249, p.57-83; p.139-155
Gulyaev Yu V	1969	JETP Lett., Vol. 9, p.37-38
Getsinger W J	1963	IEEE Trans., Vol.MTT-11,4, p.486-497
Humphreys B L	1964	Proc.IEE, Vol.111,2, p.264-274
Hickernell F S, Shulda G F & Brewer J W	1970	IEEE Ultrasonic Symposium paper G-11
Hickernell F S	1971	Acoustic Surface Wave & Acousto-optic Devices, Optosonic Press, New York, p.31-41
Hickernell F S & Brewer J W	1972	Appl. Phys. Lett., Vol. 21,8, p.389-391
Ingebrigtsen K A	1969	J.Appl. Phys., Vol. 44,6, p.2495-2503
Kurokawa K	1969	Bell Sys. Tech. J., July-August, p.1937-1955
Koerber G	1971	IEEE Trans., Vol.SU-18,2, p.73-78
Kramer C J & Araghi M N	1973	IEEE Ultrasonics Symposium Proceedings,73 CHO 807-8 SU, p.103-106
Lardat C, Maerfeld C & Tournois P	1970	Thomson-CSF Lab.Report D.ASM-85.669 CL/CM/PT
Lim T C & Farnell G W	1968	J.Appl. Phys., Vol. 39,9, p.4319-4325
Lim T C	1968	Ph.D. Thesis
Musgrave M J P	1954	Proc.Roy.Soc.(London),A226, p.339-366
Musgrave M J P	1961	Progress in Solid Mechanics, Vol.2, p.63-85
Nagao M	1966	J.Appl.Phys,Vol.37,12 p.4591-4592
Smith W R, Gerard H M, Collins J H, Reeder T M, & Shaw H J	1969	IEEE Trans., Vol. MTT-17,11, p.856-864
Schnitzler P	1967	Appl.Phys.Lett., Vol.11,9, p.273-275
Stoneley R	1955	Proc.Roy.Soc.(London) A232 p.447-458

Synge J L	1956	Proc.Roy.Irish Acad.,Vol.A58, p.13-21
Synge J L	1957	J.Math. & Phys., Vol.35, p.323-334
Schmidt R V & Voltmer F W	1969	IEEE Trans., Vol.MTT-17,11, p.920-926
Solie L P	1973	J.Appl.Phys., Vol.44,2 p.619-627
Scanlan J O & Lim J T	1964	IEEE Trans., Vol.MTT-13,6, p.827-836
Tseng C C	1967	J.Appl.Phys.,Vol.38,11, p.4281-4284
Voltmer F W, Ippen E P, White R M, Lim T C & Farnell G W	1968	Proc.IEEE, Vol.56,9, p.1634-1635
White R M & Voltmer F W	1965	Appl.Phys.Lett., Vol.7,12, p.314-316
Warner A W, Coquin G A & Fink J L	1969	J.Appl.Phys.,Vol.10,11 p.4353-4356
White R M & Tarakci U	1972	IEEE Ultrasonics Symposium Proceedings, 72 CHO 708-8 SU, p.440-445
Yamada T, Iwasaki H & Niizeki N	1972	J.Appl.Phys., Vol.43,3 p.771-775